

# Meddelelser om Grønland

## Mineralized fracture systems of the Skaergaard intrusion, East Greenland

*Dennis K. Bird, Ralph D. Rogers  
and Craig E. Manning*



**Geoscience**  
**16 · 1986**

## *Meddelelser om Grønland*

The series *Meddelelser om Grønland* was started in 1879 and has since then published results from all fields of research in Greenland. In 1979 it was split into three separate series:

*Geoscience*  
*Bioscience*  
*Man & Society*

The series should be registered as *Meddelelser om Grønland, Geoscience (Bioscience, Man & Society)* followed by the number of the paper. Example: *Meddr Grønland, Geosci. 1, 1979.*

The new series are issued by Kommissionen for videnskabelige Undersøgelser i Grønland (The Commission for Scientific Research in Greenland).

### *Correspondence*

All correspondence and manuscripts should be sent to:

The Secretary  
Kommissionen for videnskabelige Undersøgelser i  
Grønland  
Øster Voldgade 10  
DK-1350 Copenhagen K.

Questions concerning subscription to any or all of the series should be directed to the agent.

### *Agent*

Nyt Nordisk Forlag – Arnold Busck A/S, Købmagergade 49, DK-1150 Copenhagen K. Tlf. +45.1.111103.

## *Meddelelser om Grønland, Geoscience*

*Meddelelser om Grønland, Geoscience* invites papers that contribute significantly to studies in Greenland within any of the fields of geoscience (physical geography, oceanography, glaciology, general geology, sedimentology, mineralogy, petrology, palaeontology, stratigraphy, tectonics, geophysics, geochemistry). Papers primarily concerned with other areas in the Arctic or Atlantic region may be accepted, if the work actually covers Greenland or is of direct importance to continued research in Greenland. Papers dealing with environmental problems and other borderline studies may be referred to either *Geoscience* or *Bioscience* according to emphasis and editorial policy.

### *Editor – Geoscience*

T. C. R. Pulvertaft, Institute of General Geology, Øster Voldgade 10, DK-1350 Copenhagen K. Tlf. +45.1.112232. Telegr. Unigeol.

*Instructions to authors.* – See page 3 of cover.

© 1986 Kommissionen for Videnskabelige Undersøgelser i Grønland. All rights reserved. No part of this publication may be reproduced in any form without the written permission of the copyright owner.



# Mineralized fracture systems of the Skaergaard intrusion, East Greenland

*Dennis K. Bird, Ralph D. Rogers and  
Craig E. Manning*

## Table of contents

Abstract . . . . .	3
Introduction . . . . .	3
Fracture systems of the Layered Series gabbros	6
Pegmatites and pyroxene-oxide veins . . . . .	9
Transgressive granophyres and quartz veins . .	15
Amphibole veins . . . . .	19
Actinolitic hornblende-chlorite-talc-biotite .	24
Calcic amphibole-clinopyroxene-biotite . . .	25
Hornblende-actinolite-biotite . . . . .	31
Hornblende-actinolite-albite-epidote . . . . .	33
Cummingtonite-olivine . . . . .	35
Fracture systems of the Upper Border Group and the Basistoppen Sheet . . . . .	37
Fracture systems near the contact of the Skaer- gaard intrusion . . . . .	41
Uttental Pass . . . . .	44
Kraemer Ø . . . . .	46
Mellemø . . . . .	48
Ivnarmiut . . . . .	51
South and east contacts . . . . .	54
Fracture systems in the basalt host rocks . . . . .	56
Physical and chemical conditions of vein miner- alization . . . . .	57
Concluding remarks . . . . .	63
Acknowledgements . . . . .	65
References . . . . .	65



# Mineralized fracture systems of the Skaergaard intrusion, East Greenland

DENNIS K. BIRD, RALPH D. ROGERS and CRAIG E. MANNING

Bird, D. K., Rogers, R. D. & Manning, C. E. 1986. Mineralized fracture systems of the Skaergaard intrusion, East Greenland. *Meddr Grønland, Geosci.* 16: 68 pp. Copenhagen 1986-12-16.

Extensive fracture systems in the Skaergaard intrusion, including veins, sills and dikes, constitute channels for the flow of magmas and hydrothermal solutions during the subsolidus cooling and deformation of the intrusion. The abundance, orientation, transgressive relations and mineralogy of these fracture systems provides a record of fluid transport and chemical reactions during the Skaergaard's subsolidus cooling history.

The earliest mineralized fractures in the Layered Series are gabbroic pegmatites that occur as veins, sills and irregular patches. These structures are crosscut by leucocratic granophyres. Veins filled with hydrothermal minerals occur throughout the Skaergaard intrusion and its host rocks. Hydrothermal minerals in veins are similar to mineral assemblages found in metabasalts ranging in grade from upper amphibolite to zeolite facies. The earliest hydrothermal veins contain upper amphibolite facies assemblages. They are <1–2 mm wide, continuous for tens of metres and occur with frequencies of 0.2 to >1.5 and 1.4 to >20 fractures/metre in the Layered Series, and Marginal Border Group and contact metamorphosed basalts, respectively. These early veins are inferred to have formed at temperatures of >500° to 750°C and <925° to 960°C. Later vein types contain mineral assemblages characteristic of lower amphibolite, greenschist and sub-greenschist facies and occur as more localized fracture systems than the early, high temperature vein types. Compositions of secondary minerals from all of these hydrothermal vein types show systematic changes relative to both the overall fractionation trend and local modal variations in the igneous mineralogy of the Skaergaard intrusion.

Observed phase relations and fracture abundances are, in general, consistent with isotopic and transport characteristics of the Skaergaard magma-hydrothermal system reported by Taylor & Forester (1979) and Norton & Taylor (1979).

*Dennis K. Bird, Department of Geology, Stanford University, Stanford, California, 94305 U.S.A. Ralph D. Rogers, School of Geology and Geophysics, University of Oklahoma, Norman, Oklahoma, 73019 U.S.A. Craig E. Manning, Department of Geology, Stanford University, Stanford, California, 94305 U.S.A.*

Early Tertiary continental rifting that formed the North Atlantic ocean basin was associated with extensive igneous and hydrothermal activity. In East Greenland, this activity is recorded in the exposures of gabbroic and felsic plutons, in the voluminous basaltic lavas between 68° and 75° N latitude, and in the mafic dike swarms that parallel the coast between 66° and 70° N latitude (Fig. 1; Wager 1934, 1947). Glaciation and uplift in the coastal region near 68° N latitude (Brooks 1979) have provided exposures that afford an unprecedented opportunity to study the mineralogic and structural record of hydrothermal activity associated with the cooling of these igneous rocks.

The purpose of this paper is to describe the physical and chemical characteristics of mineralized fracture systems formed by the emplacement and cooling of the Skaergaard intrusion. Geometric relations between

fracture sets found within and near the intrusion have been mapped in detail on a variety of scales. These observations are combined with compositional and textural relationships among fracture-filling minerals to evaluate the intensive thermodynamic variables (i.e. temperature, pressure, and the chemical potential of thermodynamic components) associated with fluid-rock reactions and chemical mass transfer during the period of time that a given fracture set contributed to the permeability of the cooling pluton.

The Skaergaard intrusion is one of a number of Tertiary intrusions near Kangerdlugssuaq fjord in East Greenland (Fig. 2). The magma chamber was inflated about 55 million years ago (Brooks & Gleadow 1977) by the intrusion of tholeiitic magma along an unconformity between the Precambrian basement complex and the overlying sediments and basalts (Figs 2 & 3). Fig. 3

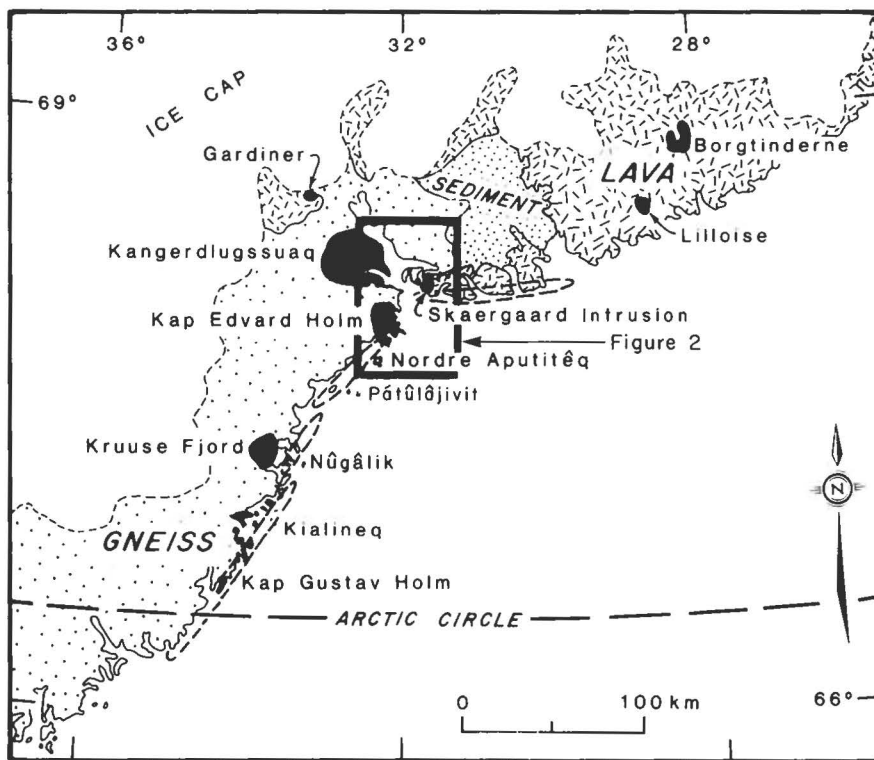
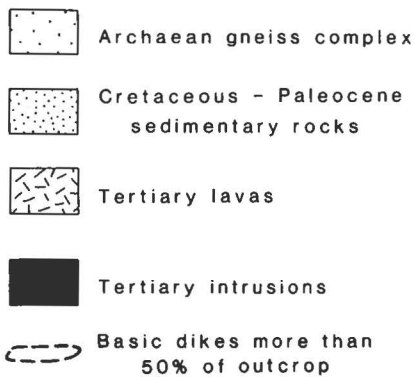


Fig. 1. Generalized geologic map of the East Greenland Tertiary igneous province between 66° and 69° North latitude. Place names refer to intrusive complexes within the coastal mountains. Compiled from maps and data reported by Wager & Brown (1967), Brooks & Nielsen (1982a,b), Bridgwater et al. (1978), and Myers (1980).



gives the distribution of the major lithologic units of the Skaergaard intrusion (after Wager & Deer 1939; Wager & Brown 1967).

Although most investigations of this intrusion have concentrated on its igneous petrogenesis, oxygen isotope analysis and numerical transport modelling of the intrusion by Taylor & Forester (1979) and Norton & Taylor (1979), respectively, have demonstrated that large scale fluid circulation and water-rock reactions occurred in the intrusion and its host rocks at subsolidus temperatures (Fig. 4). One of several important results of these studies was the prediction of a time and volume averaged permeability of the Skaergaard intrusion of  $10^{-12}$  to  $10^{-13}$  cm<sup>2</sup>.

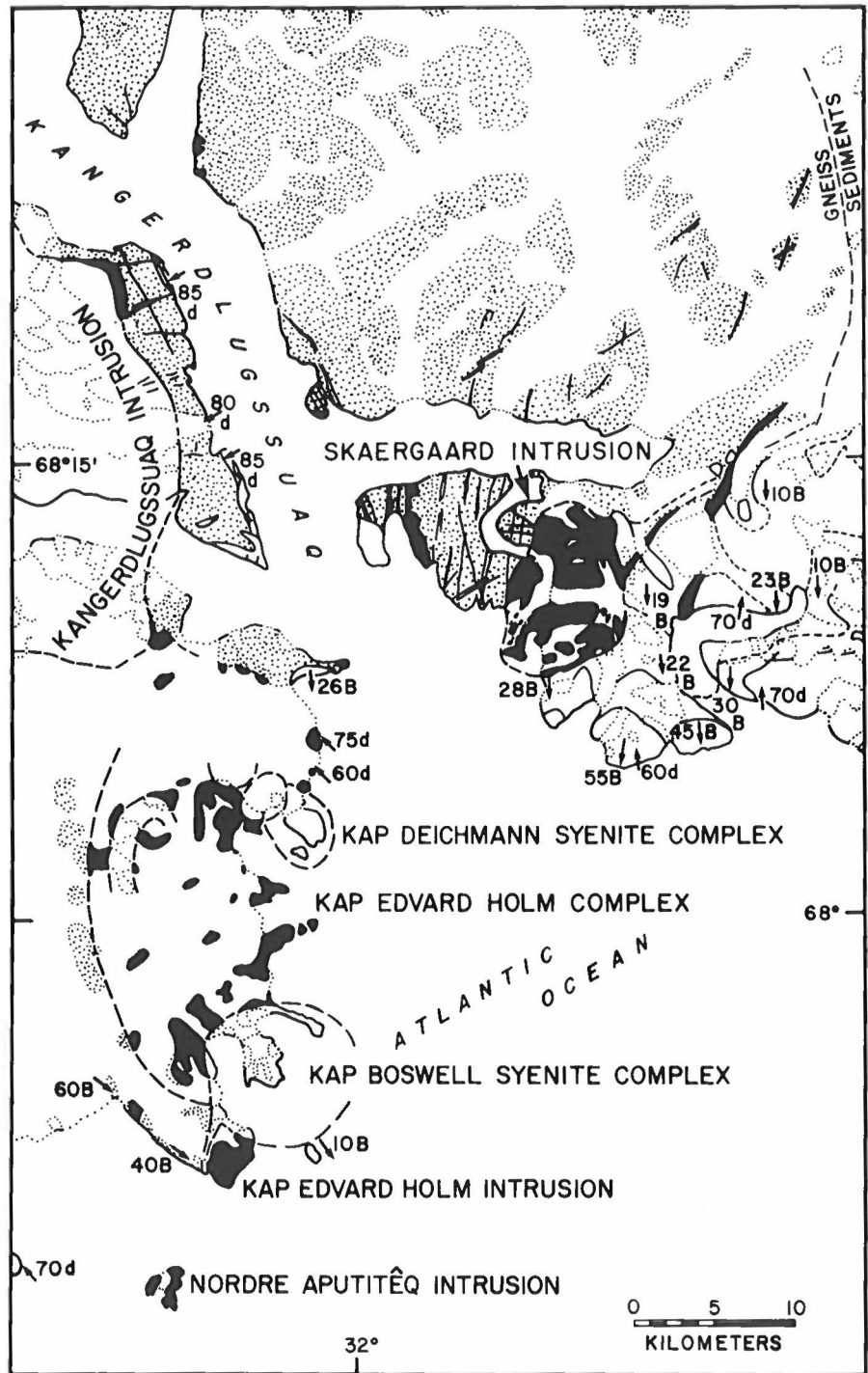
Later field investigations in the summer of 1981 by

D. Norton and D. K. Bird led to the identification of a variety of mineralized fracture systems within the Skaergaard intrusion (Norton, Taylor & Bird 1984). These fracture systems controlled the flow of hydrothermal solutions during the pluton's subsolidus cooling history and probably represent the natural porosity responsible for the permeability of the intrusion predicted by Norton & Taylor (1979). In 1982 and 1984, critical field relations were mapped in detail and samples of minerals in the veins were collected. The findings of the latter expeditions, together with mineralogic studies conducted at Stanford University are presented below and by Manning & Bird (1986) and Rogers & Bird (1987).

Fracture systems within the Skaergaard intrusion



Fig. 2. Geologic map of the Kangerdlugssuaq region (see Fig. 1 for location) showing the distribution of major plutonic complexes and mafic dikes near the Skaergaard intrusion. Stippled areas are exposures of the Precambrian basement. Solid black lines and areas denote mafic dikes and gabbroic intrusions, respectively. Numbers and arrows represent the magnitude and direction, respectively, of the dip of mafic dikes (d) and of the Blossville Kyst basalts (B). The solid lines in the Skaergaard intrusion outline the exposures of the Vandfaldsdalen Formation, Miki Formation and the Main Lavas of the Blossville Kyst Basalts. Map is compiled from references given in Fig. 1 and Wager & Deer (1938, 1939), Wager (1934, 1947), Abbott & Deer (1972), Kempe & Deer (1970) and Nielsen et al. (1981).



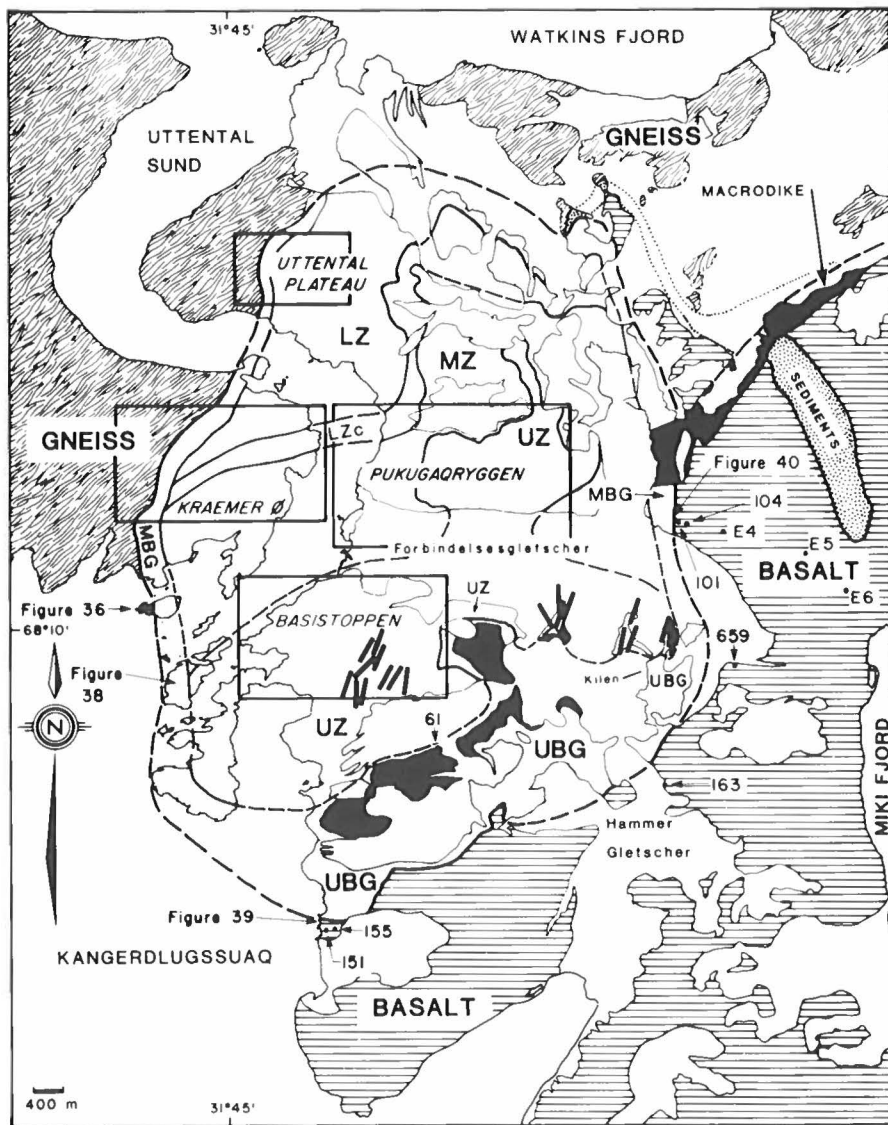


Fig. 3. Generalized geologic map of the Skaergaard intrusion showing exposures of host rock gneisses, sediments, and basalts, and the major lithologic units within the Skaergaard intrusion that are abbreviated as: LZ = Lower Zone, MZ = Middle Zone, UZ = Upper Zone, UBG = Upper Border Group, MBG = Marginal Border Group. These rock units are further subdivided based on the appearance or disappearance of various index cumulate minerals (Wager & Brown 1967). The solid black areas represent the exposures of the Basistoppen Sheet within the Skaergaard intrusion and the Macrodiike northeast of the intrusion. The short thick solid lines in the Upper Zone gabbros represent the orientation of quartz veins (see Fig. 10). Boxes outline study areas discussed in the text and are presented in Figs 5, 6, 7 & 13. These study areas are referred to as Utental Plateau, Kraemer Ø, Pukugaqryggen and Basistoppen areas in the text. The numbers 61, 101, 104, 151, 155, 163 and 659 are sample locations of veins discussed in the text. The map is compiled from data reported by Wager & Deer (1939), Wager & Brown (1967), and A. R. McBirney (personal communication, cited in Taylor & Forster 1979, fig. 3).

have characteristic and systematic mineralogic and structural relations. The distribution, crosscutting relations, abundance, and continuity of mineralized fractures were studied throughout the Layered Series, Upper Border Group and contact zones of the intrusion (Fig. 3). Approximately 1500 measurements of fracture orientations were made in these study areas, and hand samples of fracture mineralization and crosscutting relations were obtained for laboratory analysis. These data, summarized in the maps presented in this paper, constitute the structural record of fractures that controlled the transport of reactive fluids during the subsolidus cooling history of the Skaergaard magma-hydrothermal system. The fracture systems of the intrusion are discussed below in terms of the major lithologic divisions in which they occur.

### Fracture systems of the Layered Series gabbros

In the Layered Series gabbros, large scale reconnaissance mapping and traverses, as well as small scale detailed maps were made at Utental Plateau, Kraemer Ø, and on the west slopes of Basistoppen and Pukugaqryggen (Fig. 3). Within these areas are several important igneous structures of the Skaergaard Layered Series, including the zone of Upper Border Group stope blocks and the Triple Group layering in the Middle Zone gabbros, and the Trough Band structures of the Upper Zone a rocks (Wager & Deer 1939, Wager & Brown 1967). The maps given in Fig. 5 show the details of these geologic features within the Kraemer island (Kraemer Ø), Pukugaqryggen, and Basistoppen study



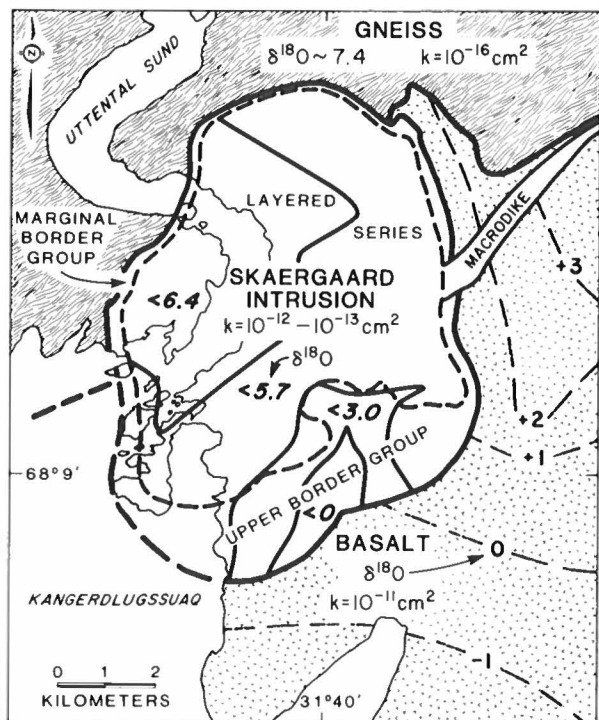


Fig. 4. Generalized geologic map of the Skaergaard intrusion showing the oxygen isotope and transport characteristics of the intrusion and the host rocks reported by Taylor & Forester (1979) and Norton & Taylor (1979). Isoleths of  $\delta^{18}\text{O}$  within the intrusion denote values for plagioclase, but those in the host rocks represent whole rock values. Permeabilities ( $k$ ) are time and volume averaged values used by Norton & Taylor (1979) in their numerical analysis of fluid circulation and  $^{18}\text{O}$  mass transfer during the cooling of the Skaergaard intrusion.

areas. The distribution of hydrothermal veins, transgressive granophyres, pegmatites and mafic dikes have been studied in detail within the map areas.

The simple geologic history and excellent exposures of the Skaergaard intrusion permit detailed geometric analysis of fracture genesis. However, paragenetic relations observed among the various mineralized fractures are locally intricate and complex. Early fracture networks within the crystallized and cooling Layered Series gabbros had a conspicuous influence on subsequent fracture orientations. Superimposition of fracturing is recorded in overlapping fracture-filling mineralization that may include hornblende-biotite-clinopyroxene veins, felsic granophyres, chlorite-actinolite veins, quartz veins and mafic dikes. In a number of localities where several types of fracture sets occur we have been able to identify the relative timing of different fracture types as well as the relations of the various fracture sets to different intrusive and deformational events.

Norton, Taylor & Bird (1984) identifies four general fracture types within the Skaergaard intrusion. The earliest fracturing was associated with local transport of re-

sidual magma that formed hybrid gabbro pegmatites in fractures that are typically concordant with the igneous layering. Near vertical fracture systems that acted as channels for the flow of hydrothermal solutions crosscut the pegmatites. Reactions between these aqueous solutions and the Layered Series gabbros have produced mineral assemblages typical of upper amphibolite facies metamorphism of basaltic rocks. These high temperature fractures are locally crosscut by leucocratic transgressive granophyres that do not have chilled margins with the gabbros and a closely related set of drusy amphibole mineralized veins. Mineralized fractures formed during the final stages of the subsolidus cooling history of the Skaergaard intrusion contain lower amphibolite facies metamorphic mineral assemblages with minor amounts of later greenschist to zeolite facies assemblages. It is evident from the work of Norton, Taylor & Bird (1984), and the present study, that amphibole veins formed continuously during the cooling of the Layered Series. The amphibole veins formed prior to, during and subsequent to the emplacement of the transgressive granophyres. The four fracture types are interpreted by Norton, Taylor & Bird (1984), and in this study, as expressions of brittle deformation and mineralization associated with the subsolidus cooling of the Skaergaard intrusion.

In addition to these fractures, the study areas of Fig. 3 are crosscut by mafic dikes (Nielsen 1978) and a closely associated parallel set of chlorite mineralized veins (Rogers & Bird 1987) that postdate all of the fracture systems mentioned above. All the mafic dikes examined have chilled margins to their host rocks. Mafic dikes within the Layered Series gabbros have several prominent orientations including north-south and east-west in the southern map areas, and east-west and northeast in the northern most study areas near Utental Plateau (Fig. 6). These dikes are usually less than five meters wide and rarely exceed 10 meters in width. In many cases they are continuous for hundreds of meters. Fracture systems represented by these mafic dikes form a complex grid pattern over the map areas of Fig. 6 and also on a regional scale in the Kangerdlugssuaq fjord region as shown in Fig. 2. Dike intersections define blocks that are tens to hundreds of meters wide. These blocks contain the older mineralized fracture sets that are the subject of this communication. The youngest mineralized fractures in the area are associated with calcite and zeolite fillings of fault zones.

The mineralized fracture systems outlined above for the Layered Series can be divided into four groups based on the dominant fracture-filling mineralogy. These include 1) gabbro pegmatites and pyroxene-oxide veins, 2) leucocratic transgressive granophyres and quartz veins, 3) amphibole veins, and 4) chlorite veins. The geometric characteristics and mineralogic phase relations within and near the first three groups of these mineralized fracture types are presented below. The mineralogy and field relations of chlorite veins that are

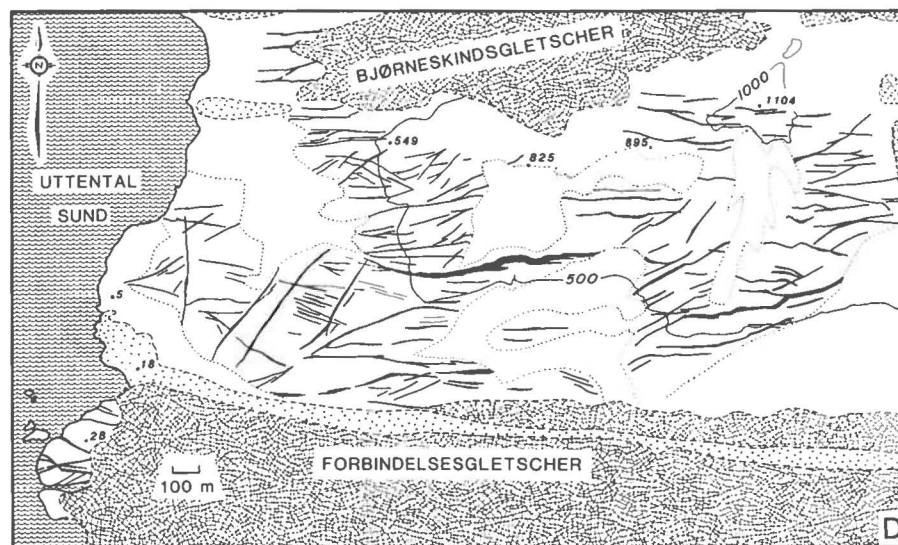
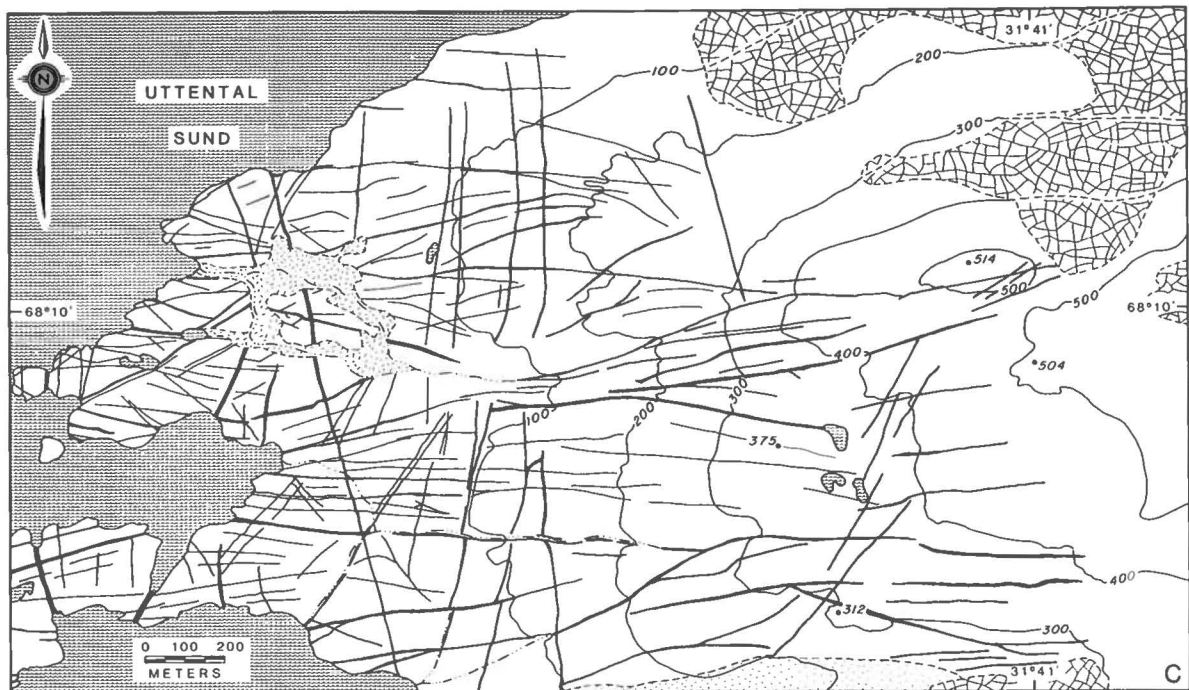


Fig. 6 C-D. Aerophotograph interpretation of the distribution of mafic dikes within the Basistoppen (C) and Pukugaqryggen (D) study areas of the Skaergaard intrusion (see Fig. 3 for map locations).

clase and pyroxene with open space vugs lined with  $\beta$ -quartz, plagioclase, orthoclase and micaceous material. Their description of the hybrid patches is similar to the description of the pegmatitic veins in the Upper Zone gabbros given by Norton, Taylor & Bird (1984: fig. 7). Plagioclase-rich lenses and closely associated veins were also found in the Lower Zone c gabbros at Utental Plateau and in the Middle Zone gabbros on the west slopes of Pukugaqryggen (Irvine 1980).

Coarse-grained calcium-poor pyroxene and Fe-Ti oxide veins that occur in the region of fallen Upper Border

Group blocks in the Middle Zone gabbros of Kraemer Ø are similar in appearance but mineralogically distinct from the gabbro pegmatites in the Layered Series gabbros described above. Coarse-grained inverted pigeonite, Fe-Ti oxides and minor augite fill both irregular shaped and near linear fracture systems within the larger Upper Border Group blocks (Fig. 8A). Unlike these veins, the thicker pegmatitic veins in the Layered Series gabbros may contain about 20% plagioclase with crystals up to 2 cm long. The pyroxene-oxide veins are typically less than 3 cm wide, are continuous for up to



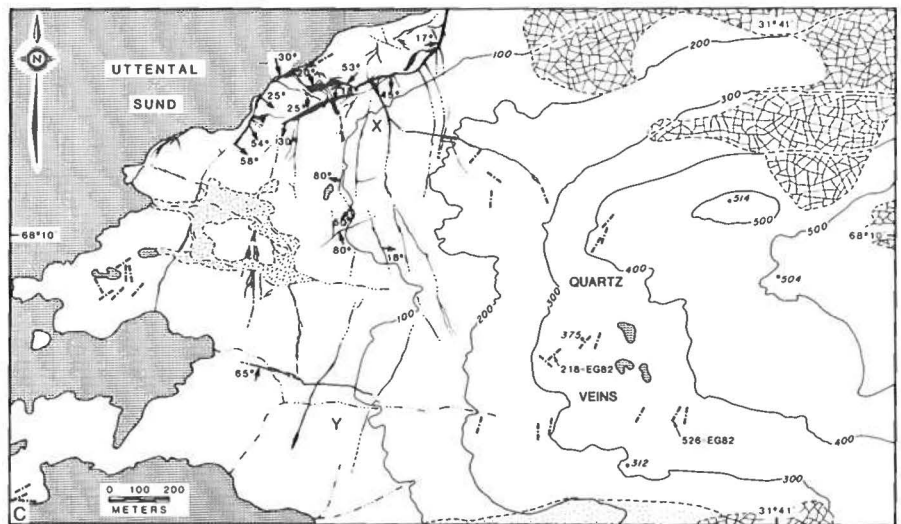
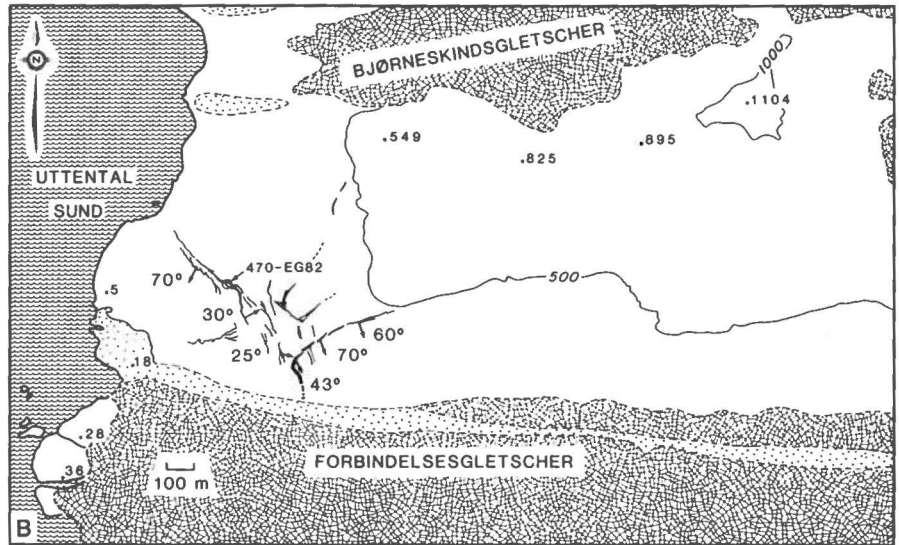
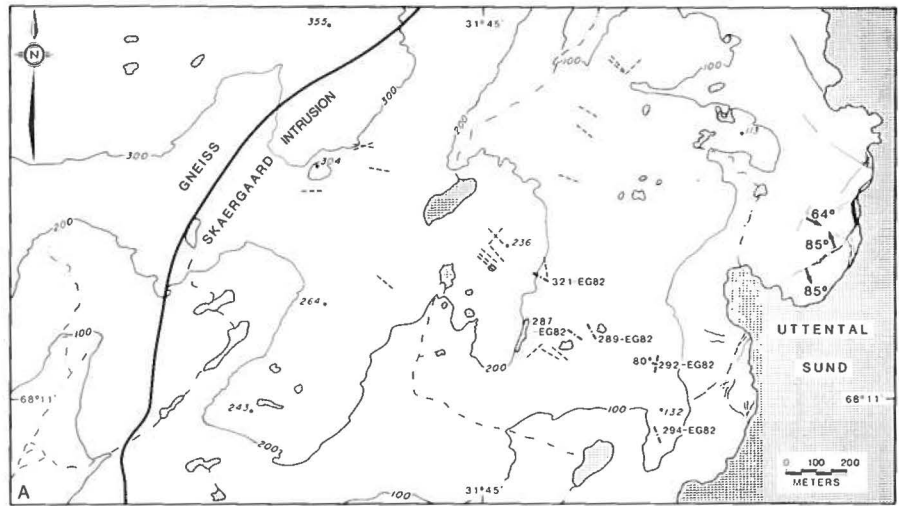


Fig. 7. Distribution of transgressive acid granophyres (solid and dashed lines), pyroxene-Fe-Ti oxide veins in Upper Border Group xenoliths of the Middle Zone gabbros (dash-dot-dash lines in map A) and quartz-iron silicate veins in the Upper Zone b and Upper Zone c gabbros (dash-dot-dash lines in map C) within the Kraemer Ø (A), Pukugaqryggen (B) and Basistoppen (C) study areas (see Fig. 3 for map locations). Contour intervals are 100 meters in maps A and C and 500 meters in map B.

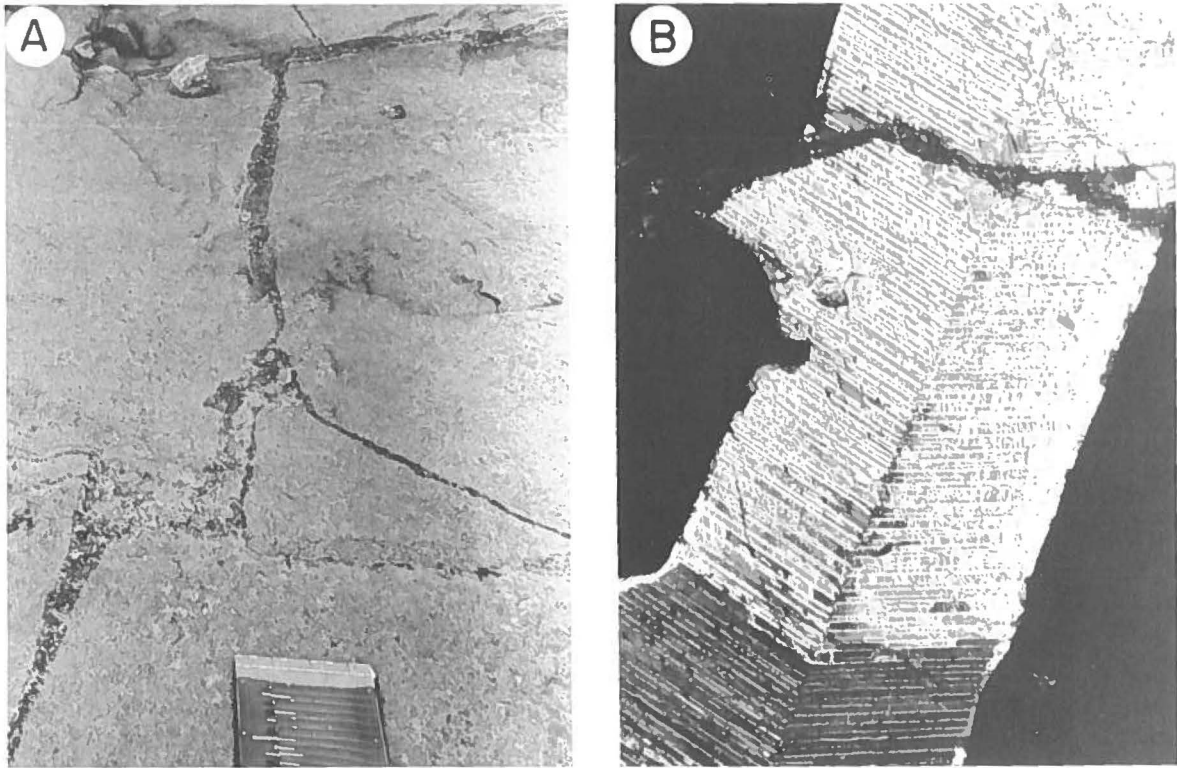


Fig. 8. Pyroxene-oxide veins in Upper Border Group stope blocks in the Middle Zone gabbros. A) exposures of veins in Upper Border Group block near locality 321-EG82 in Fig. 7A. B) photomicrograph of inverted pigeonite and oxides in vein 321-EG82 (field of view is 8 mm wide).

10–15 meters, and appear to be restricted to the stoped blocks. In the 800 meter traverse between sample 321-EG82 southeast to 294-EG82 (Fig. 7A), five sets of these fracture systems were observed, suggesting a wide distribution of the pyroxene-oxide veins in the zone of the fallen blocks. These veins generally trend northwest (Fig. 7A), although more complicated local structures were apparent in the field (Fig. 8A). An example of the field geometry of these fractures can be seen in the small stope block in the lower right hand corner of Fig. 15B.

Pyroxene-oxide veins transgress the boundary of the fallen blocks and the Middle Zone gabbros in only a few localities. In these places the mineralized fractures have sharp contacts with the host gabbros, are typically greater than 5 cm wide and are up to several meters in length. This is in contrast to the more common irregular shaped veins that appear to terminate near the magnetite-rich margins of the Upper Border Group xenoliths. As noted by McBirney (1979), concentrations of iron oxides are common near the margins of many of the xenoliths within the Layered Series gabbros.

The pyroxene-oxide veins in the fallen blocks have irregular contacts with the plagioclase-rich host rock.

Contacts between the plagioclase and the vein minerals are sharp, displaying concave embayments in the cumulate plagioclase. Rounded plagioclase crystals may also be completely surrounded by the oxide mineral aggregates. This results in an irregular and poorly defined microscopic boundary between the vein and the host rock. About two-thirds of the veins are filled with Fe-Ti oxides with lesser amounts of coarse-grained inverted pigeonite (up to 2 cm long) and minor augite. Representative chemical analyses of vein-filling minerals are given in Table 1.

Unaltered pyroxene-oxide vein samples contain oxide aggregates that consist of about 60% titanomagnetite and 40% ilmenite (Analyses 4 & 5, Table 1). Ilmenite grains are typically surrounded by titanomagnetite, and occur as coarse-grained composite inclusions with subhedral terminations parallel to the {111} planes of the magnetite. Minor amounts of thin trellis exsolution lamellae of ilmenite also occur in the magnetite. Based on microprobe analyses, cell edge refinement of XRD analyses and lattice constant composition relations reported Lindsley (1965), the titanomagnetite contains up to 45 mole percent ulvospinel, whereas the ilmenite has less than 5 mole percent hematite component.

Table 1. Selected electron microprobe analyses of pyroxene-oxide vein minerals.<sup>a</sup>

	1 321-8 Augite lamellae	2 321-19 Inverted pi- geonite host	3 321-26 Olivine (Hortonalite)	4 321-11 Titaniferous magnetite	5 321-12 Ilmenite	6 294-10b Inverted pi- geonite host	7 294-13 Augite lamellae
SiO <sub>2</sub>	51.96	52.71	36.53	0.17	0.10	52.93	51.32
Al <sub>2</sub> O <sub>3</sub>	1.61	0.71	b.d. <sup>b</sup>	4.51	0.02	0.74	1.79
FeO	14.01	26.22	39.38 <sup>c</sup>	44.52	43.13	24.48	13.42
Fe <sub>2</sub> O <sub>3</sub>	0.00 <sup>d</sup>	0.00 <sup>d</sup>		34.52 <sup>d</sup>	2.22 <sup>d</sup>	0.00 <sup>d</sup>	0.19 <sup>d</sup>
MgO	12.50	18.56	24.64	1.05	2.24	18.62	13.49
MnO	0.37	0.63	0.56	0.26	0.39	0.54	0.29
TiO <sub>2</sub>	0.71	0.36	0.11	15.28	52.71	0.41	0.91
CaO	18.98	1.63	0.07	b.d.	b.d.	3.10	18.21
Na <sub>2</sub> O	0.21	b.d.	b.d.	b.d.	b.d.	b.d.	0.24
Cr <sub>2</sub> O <sub>3</sub>	b.d.	0.02	0.04	0.09	b.d.	0.01	0.03
Total	100.35	100.84	101.33	100.40	100.81	100.83	99.88
Basis (Oxygens):	6	6	4	8	3	6	6
Si	1.960	1.988	1.018	0.012	0.003	1.987	1.940
Al <sup>IV</sup>	0.040	0.012				0.013	0.060
Al <sup>VI</sup>	0.032	0.019				0.000	0.020
ΣAl	0.072	0.031	0.000	0.389	0.000	0.013	0.080
Fe <sup>2+</sup>	0.442	0.827	0.918	2.723	0.905	0.769	0.424
Fe <sup>3+</sup>	0.000	0.000		1.900	0.003	0.00	0.006
Mg	0.703	1.043	1.024	0.115	0.084	1.042	0.760
Mn	0.012	0.020	0.013	0.016	0.009	0.017	0.009
Ti	0.020	0.010	0.002	0.840	0.996	0.012	0.026
Ca	0.767	0.066	0.002	0.000	0.000	0.125	0.738
Na	0.015	0.000	0.000	0.000	0.000	0.000	0.018
Cr	0.000	0.001	0.001	0.005	0.000	0.000	0.001
Total	3.991	3.986	2.978	6.000	2.000	3.985	4.000

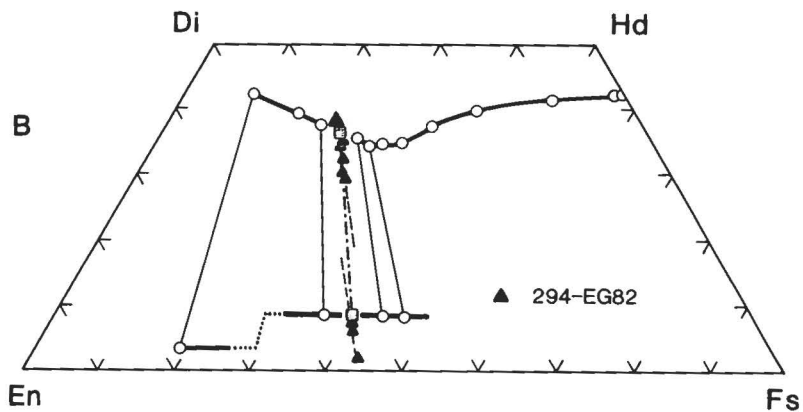
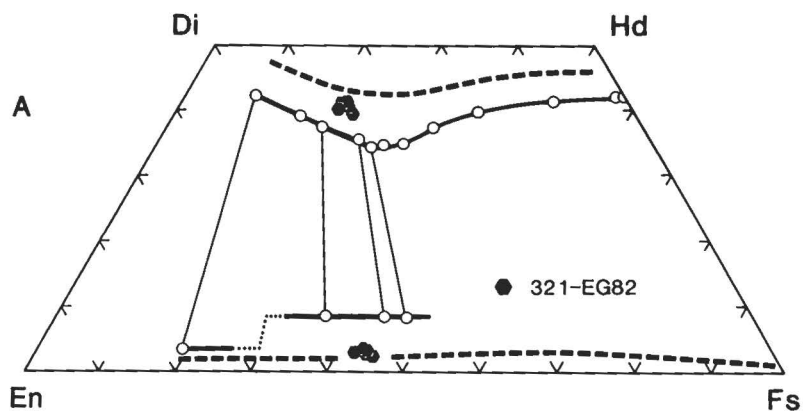
<sup>a</sup> Samples were analyzed using the Stanford University JEOL 733A automated electron microprobe with 5 wavelength dispersive spectrometers. A 15 Kv accelerating voltage was used, with a sample current of 15 nA, 20 seconds maximum counting time and beam diameters of 1-3 microns. The Bence-Albee (1968) matrix correction method was employed. Calculations for ferric iron content in this and subsequent tables are after Papike et al. (1974). Amphibole and pyroxene nomenclature is adopted from Leake (1978) and Poldevaart & Hess (1951), respectively. <sup>b</sup> Below detection limit. <sup>c</sup> All Fe as FeO. <sup>d</sup> Fe<sub>2</sub>O<sub>3</sub> calculated by charge balance.

The dominant vein pyroxenes are inverted pigeonites ( $X_{Fe^{2+}} = 0.41-0.44^+$ , Analyses 2 & 6, Table 1) that occur as subhedral twinned crystals up to 1 cm long (Fig. 8B). Broad lamellae of augite ( $X_{Fe^{2+}} = 0.35-0.39$ , Analyses 1 & 7, Table 1) are exsolved parallel to (001) of pigeonite. Very thin lamellae of orthopyroxene are formed between the augite lamellae parallel to the (100) twin plane of the original pigeonite, and are interpreted as evidence for inversion of pigeonite to orthorhombic pyroxene. (100) twinned crystals of pigeonite have inverted into two or more irregular shaped crystals of orthopyroxene similar to the cumulate pigeonites in the Middle Zone gabbros reported by Wager & Brown (1967:

fig 21C). Olivine ( $X_{Fe} = 0.47$ , Analysis 3, Table 1) is formed as a thin reaction rim separating the oxides from the pyroxenes (Fig. 8B). Trace amounts of biotite also occur in these veins.

Microprobe analyses of exsolved augites and inverted pigeonites from 294-EG82 and 321-EG82 are given in Fig. 9. Also shown in the figure are the pyroxene solidus trends defined by Brown (1957) and Brown & Vincent (1963) and the compositional trends in exsolved Layered Series pyroxenes reported by Nwe (1976). Analyses from vein 321-EG82 (Fig. 9A) represent an inverted pigeonite host and its Ca-rich exsolution lamellae (Fig. 8B). In contrast, analyses reported for vein 294-EG82 (Fig. 9B) represent an inverted pigeonite host and an augite host, both of which are only slightly exsolved in comparison to pyroxenes from vein 321-EG82. Pyroxene compositions that are between Brown & Vincent's Skaergaard pyroxene solidus trends are mixed analyses of the host pyroxene and thin exsolution lamel-

<sup>+</sup>  $X_{Fe^{2+}}$  denotes mole fraction of ferrous iron calculated such that  $X_{Fe^{2+}} = n_{Fe^{2+}} / (n_{Fe^{2+}} + n_{Mg^{2+}})$  where n represents the number of moles of the subscripted element per formula unit. Ferrous and ferric iron are calculated by charge balance using the method of Papike et al. (1974). The subscript Fe<sup>\*</sup> denotes all iron as ferrous iron.







-  CRYSTALLIZATION TREND LAYERED SERIES & MARGINAL BORDER GROUP (BROWN 1957, BROWN & VINCENT 1963)
-  COMPOSITIONAL EXTREMES IN EXSOLVED PYROXENES, LAYERED SERIES (NWE 1976)
-  PYROXENE COMPOSITIONS FROM PYROXENE-Fe Ti OXIDE VEINS IN
-  UPPER BORDER GROUP XENOLITHS, MIDDLE ZONE

Fig. 9. Compositions of pyroxenes from pyroxene-oxide veins in Upper Border Group xenoliths of the Middle Zone gabbros of the Skaergaard intrusion. See Fig. 7A for sample locations. Thick solid lines and open round symbols represent the solidus compositions of pyroxenes reported by Brown (1957) and Brown & Vincent (1963). The thick dashed curves are the subsolidus exsolved compositions of Ca-rich and Ca-poor pyroxenes reported by Nwe (1976). Hexagons in diagram A are the compositions of an inverted pigeonite host and its Ca-rich exsolution lamellae vein 321-EG82. Triangles in diagram B are compositions of augite and inverted pigeonite crystals in vein 294-EG82. Thin dashed lines in diagram B denote partial tie lines between exsolved phases and the dot dashed line and boxes represent the predicted solidus compositions of the pyroxene pairs in 294-EG82. The abbreviations Di, Hd, En and Fs denote the components  $\text{CaMgSi}_2\text{O}_6$ ,  $\text{CaFeSi}_2\text{O}_6$ ,  $\text{Mg}_2\text{Si}_2\text{O}_6$  and  $\text{Fe}_2\text{Si}_2\text{O}_6$  respectively.

lae. Changes in the proportion of host and lamellae in mixed analyses define a linear trend in the pyroxene quadrilateral composition space (dashed lines in Fig. 9B). The intersection of these lines with the solidus trend approximates the solidus compositions of coexisting pyroxenes (e. g. Coleman, 1978; Nobugai et al., 1978). The tie-line joining the inferred solidus compositions of Ca-rich and Ca-poor pyroxenes (shaded squares) has the same orientation as the tie-lines joining solidus compositions of pyroxene pairs in the adjacent Layered Series gabbros. This implies similar element distribution between the coexisting pyroxenes in the pyroxene-oxide veins and those in the adjacent Layered Series and suggests that the vein pyroxenes formed at

temperatures close to the solidus temperatures of the Middle Zone magma.

The largest mineralized fracture found in the study area of Fig. 7A consists of a coarse-grained pegmatite (sample 292-EG82) similar in appearance to the hybrid patches and pegmatitic veins in the Upper Zone a gabbros. This pegmatite is about one meter thick and ~ 20 meters long, with distinct linear contacts to the Middle Zone gabbros and the Upper Border Group xenoliths. Minerals that form this pegmatite and some pyroxene-oxide veins have locally reacted with hydrothermal solutions near crosscutting late stage fracture systems. In the pegmatite sample of 292-EG82 east-west-trending hornblende-actinolite-albite-epidote veins (see below)



crosscut the pegmatite. Pyroxenes are replaced by iron-rich actinolite ( $X_{Fe^{2+}} > 0.60$ ) and titanomagnetite is oxidized to subhedral aggregates of ilmenite-hematite solid solution. Plagioclase in the wall rock is replaced by iron-rich chlorite ( $X_{Fe^{2+}} < 0.70$ ), albite and apatite.

Oxygen isotope gradients across the Upper Border Group fallen blocks are apparent in the data presented by Taylor & Forester (1979) suggesting that the blocks have reacted with meteoric hydrothermal solutions prior to breaking apart near the roof of the pluton. It is probable that some of the mineralized fractures discussed above formed before the blocks fell from the roof of the magma chamber and represent paleo-flow channels that localized the flow of hydrothermal solutions through the top of the intrusion. These fractures were probably filled with hydrous alteration minerals and isolated fluid-filled pores. Conductive heating of the blocks in the Middle Zone magma would have generated large fluid pressures in the pores (Knapp & Knight 1977). This process probably resulted in the formation of hydrolic fractures which were filled by the pyroxene-oxide veins.

#### Transgressive granophyres and quartz veins

Fracture systems associated with the emplacement of granitic magmas in the Layered Series occur in the Middle Zone and Upper Zone gabbros near the region of Uttental Sund. These vein-, sill- and dike-like bodies are referred to as transgressive acid granophyres by Wager & Deer (1939) and Wager & Brown (1967). The lack of fine-grained chill margins with the gabbro host rocks suggests that these intrusions formed during brittle deformation of the crystallized Layered Series gabbros at high temperatures. Oxygen, strontium and lead isotopic analyses of these granophyres reported by Taylor & Forester (1979), Leeman & Dasch (1978) and Hamilton (1963) indicate that some of the granitic melt was isotopically similar to the Precambrian basement gneisses in the Kangerdlugssuaq region. This is consistent with Wager & Deer's (1939) conclusion that the smaller transgressive granophyre dikes in the Layered Series gabbros originated by fusion and later local redistribution of entrained blocks of the basement within the magma chamber. Norton, Taylor & Bird (1984) suggest that the complex fracture systems now filled with transgressive acid granophyres formed between 750° and 850°C.

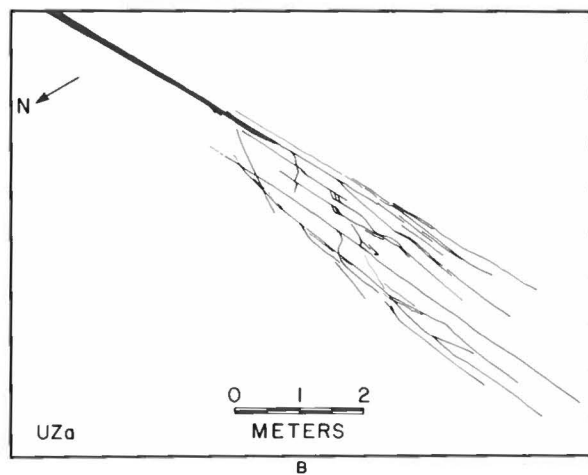
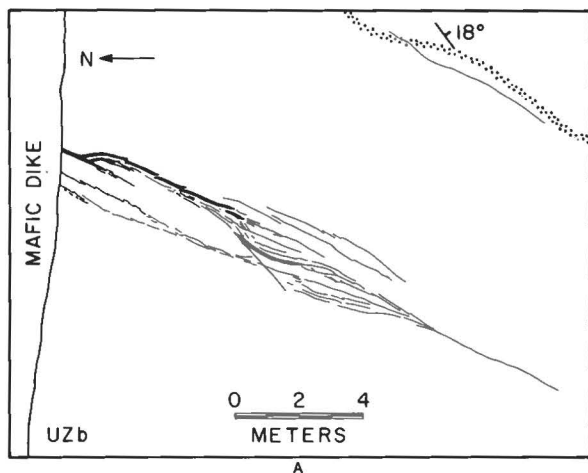
The granophyres weather buff-white to light grey in color. They have sharp contacts with the Skaergaard gabbros and transgress all igneous structures and the coarse-grained pyroxene-oxide veins and hybrid gabbroic veins, sills and patches. In the Layered Series gabbros these granophyres are leucocratic medium- to fine-grained intrusives composed of about 60% feldspar and 30% quartz. The feldspars are albite-rich plagioclase and minor amounts of microcline perthites. Well developed micrographic intergrowths of quartz and alkali

feldspars have been found in only a few samples. Feldspars are cloudy and sometimes partially replaced by fine-grained sericites. Accessory minerals consist of variable amounts of chloritized biotite, titanite, allanite, apatite, zircon and iron oxides (Wager & Deer 1939). Mirolitic cavities up to 10 cm long are common in many of the smaller granophyre veins. The smaller cavities are equant whereas the larger cavities are elongate parallel to or at slight acute angles to the vein walls. Mirolitic vugs are lined with euhedral crystals of quartz, albite and microcline perthite that may be greater than 1 cm in length. Apatite and hexagonal books of micaceous material (probably stilpnomelane) have also been found in some of the larger vugs. Near sample 470-EG82 (Fig. 7B) large mirolitic cavities occur in the granophyres along with numerous amphibole-mineralized veins in the Middle Zone gabbro host rocks. In this area the matrix feldspars of the granophyres are albites. These albites have cores with numerous chlorite and fluid filled elongate inclusions, and inclusion-free rims that may have euhedral crystal faces to the mirolitic cavities.

Transgressive granophyres and spatially related quartz veins were mapped by reconnaissance traverses and small scale survey maps within the study areas of Fig. 3. As shown in Fig. 7 they are continuous for hundreds of meters. The intrusions range from >10 meter wide shallow-dipping bodies to thin <1 cm wide quartz-rich veins. The largest transgressive granophyres are found near the shores of Uttental Sund (see Fig. 7). Some of these intrusions are several meters wide and dip away from the shoreline on the eastern, western and southern portions of Uttental Sund. Their distribution appears to be concentrated about the gravity high in Uttental Sund (Blank & Gettings 1973) that has been interpreted by a number of workers as the location of the deep feeder system during the inflation of the Skaergaard magma chamber.

Near the southern shore of Uttental Sund in Fig. 7C the larger intrusions dip 18° to 30° to the south. The Layered Series gabbros in this area dip about 19° to the south, indicating that some of the granophyres were intruded as low-angle sill-like bodies. Extending from this intrusive complex are a number of thin (<1 meter wide) near vertical vein systems trending approximately north-south (see region between symbols A and B in Fig. 7C). A minor set of east-west trending veins of similar continuity can also be seen in Fig. 7C. Together these veins form an array of mineralized fractures that extend for at least 1.3 kilometers to the south of Uttental Sund, and outcrop over a vertical extent from sea level in the Upper Zone gabbros to an elevation of about 300 meters in the uppermost portions of Upper Zone b.

Stratigraphically above these granophyre intrusions is an extensive north-northeast fracture system composed of quartz veins and thin granophyres (Fig. 7C). Many of the veins are less than 2-3 cm wide, are continuous for



- MINERALOGIC LAYERING AND DIP OF UPPER ZONE GABBROS
- TRANSGRESSIVE GRANOPHYRES
- AMPHIBOLE - CLINOPYROXENE - BIOTITE MINERALIZED VEINS

Fig. 11. Maps of black weathering amphibole-clinopyroxene-biotite veins near the terminations of transgressive acid granophyres in the Upper Zone gabbros. See Fig. 5C for map locations.

magnetite fill similar cavities in the quartz vein of sample 526-EG82. The cavity-filling fayalitic olivine is monocrystalline with randomly oriented rod-shaped microcrystalline inclusions. Very fine-grained disseminated dark brown iron oxides and silicates have been formed between the fayalitic olivine and the euhedral quartz crystals. Trace amounts of hedenbergite  $X_{Fe^{2+}} = 0.97$ , Analysis 5, Table 2) occur within the quartz matrix of the olivine-bearing veins.

Complex fracture systems are associated with the ter-

minations of the transgressive granophyres (for example see Norton, Taylor & Bird, 1984: fig. 12). At a number of localities in the Middle Zone and Upper Zone a gabbros (Fig. 7) we have noted the formation of drusy, black weathering amphibole mineralized fracture systems both parallel to the granophyres and extending in complex arrays from the terminations of the granophyres. Examples of the exposures of amphibole mineralized veins near the terminations of granophyre filled fractures are shown in the maps of Fig. 11. Some of the fractures marginal to the granophyres may have formed as a result of elastic deformation during emplacement. In other cases, the granophyres are probably filling fractures that formed as they were emplaced, because vein systems such as those in Fig. 11 are not present. Elastic models such as those developed by Rogers & Bird (1987) for chlorite veins marginal to the mafic dikes in the Layered Series gabbros are not compatible with the size or complexity of fracture geometries shown in Fig. 11.

The maps in Fig. 11 illustrate two geometric types of mineralized fracture arrays associated with the granophyre crack tips. In Fig. 11B the amphibole mineralized veins form arrays subparallel to the granophyre that diverge with increasing distance from the granophyre. Small rhombohedral fracture networks are formed between en echelon vein sets that are associated with cavities lined with euhedral brown hornblende and later overgrowths of grunerite. Fig. 11A illustrates the more typical fracture geometry, where the fracture array near the granophyre converges to a single fracture at about 6 meters from the granophyre crack tip. The single fracture may extend for tens of meters beyond the granophyre. Although the field evidence is not conclusive, it is probable that this single fracture was formed prior to the intrusion of the granophyre and represents the high temperature amphibole-clinopyroxene-biotite veins that are locally crosscut and offset by the granophyres (see below). Similar field observations within the area of Fig. 7 indicate that some of the transgressive granophyres are locally emplaced along pre-existing hydrothermal vein systems.

In the Lower and Middle Zone gabbros of Kraemer Ø there are northwest-trending quartz-rich granophyres and veins that are continuous for tens of meters and less than 0.75 meters wide (thin dashed lines in Fig. 7A). These intrusions are geometrically distinct from the transgressive granophyres described above and are crosscut by all the types of amphibole-mineralized veins in the area. This is in contrast to the granophyres near Uttental Sund that locally transect and offset high temperature amphibole-clinopyroxene-biotite veins described below. Based on these geometric relations, it appears that the northwest-trending quartz and granophyre vein set on Kraemer Ø is older than the granophyres near Uttental Sund described above. Fig. 12 is a map of a portion of a 50 meter long exposure of one of these granophyres and subparallel quartz veins in the

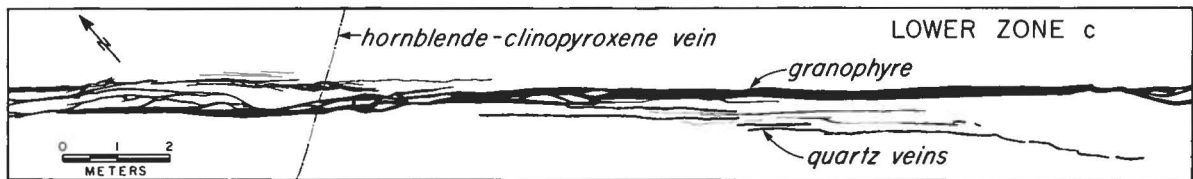


Fig. 12. Map of transgressive granophyres and parallel quartz veins in Lower Zone c gabbros on Kraemer Ø (see Fig. 5A for map location). The leucocratic granophyre is crosscut and offset by the black weathering calcic amphibole-clinopyroxene-biotite vein in the map area.

Lower Zone c gabbros of Kraemer Ø (see Fig. 5A for location). The granophyre-gabbro contacts are undulatory and locally enclose blocks of the gabbro host rocks. Thin quartz veins fill fractures that parallel the granophyres. Although it is not apparent from this map, the N70E hornblende-clinopyroxene vein crosscuts and offsets the granophyre (<10 mm right lateral offset). It can be seen in Fig. 7A that the northwest trend of these granophyres and quartz veins is parallel to the orientation of the pyroxene-oxide veins; however, we have not observed any direct relationships between these two vein types in the field.

#### Amphibole veins

In addition to fractures filled by material crystallized from silicate-rich magmas, at least five geometrically and mineralogically distinct hydrothermal vein sets occur within the Skaergaard Layered Series. These veins represent the outcrop expression of fracture sets that acted as conduits for the circulation of hydrothermal solutions during the subsolidus cooling history of the Skaergaard intrusion. The veins are characterized by mineral assemblages typical of hydrothermal alteration and metamorphism of rocks of basaltic composition. Secondary minerals associated with these fractures include calcic and Fe-Mg amphiboles, biotite, ortho- and clinopyroxene, talc, epidote, prehnite, K-feldspar, albite, quartz, calcite, Fe-Ti oxides, Ca-rich zeolites, sericite and titanite. Within the Layered Series gabbros, calcic amphiboles, primarily hornblende, are the dominant fracture-filling mineral.

Measured orientations of the black to dark-brown weathered amphibole mineralized veins found on reconnaissance traverses in the study areas of Fig. 3 are given in the maps of Fig. 13. These maps provide a general representation of the large scale geometry of hydrothermal vein systems in the Layered Series gabbros. Data presented in the rose diagrams denote the orientation and abundance of near vertical amphibole mineralized fractures measured on 20 to 50 meter long traverses. These veins are typically less than 1–2 mm wide and are continuous for tens of meters as shown in the photographs of Fig. 14. The surveyed traverses were oriented approximately perpendicular to the strike of the most abundant fracture set. It can be seen in Fig. 13 that the frequency of the veins is between 0.20 and 1.65

fractures per meter. Near the margins of the intrusion hydrothermal veins in the Layered Series appear to form approximately perpendicular to the walls of the magma chamber suggesting that the stress field that controlled fracture propagation was influenced in turn by the geometry of intrusion (Figs 13A & B). Near the central part of the Layered Series on the western slopes of Pukugaqryggen and Basistoppen (Figs 13C & D) more complex fracture patterns are apparent. Fractures in the former location appear to be subparallel to the transgressive granophyres (compare Fig. 7B with rose diagrams T5, T6 and T7 in Fig. 13C). The east-west veins near traverse T8 in Fig. 13C represent a set of rust-brown colored veins that appear to be associated with large east-west trending mafic dikes in the area (see Fig. 6C and below). Although many of the amphibole mineralized veins parallel the general trend of the transgressive granophyres in the area of the Trough Bands west of Basistoppen (compare Figs 7C & 13D), other vein orientations are apparent that are not readily explained in terms of the local structure and stratigraphy of the Skaergaard intrusion.

In some of the selected map areas, crosscutting relations between different fracture types can be determined. An example of one such area is shown in Fig. 15, which is a map of the lithology and mineralized fractures near a 10 meter wide mafic dike shown at the top of the map area. Marginal to the dike and subparallel to its strike are numerous brown weathering chlorite-mineralized fractures (dot-dash lines). Although it is not apparent in Fig. 15, the chlorite veins crosscut black weathering fractures filled primarily with calcic amphiboles, (solid lines of Fig. 15B). The latter fractures are more abundant in the southern portions of the map area away from the rust colored, weathered outcrops that contain chlorite veins. Within distances of about 20 meters of the large mafic dike east-west chlorite veins are abundant. It is apparent from this and other similar observations (e.g. fracture abundance traverse T8 in Fig. 13C) that the chlorite mineralized fractures are related to brittle deformation and hydrothermal alteration associated with the intrusion of mafic dikes that postdate the cooling of the Skaergaard pluton. Mineralogical and structural properties of these veins are presented by Rogers & Bird (1987), and are not considered further in this discussion. It is important to note that at least two generations of hornblende mineralized fractures occur

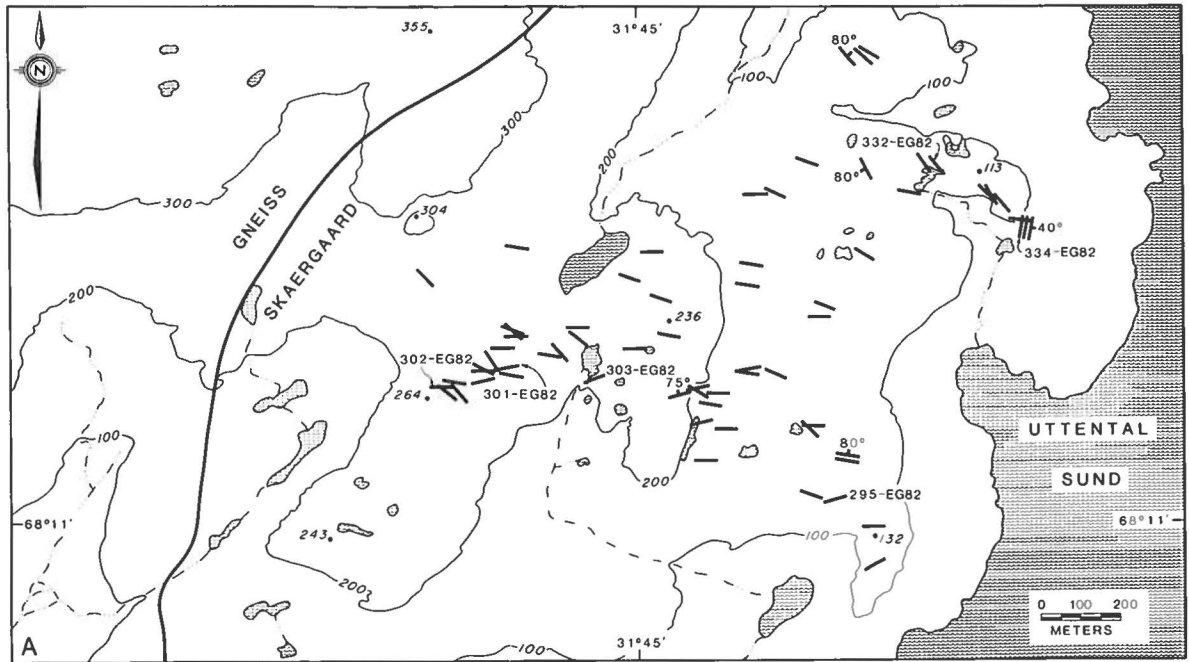
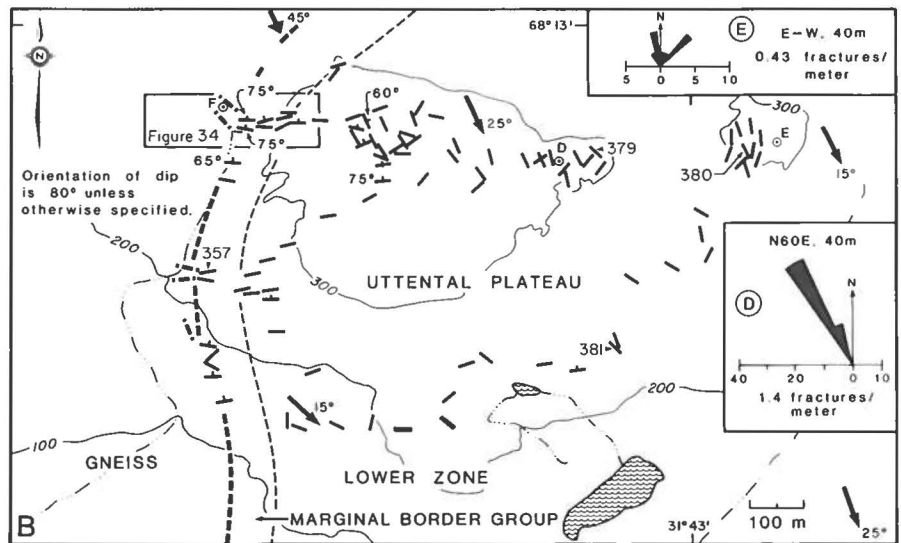


Fig. 13 A-B. Orientation and abundance of amphibole veins (solid lines) within the Layered Series gabbros of the Kraemer Ø (A) and Uttental Plateau (B). The rose diagrams denote the strike and abundance of black and brown weathering amphibole veins along measured traverses. Unless specified, all veins dip within 10° of vertical. Distance and orientation of the traverses are given with the rose diagrams. Dashed lines in B are epidote and alkali feldspar veins in the Precambrian basement near the intrusion, and the double lines in B denote prehnite veins in the Lower Zone gabbros. Fracture abundances reported for the rose diagrams in B represent the total number of veins encountered divided by the total distance of the traverse. The numbers 357, 379, 380 and 381 in map B denote sample locations discussed in the text. See Fig. 3 for location of maps. Elevations are given in meters.



in the southern portion of the map area Fig. 15B. Based on crosscutting relations, the northwest fracture set which contains the assemblage of hornblende-clinopyroxene-biotite is the oldest. Similar observations have been made at several other locations in the Middle Zone gabbros.

The compositions of fracture-filling calcic amphiboles vary systematically with respect to stratigraphic height within the Layered Series gabbros and to local mineralogic phase relations within and near the veins. Repre-

sentative chemical analyses of calcic amphiboles from five fractures within the Layered Series gabbros and the Marginal Border Group are given in Fig. 16. The mole fraction of octahedral  $Fe^{2+}$  in calcic amphiboles increases from ~ 0.10 in the Marginal Border Group to >0.98 in Upper Zone c of the Layered Series. These compositional changes are a consequence of variations in bulk rock chemistry as represented by the Skaergaard fractionation trend. Biotites show similar iron enrichment with increasing stratigraphic height as noted by



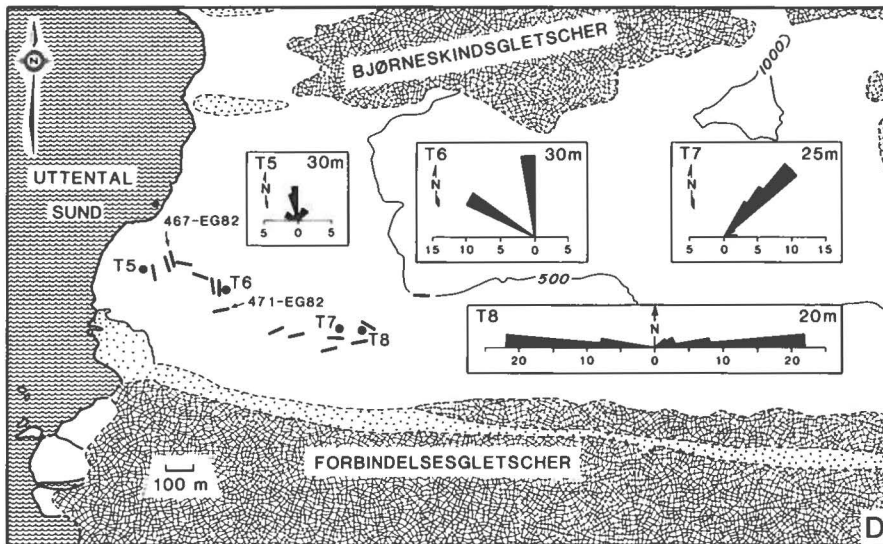
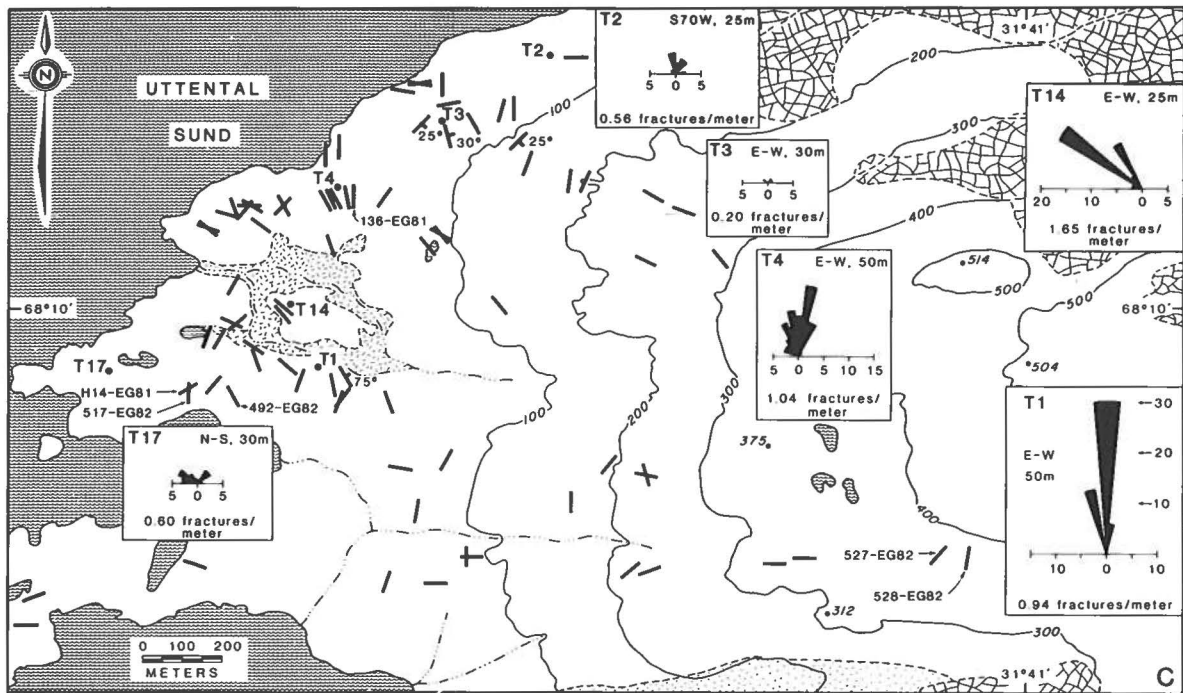


Fig. 13C-D. Orientation and abundance of amphibole veins (solid lines) within the Layered Series gabbros of the Basistoppen (C) and Pukugaarqyryggen (D) study areas given in Fig. 3. See Fig. 13 A-B for explanation. Fracture abundances reported for the rose diagrams in C represent the total number of veins encountered divided by the total distance of the traverse. Fracture abundances for traverses T5, T6, T7 and T8 in D are 0.5, 0.8, 1.0 and 1.3, respectively. See Fig. 3 for location of maps.

Nash (1976), as do hydrothermal clinopyroxenes (see below). The concentration of tetrahedral Al in vein filling calcic amphiboles ranges from  $\sim 0$  to  $>2$  (moles/23 oxygens) within a single fracture sample from the Middle Zone gabbros (Fig. 16). It is apparent from the tetrahedral concentrations of  $Al^{3+}$  given in the figure that both subsolvus and supersolvus amphiboles of the actinolite-hornblende solid solution are formed in these fracture systems (see Robinson et al. 1982, and references therein).

The compositional characteristics of amphiboles given in Fig. 16 are closely related to the types of vein mineral assemblages within the various mineralized fracture systems. At least five distinct types of mineralogic phase relations have been observed in amphibole veins of the Layered Series gabbros. The earliest high-temperature hydrothermal veins are characterized by metasomatic replacement of cumulate olivines and augites by talc, clinopyroxene, and rarely orthopyroxene. Igneous plagioclases are only slightly altered near these

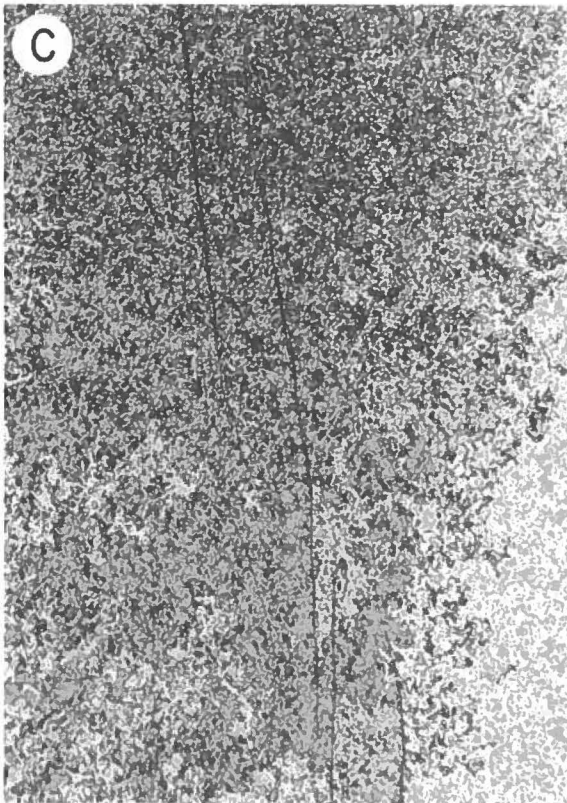


Fig. 14. Calcic amphibole-clinopyroxene-biotite veins in the Layered Series gabbros. A) exposure of a dip slope of the layering in the Upper Zone a gabbros showing black weathering veins that appear in outcrop as thin ridges transecting the gabbros (knife is 21 cm long). B) veins in Middle Zone gabbros of Kraemer Ø (hammer is 40 cm long). C) an echelon fracture array of veins in the Upper Zone gabbros (field of view is 15 cm wide).

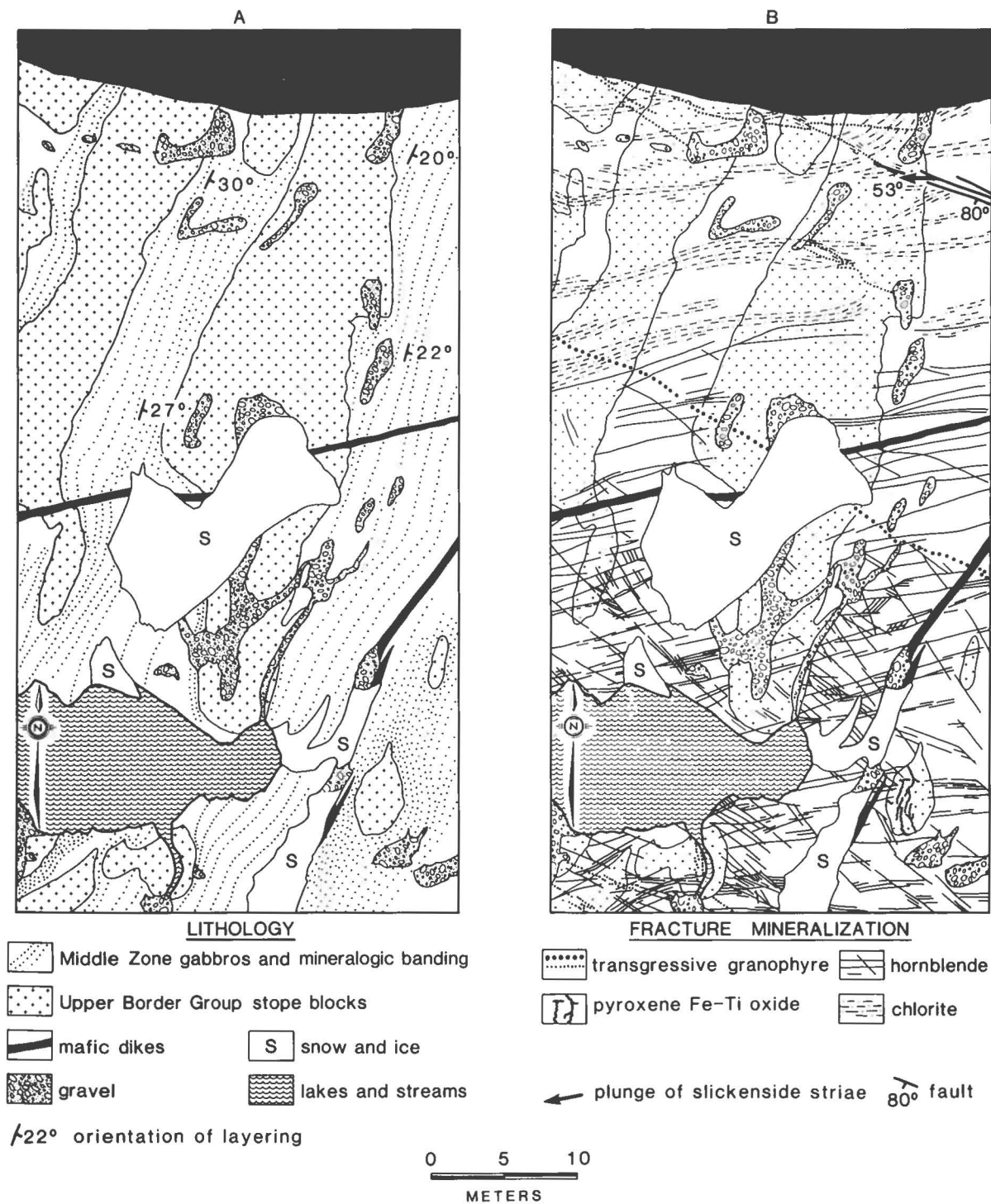


Fig. 15. Geology and vein distribution near a 10 meter wide mafic dike (top of the map) in the Middle Zone gabbros of Kraemer Ø. Solid lines in B denote calcic amphibole-clinopyroxene-bioite veins. See Fig. 5A for map location.

Table 3. Selected electron microprobe analyses of actinolitic hornblende-chlorite-talc-biotite vein minerals.

	1 379D-4 Talc	2 379D-12 Talc	3 379D-21 Cumming- tonite	4 379A-1 Ferrosalite	5 379A-4 Actinolitic hornblende	6 380A-24 Chlorite	7 380A-22 Biotite
SiO <sub>2</sub>	63.89	60.22	53.57	50.51	51.27	27.05	37.47
Al <sub>2</sub> O <sub>3</sub>	0.37	1.58	1.61	0.04	5.15	18.88	15.09
FeO	2.44 <sup>a</sup>	8.26 <sup>a</sup>	17.17	20.66	12.98	26.22 <sup>a</sup>	18.50 <sup>a</sup>
Fe <sub>2</sub> O <sub>3</sub>			0.34 <sup>b</sup>	0.08 <sup>c</sup>	1.32 <sup>b</sup>		
MgO	28.19	24.77	18.28	4.79	14.07	15.57	13.77
MnO	0.04	0.08	1.09	0.67	0.11	0.24	0.10
TiO <sub>2</sub>	0.07	0.09	0.12	0.02	0.40	0.04	1.53
CaO	0.04	0.09	3.11	23.45	12.69	0.02	0.06
Na <sub>2</sub> O	0.11	0.27	0.32	0.07	0.70	b.d.	0.13
K <sub>2</sub> O	0.04	0.06	b.d.	n.a.	0.03	b.d.	9.05
Total	95.18	95.42	95.61 <sup>d</sup>	100.29	98.72	88.01	95.70
Basis (Oxygens):	11	11	23	6	23	14	11
Si	4.067	3.950	7.862	2.002	7.372	2.850	2.824
Al <sup>IV</sup>	0.000	0.050	0.138	0.000	0.628	1.150	1.176
Al <sup>VI</sup>	0.028	0.072	0.141	0.002	0.245	1.194	0.164
ΣAl	0.028	0.122	0.279	0.002	0.873	2.344	1.340
Fe <sup>2+</sup>	0.130	0.453	2.108	0.685	1.561	2.309	1.166
Fe <sup>3+</sup>			0.038	0.002	0.143		
Mg	2.675	2.422	3.998	0.283	3.015	2.445	1.547
Mn	0.002	0.004	0.135	0.022	0.013	0.021	0.006
Ti	0.003	0.004	0.013	0.001	0.043	0.003	0.087
Ca	0.003	0.006	0.489	0.996	1.955	0.003	0.005
Na	0.014	0.034	0.091	0.005	0.195	0.000	0.019
K	0.003	0.005	0.000	—	0.006	0.000	0.870
Total	6.925	7.000	15.014	3.998	15.176	9.975	7.864

<sup>a</sup> All Fe as FeO. <sup>b</sup> Fe<sub>2</sub>O<sub>3</sub> is midpoint between minimum and maximum. <sup>c</sup> Fe<sub>2</sub>O<sub>3</sub> calculated by charge balance. <sup>d</sup> Low total probably due to poor polish. All abbreviations and analytical techniques as in Tables 1 and 2.

b. The distribution and orientation of these pyroxene-bearing veins is given in fig. 1 of Manning & Bird (1986). In some cases these veins form an echelon fracture sets with complex rhombohedral shaped fracture networks joining overlapping fractures (see the lower portion of Fig. 15B). It is common, however, to find one dominant fracture orientation at a given locality.

On a thin section scale there is significant variation in vein width as expressed by secondary minerals (alteration aperture) within these veins. Apertures across igneous plagioclase grains are commonly no greater than 1 mm, whereas apertures across magmatic pyroxenes or olivines can be up to 10 mm. Cumulate plagioclase shows very little mineralogic alteration in many of the fractures (Fig. 19A). Mineralogical and structural alteration of igneous pyroxenes near the vein margins is characterized by recrystallization, exsolution coarsening, and partial replacement by calcic amphiboles (Figs 19B & 20).

Minerals that characterize this vein type include calcic amphiboles ranging in composition from actinolite to hornblende, clinopyroxene, biotite. Accessory minerals include minor amounts of Fe-Mg amphiboles, Fe-Ti ox-

ides, orthopyroxene, talc and chlorite. Late stage void-filling Ca zeolites, albite and prehnite may occur in some of the veins.

Compositions of fracture-filling calcic amphiboles in these veins are highly variable both within individual fractures and throughout the intrusion. It can be seen in Fig. 21 that the concentration of tetrahedral Al ranges continuously from <0.3 to >2.0 (moles/23 oxygens) within a single fracture sample 471-EG82 (see Fig. 13C for location and Table 4, Analyses 1-4 for representative compositions). In this vein sample variations in the compositional characteristics of calcic amphiboles show systematic relations with respect to the cumulate mineralogy of the wall rock gabbros. The example from the Middle Zone gabbros given in Fig. 21 illustrates how the calcic vein amphibole compositions vary with respect to the wall rock mineralogy. Note that hornblendes adjacent to igneous plagioclase have higher concentrations of Fe<sup>2+</sup>, Al, and Ti than do amphiboles near other types of wall rock minerals. Amphiboles coexisting with hydrothermal clinopyroxenes have a very restricted solubility of tetrahedral Al between about 0.5 to 1.3 (per 23 oxygens). The latter observation was found to be the



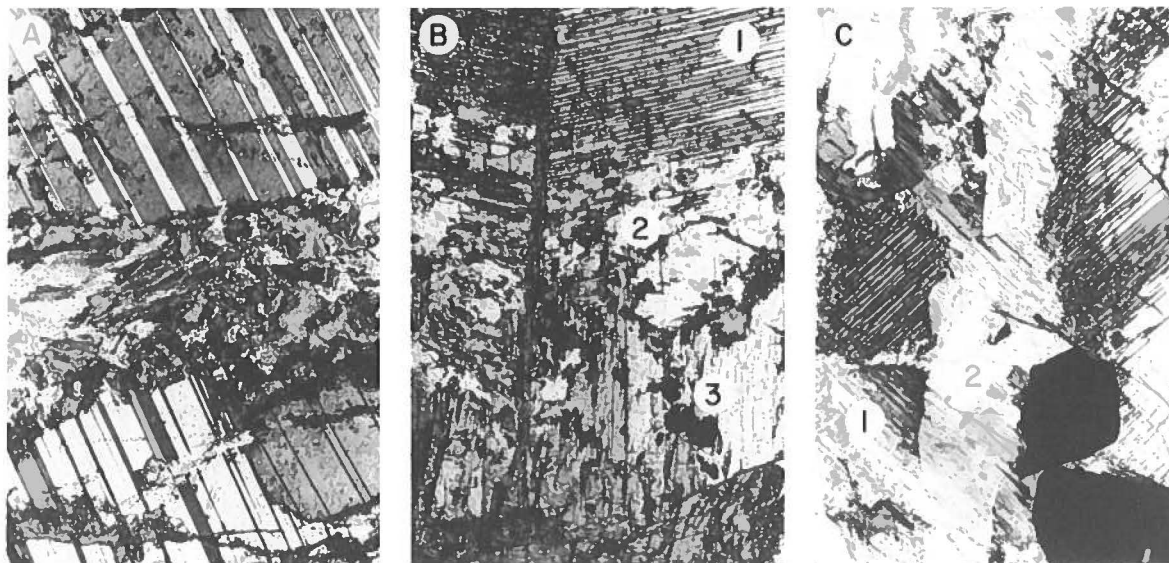


Fig. 19. Photomicrographs of calcic amphibole-clinopyroxene-biotite veins. A) hornblende vein crosscutting plagioclase in the Lower Zone c gabbros of Kraemer Ø (field of view is 1 mm wide). B) vein 298-EG82 in the Lower Zone c gabbros of Kraemer Ø showing coarsening of exsolution lamellae in magmatic augite (1), hydrothermal clinopyroxene and ilmenite at vein margin (2), and edenitic hornblende within the vein (3) (field of view is 0.8 mm wide). C) vein 332-EG82 of the Lower Zone c gabbros showing coarsening and alteration of exsolution lamellae in magmatic augites marginal to the amphibole-filled vein (field of view is 1.5 mm wide). Note that the vein contains two generations of amphiboles: the early brown calcic amphiboles (1) are crosscut by a second generation of pale-green calcic amphiboles (2).

case for calcic amphibole-clinopyroxene-biotite veins stratigraphically between Lower Zone c and Upper Zone b. In many veins actinolites are formed primarily by reaction of hydrothermal fluids with orthopyroxenes and olivines.

Reactions between hydrothermal solutions and cumulate augites at the fracture walls results in the forma-

tion of hydrothermal clinopyroxenes. The hydrothermal clinopyroxenes can be distinguished from their igneous counterparts because they are colorless and show no optically visible exsolution fabrics, whereas igneous augites are pink to brownish and display prominent (001) exsolution lamellae (Fig. 19B). Secondary clinopyroxenes are depleted in Al, Ti, and Na, but enriched in Ca

Fig 20. Compositions of pyroxenes from amphibole-pyroxene-biotite veins in the Layered Series and Marginal Border Group. Solid lines denote the pyroxene crystallization trend (Brown 1957; Brown & Vincent 1963) and the dashed lines represent the subsolidus compositional limits of exsolved igneous pyroxenes (Nwe 1976). See Fig. 9 for abbreviations.

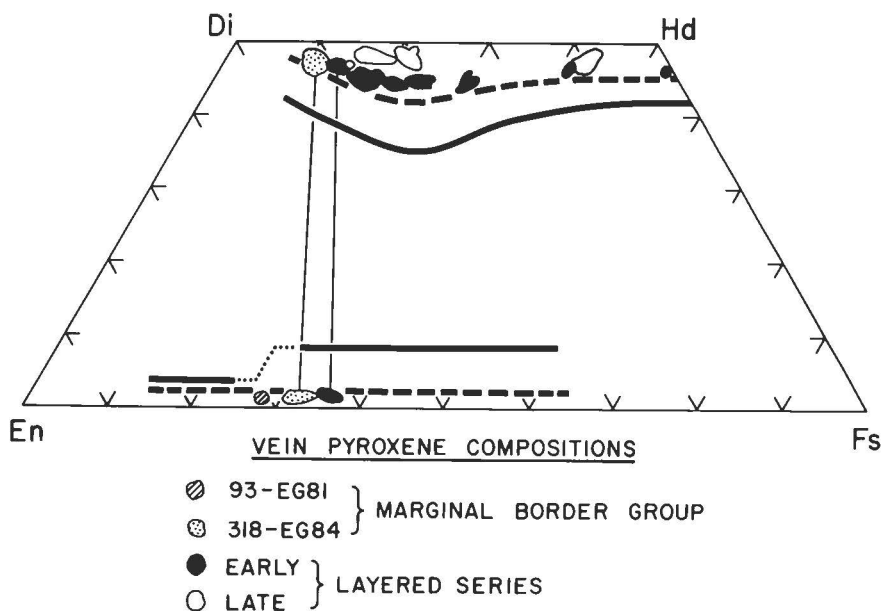


Table 4. Selected electron microprobe analyses of calcic amphibole-clinopyroxene-biotite vein minerals from the Middle Zone.

	1 471A-6 Ferroan paragasite	2 471C-22 Actinolite	3 471C-19 Magnesio- hornblende	4 471C-16 Actinolite hornblende	5 471C-9 Augite	6 471B-5 Biotite
SiO <sub>2</sub>	38.23	52.55	48.49	50.61	52.57	35.89
Al <sub>2</sub> O <sub>3</sub>	14.52	2.45	5.58	3.53	0.32	15.65
FeO	19.97	15.81	14.54	14.99	11.20	19.95 <sup>a</sup>
Fe <sub>2</sub> O <sub>3</sub>	0.83 <sup>b</sup>	1.20 <sup>b</sup>	4.08 <sup>b</sup>	2.91 <sup>b</sup>	0.00 <sup>c</sup>	
MgO	6.17	13.33	12.02	12.69	13.01	11.91
MnO	0.11	0.21	0.23	0.21	0.32	0.05
TiO <sub>2</sub>	3.40	0.35	0.91	0.59	0.09	3.29
CaO	11.88	10.91	11.00	11.37	21.64	0.12
Na <sub>2</sub> O	2.12	0.52	1.12	0.68	0.10	0.42
K <sub>2</sub> O	0.56	0.07	0.29	0.16	n.a.	8.53
Total	97.79	97.40	98.26	97.74	99.25	95.80
Basis (Oxygens):	23	23	23	23	6	11
Si	5.889	7.707	7.142	7.452	1.994	2.725
Al <sup>IV</sup>	2.111	0.293	0.858	0.548	0.006	1.275
Al <sup>VI</sup>	0.526	0.131	0.111	0.065	0.008	0.126
ΣAl	2.637	0.424	0.969	0.613	0.014	1.401
Fe <sup>2+</sup>	2.572	1.939	1.791	1.846	0.355	1.267
Fe <sup>3+</sup>	0.096	0.133	0.453	0.323	0.000	
Mg	1.416	2.914	2.639	2.785	0.736	1.348
Mn	0.014	0.026	0.029	0.026	0.010	0.003
Ti	0.394	0.039	0.101	0.065	0.003	0.188
Ca	1.961	1.715	1.736	1.794	0.880	0.010
Na	0.633	0.148	0.320	0.194	0.007	0.062
K	0.110	0.013	0.055	0.030	-	0.826
Total	15.722	15.057	15.235	15.128	4.000	7.830

<sup>a</sup> All Fe as FeO. <sup>b</sup> Fe<sub>2</sub>O<sub>3</sub> is midpoint between minimum and maximum. <sup>c</sup> Fe<sub>2</sub>O<sub>3</sub> by charge balance. All abbreviations and analytical techniques as in Tables 1 and 2.

and Si relative to cumulate augites (Manning & Bird 1986; see Analysis 5, Table 4 for representative analysis). Exsolution lamellae in igneous augites near the hydrothermal veins are commonly coarsened and may be altered to amphiboles.

Pyroxenes from samples ranging over the stratigraphic section between Lower Zone c and Upper Zone c of the Skaergaard Layered Series were analyzed. Fig. 20 illustrates the quadrilateral compositions of these hydrothermal pyroxenes of the Skaergaard intrusion. The pyroxene crystallization trends of Brown (1957) and Brown & Vincent (1963) and the limits of compositional change due to exsolution in igneous pyroxenes as described by Nwe (1976) are also given in the figure. Note that all the hydrothermal clinopyroxenes are more calcic than the exsolved igneous augites reported by Nwe (1976).

In Fig. 20 we make the distinction between vein pyroxenes in "early" and "late" veins in the Layered Series gabbros. The "early" veins refer to calcic amphibole-clinopyroxene-biotite veins discussed here. These veins are characterized by calcic amphiboles with Al<sup>IV</sup> concentrations ranging between ~0.3 and 2.0 moles per

23 oxygens. "Late" veins denote hydrothermal pyroxene-bearing veins that contain calcic amphiboles with a distinct gap in Al<sup>IV</sup> concentration between the compositions of actinolite and hornblende (see hornblende-actinolite-biotite vein discussion below). It should be noted that pyroxenes in the early veins have a lower concentration of the CaSiO<sub>3</sub> component than the late vein pyroxenes.

Black weathering iron-rich analogs of the calcic amphibole-clinopyroxene-biotite veins described above are found in the Upper Zone c gabbros. However, these veins do not contain biotite or chlorite and are not as abundant as the black weathering amphibole veins below Upper Zone b. Green amphiboles and abundant oxides fill the veins. The amphiboles range in composition from ferro-actinolites to Fe hornblendes (see Fig. 16, sample 528-EG82). Recrystallized pyroxenes marginal to the vein are hedenbergites. Minor amounts of grunerite, albite and quartz also occur in some of the veins.

A remarkable set of mineralized fractures are found in close association with the transgressive acid granophyres in the Upper Zone and Middle Zone gabbros

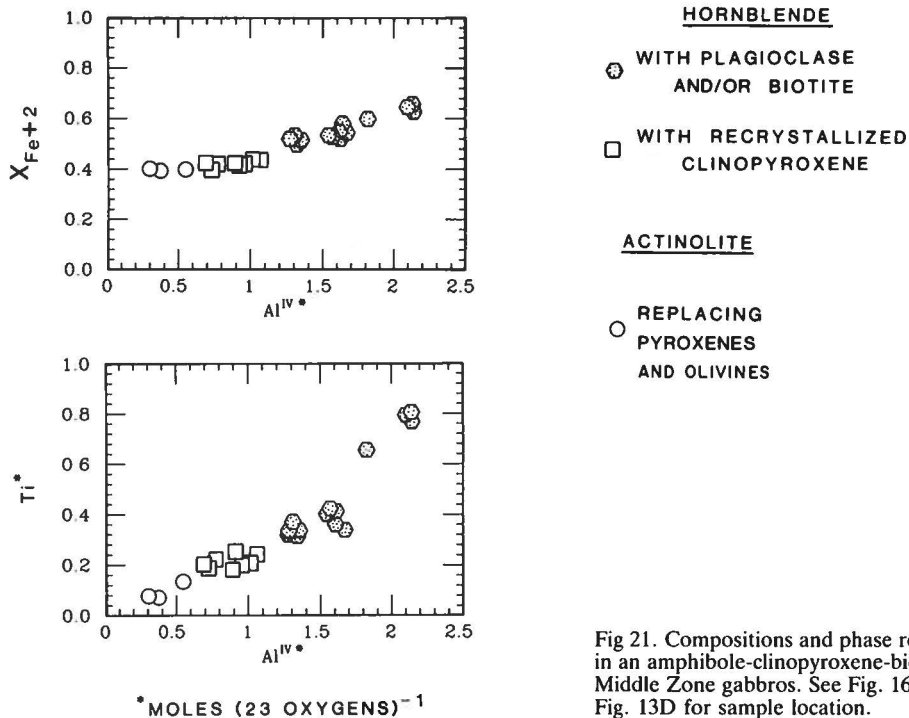


Fig 21. Compositions and phase relations of calcic amphiboles in an amphibole-clinopyroxene-biotite vein (471-EG82) of the Middle Zone gabbros. See Fig. 16 caption for explanation and Fig. 13D for sample location.

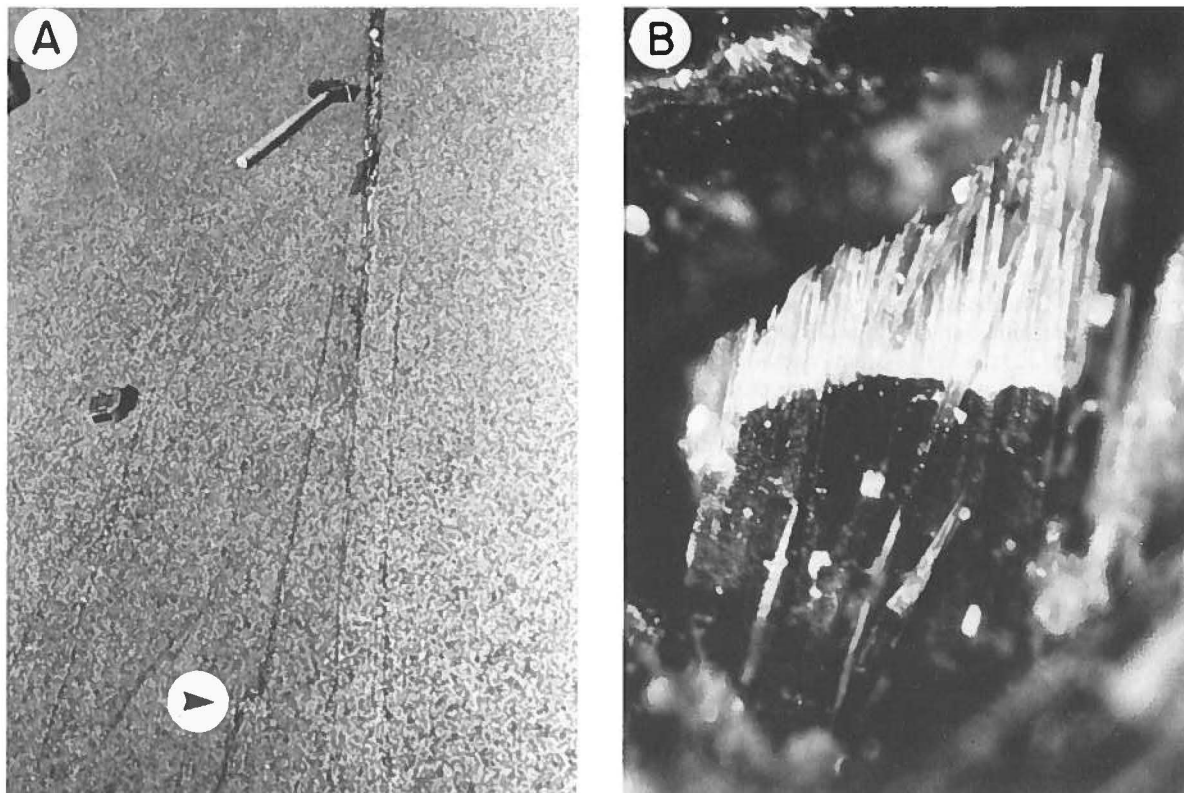


Fig. 22. Calcic amphibole-clinopyroxene-biotite veins near transgressive granophyres. A) exposures at locality of Fig. 11B. Arrow shows location of amphibole-lined open space (1×5 cm). B) macrophoto of hornblende crystal with fibrous grunerite overgrowths in pores within the fracture network (field of view is 1 mm wide).

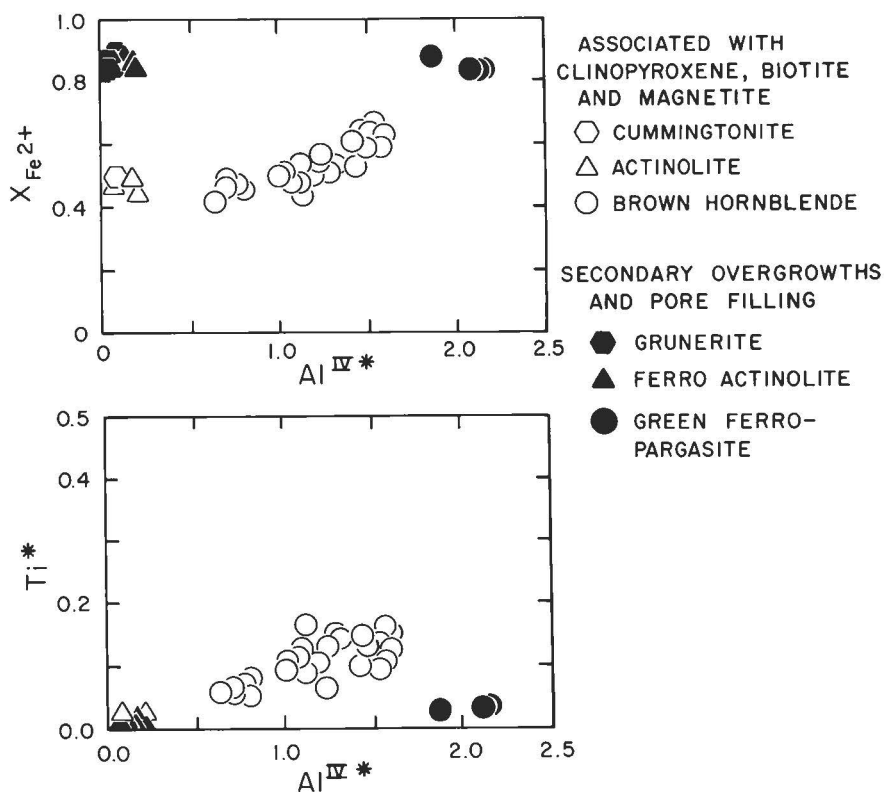


Fig. 23. Composition of calcic and Fe-Mg amphiboles from an amphibole-clinopyroxene-biotite vein system (136-EG82) extending from the termination of a transgressive granophyre in the Upper Zone a gabbros. See Fig. 16 caption for explanation and Fig. 13C for sample location.

(see Figs 7 & 11). Unlike the calcic amphibole-clinopyroxene-biotite veins described above that are locally crosscut by the transgressive granophyres, the fractures and the vein mineral paragenesis of these veins appear to be closely related to the emplacement of the granophyres. These black weathering veins are distinct in at least four ways: (1) the fractures parallel the granophyres and form complex fracture arrays that occur only near the terminations of granophyre filled fractures (Figs 11 & 22), (2) the vein systems contain large open space cavities up to 10 cm long that are partially filled with hydrothermal minerals including <4 mm long euhedral crystals of brown-green hornblende with overgrowths of actinolite and fibrous grunerite (Fig. 22B), (3) microfractures and replacement of the Layered Series gabbros are more extensive near these veins (up to 3 cm from individual veins and large mineralized cavities), and (4) the paragenetic relations within the veins indicate several stages of brittle failure and mineralization of compositionally distinct amphiboles (Figs 19C, 22 & 23).

At least two distinct stages of mineralization are apparent from the textures and compositions of amphiboles shown in Figs 22B & Fig. 23. These minerals formed in a 10 cm long cavity one meter from the termination of a transgressive granophyre in the Upper Zone a gabbros (136-EG81, see Fig. 13D for location). The main stage of alteration was associated with metasoma-

tism of the wall rock within ~2 cm of the cavity. The earliest amphiboles formed were brown-green magnesian- and ferro-hornblendes, actinolite and cummingtonite ( $X_{Fe^{2+}} = 0.42-0.68$ , Fig. 23A & Analyses 1 & 4-7, Table 5). These amphiboles occur both in the wall rock and lining large cavities. A secondary stage of mineralization formed on cavity-lining hornblendes and in microcracks in the gabbro, and consists of euhedral dark green ferro-pargasitic hornblende ( $X_{Fe^{2+}} > 0.80$ ). The earlier brown hornblende crystals in the cavity are also overgrown by ferro-actinolite and fibrous grunerite ( $X_{Fe^{2+}} = 0.84-0.87$ , Analyses 2 & 3, Table 5).

Wall rock alteration at the margin of this cavity consists of metasomatic replacement of cumulate olivine by fine-grained aggregates of talc ( $X_{Fe} = 0.17$ , Analysis 9, Table 5) and magnetite, and replacement of igneous augite by well-crystallized hydrothermal clinopyroxene ( $X_{Fe^{2+}} = 0.39$ , Analysis 8, Table 5), hornblende and fine-grained ilmenite. Biotite is abundant within the metasomatic alteration haloes of the veins and is usually in close association with opaques.

Based on the compositions of hydrothermal clinopyroxenes and amphiboles, the vein assemblages near the terminations of small transgressive granophyres are indicative of conditions spanning both the early and late vein types described above. The mineral assemblages in sample 136-EG81 include subsolvus amphiboles and clinopyroxenes that are more calcic than those found in



Table 5. Selected electron microprobe analyses of calcic amphibole-clinopyroxene-biotite vein minerals near granophyre crack tips.

	1 136E-3 Magnesian hastingsitic hornblende	2 136E-8 Ferro-actinolite	3 136E-12 Grunerite	4 136D-15 Ferroedenite	5 136D-14 Cummingtonite	6 136A-22 Magnesiohornblende	7 136A-28 Actinolite	8 136H-2 Salite	9 136G-1 Talc
SiO <sub>2</sub>	42.13	49.82	48.48	45.59	52.68	48.41	52.49	52.80	55.40
Al <sub>2</sub> O <sub>3</sub>	10.16	1.35	0.77	7.88	0.82	5.80	1.79	0.06	b.d.
FeO	21.06	31.45	40.41	18.26	25.95	15.89	18.31	12.42	8.60 <sup>a</sup>
Fe <sub>2</sub> O <sub>3</sub>	3.02 <sup>b</sup>	0.74 <sup>b</sup>	0.23 <sup>b</sup>	3.24 <sup>b</sup>	0.44 <sup>b</sup>	2.33 <sup>b</sup>	1.11 <sup>b</sup>	0.01 <sup>c</sup>	
MgO	6.68	2.77	3.83	9.07	14.79	11.43	13.19	10.97	23.37
MnO	0.19	0.47	1.46	0.23	0.74	0.16	0.45	0.27	b.d.
TiO <sub>2</sub>	1.19	0.08	0.06	0.90	0.03	0.72	0.15	0.04	0.04
CaO	11.02	11.21	1.28	10.74	1.01	11.43	8.47	23.80	b.d.
Na <sub>2</sub> O	2.25	0.32	0.12	1.90	0.24	1.21	0.51	0.07	b.d.
K <sub>2</sub> O	0.43	b.d.	b.d.	0.32	b.d.	0.23	b.d.	n.a.	b.d.
F	0.05	0.29	b.d.	0.14	0.15	0.46	0.28	n.a.	b.d.
Cl	0.78	0.02	0.05	0.54	0.02	0.30	0.02	n.a.	b.d.
Total <sup>d</sup>	98.76	98.39	96.67	98.63	96.79	98.11	96.91	100.44	87.41 <sup>e</sup>
Basis (Oxygens):	23	23	23	23	23	23	23	6	11
Si	6.485	7.841	7.914	6.868	7.918	7.192	7.798	2.001	3.985
Al <sup>IV</sup>	1.515	0.159	0.086	1.132	0.082	0.808	0.202	0.000	
Al <sup>VI</sup>	0.329	0.091	0.062	0.268	0.063	0.208	0.112	0.003	
ΣAl	1.844	0.250	0.148	1.400	0.145	1.016	0.314	0.003	0.000
Fe <sup>2+</sup>	2.711	4.140	5.517	2.301	3.261	1.975	2.274	0.394	0.517
Fe <sup>3+</sup>	0.350	0.088	0.028	0.367	0.050	0.261	0.124	0.000	
Mg	1.532	0.650	0.932	2.036	3.313	2.531	2.920	0.620	2.506
Mn	0.025	0.063	0.202	0.029	0.094	0.020	0.057	0.009	0.000
Ti	0.138	0.010	0.007	0.102	0.003	0.080	0.017	0.001	0.002
Ca	1.818	1.890	0.224	1.734	0.163	1.820	1.391	0.967	0.000
Na	0.672	0.098	0.038	0.555	0.070	0.349	0.147	0.005	0.000
K	0.084	0.000	0.000	0.062	0.000	0.044	0.000	—	0.000
Total	15.659	15.660	15.010	15.454	15.017	15.288	15.042	4.000	7.010

<sup>a</sup> All Fe as FeO. <sup>b</sup> Fe<sub>2</sub>O<sub>3</sub> is midpoint between minimum and maximum. <sup>c</sup> Fe<sub>2</sub>O<sub>3</sub> calculated by charge balance. <sup>d</sup> Adjusted for F,Cl=O. <sup>e</sup> Low total probably due to poor polish. All abbreviations and analytical techniques as in Tables 1 and 2.

early veins. In similar veins near Pukugaqryggen (Fig. 7B) this type of late vein mineral assemblage is superimposed on supersolvus amphiboles and less calcic clinopyroxenes that are typical of early vein assemblages (see Figs 20 & 21).

Amphibole mineralization was followed by the formation of prehnite, chlorite, albite and Ca zeolites in the cavities. These late stage void-filling minerals imply reaction between the aqueous solutions in these fractures with the host gabbros over a wide range of temperatures.

*Hornblende-actinolite-biotite:* A texturally and mineralogically distinct set of black weathering, calcic amphibole mineralized veins occurs at stratigraphic intervals between Lower Zone c and Upper Zone b. These veins are less abundant than the veins described above. In thin section they are characterized by (1) microbrecciation and rotation of angular wall rock fragments <1 mm

wide, (2) abundant microfractures parallel to the main amphibole mineralized vein and (3) metasomatic reaction haloes that extend up to 5 mm from vein centers.

These veins are filled by two types of hornblendes: brown hornblende and a later stage green hornblende that forms overgrowths on, or fracture fillings within, the brown hornblende (Fig. 24B). Near vein margins, minor amounts of actinolite replace igneous pyroxenes. Biotite is usually found in close association with cumulate oxides in the wall rock near veins. Trace amounts of prehnite, titanite, chlorite, albite and Ca-zeolites occur in irregular cavities near the vein centers. Within tens of meters from the transgressive granophyres some of these fractures have thin (<1 cm wide) white alteration haloes where igneous plagioclase has been replaced by sericite and/or albite (Fig. 24A). Where these veins crosscut the transgressive granophyres, actinolite and euhedral quartz crystals fill the veins.

Compositional characteristics of vein-filling calcic



Fig. 27. Hornblende-actinolite-albite-epidote veins in the Layered Series gabbros. A) photomicrograph of trellis-type networks of ilmenite that enclose iron-rich ripidolitic chlorite and titanite marginal to a 0.5 cm wide hornblende-albite-epidote vein (302-EG82) in the Lower Zone c gabbros. Pyroxenes are replaced by hornblende and plagioclase is replaced by epidote, prehnite and albite (field of view is 5 mm wide, see Fig. 13A for sample location). B) photomicrograph of vein in Trough Band H (H14-EG81, Fig. 13C) showing albite alteration of wall rock plagioclase. Vein is filled by tabular green hornblende crystals with interstitial epidote (field of view is 3 mm wide).

gap in the distribution of the analyses between  $\sim 0.6$  and  $0.9$ . The amount of  $Al^{IV}$  increases in the calcic amphibole with increasing  $Fe^{2+}$  substitution (Fig. 28). In contrast,  $Al^{IV}$  concentrations in chlorites are essentially independent of the total octahedral iron concentration (Fig. 17).

Compositional characteristics of coexisting epidotes and prehnites marginal to vein 302-EG82 are given in Fig. 29 (cf. Analyses 3 & 4, Table 6A). Epidote and prehnite pairs define two groups: a high iron group in which  $X_{Fe^{3+}}$  in epidote ranges from 0.26 to 0.28 and  $X_{Fe^{3+}}$  in prehnite ranges from 0.18 to 0.23, and a low iron group in which  $X_{Fe^{3+}}$  in epidote ranges from 0.13 to 0.17 and  $X_{Fe^{3+}}$  in prehnite ranges from 0.02 to 0.08. Prehnites which do not coexist with epidote are also low in iron ( $X_{Fe^{3+}} = 0.02-0.06$ ). It can also be seen in Fig. 29 that there is a close agreement between the partitioning of  $Fe^{3+}$  and  $Al^{3+}$  in these epidotes and prehnites and those observed in the Cerro Prieto geothermal system (Bird et al. 1984) and the fossil hydrothermal system of the Del Puerto ophiolite (Evarts & Schiffmann 1983).

Similar vein types occur near the axial portion of

Trough Band H (sample H14-EG81, Fig. 13D) in an area about 150 metres square. In this area the rust colored gabbros are bleached and fractured. Irregularly shaped veins occur with green lens-shaped pockets up to 4 mm wide and 10 cm long. Pink and white albite alteration haloes occur about the veins. Just outside the bleached areas these veins appear to merge with the more uniform black-weathering amphibole-clinopyroxene-biotite veins. The lens-shaped pockets are filled with several generations of amphiboles. Epidote was formed interstitial to the euhedral amphiboles and albite occurs along the margins of the vein and in microcracks parallel to the main mineralized fractures (Fig. 27B and Analyses 4 & 5, Table 6B). Cavities within the pockets are now filled with Ca zeolites (e.g. stilbite, Analysis 6, Table 6B). Textural relations and compositions (Fig. 28) indicate at least three distinct types of amphiboles formed within the veins. The earliest amphiboles (solid circles in Fig. 28) are euhedral brown-green ferro-edenitic hornblendes that contain  $\sim 0.1$  moles Ti per 23 oxygens (Analysis 1, Table 6B). These hornblendes have formed near the vein walls. Over-

Table 6A. Selected electron microprobe analyses of hornblende-actinolite-albite-epidote vein minerals.

	1 302IIB-5 Ferroan pargasite	2 302IA-8 Magnesio- hornblende	3 302IIB-50 Epidote	4 302IIB-49 Prehnite	5 302IA-4 Chlorite	6 302IIB-7 Chlorite	7 302IA-2 Titanite
SiO <sub>2</sub>	40.27	46.24	37.47	42.58	27.37	24.70	30.83
Al <sub>2</sub> O <sub>3</sub>	12.71	6.36	24.90	22.54	19.07	20.99	3.45
FeO	20.31	15.18			24.34 <sup>b</sup>	35.21 <sup>b</sup>	0.96 <sup>b</sup>
Fe <sub>2</sub> O <sub>3</sub>	4.10 <sup>a</sup>	4.02 <sup>a</sup>	13.40 <sup>c</sup>	3.47 <sup>c</sup>			
MgO	5.82	11.42	b.d.	b.d.	17.98	8.20	b.d.
MnO	0.09	0.13	0.14	b.d.	b.d.	0.14	b.d.
TiO <sub>2</sub>	0.79	1.40	b.d.	0.04	0.21	0.25	34.28
CaO	11.66	11.09	23.06	26.87	0.08	0.06	29.35
Na <sub>2</sub> O	2.09	1.49	b.d.	0.03	0.02	0.08	0.17
K <sub>2</sub> O	0.47	0.05	b.d.	b.d.	b.d.	b.d.	b.d.
F <sup>-</sup>	0.10	b.d.	b.d.	b.d.	b.d.	b.d.	0.61
Cl	0.70	0.12	0.03	0.02	0.03	0.04	0.04
Total <sup>d</sup>	98.91	97.47	98.99	95.55	89.09	89.66	99.43
Basis (Oxygens):	23	23	12.5	11	14	14	5
Si	6.200	6.926	2.949	2.968	2.816	2.684	1.016
Al <sup>IV</sup>	1.800	1.074	0.051	1.032	1.184	1.316	
Al <sup>VI</sup>	0.507	0.049	2.261	0.821	1.129	1.373	0.134
ΣAl	2.307	1.123	2.312	1.853	2.313	2.689	0.134
Fe <sup>2+</sup>	2.615	1.901			2.095	3.201	0.027
Fe <sup>3+</sup>	0.476	0.453	0.794	0.182			
Mg	1.335	2.549	0.000	0.000	2.758	1.329	0.000
Mn	0.012	0.017	0.009	0.000	0.000	0.013	0.000
Ti	0.092	0.158	0.000	0.002	0.017	0.020	0.849
Ca	1.924	1.780	1.945	2.007	0.009	0.007	1.036
Na	0.624	0.433	0.000	0.002	0.004	0.018	0.011
K	0.092	0.010	0.000	0.000	0.000	0.000	0.000
Total	15.677	15.350	8.009	7.014	10.012	9.961	3.073

<sup>a</sup> Fe<sub>2</sub>O<sub>3</sub> is midpoint between minimum and maximum. <sup>b</sup> All Fe as FeO. <sup>c</sup> All Fe as Fe<sub>2</sub>O<sub>3</sub>. <sup>d</sup> Adjusted for F, Cl=O. All abbreviations and analytical techniques as in Tables 1 and 2.

growths and separate euhedral crystals of dark green low-titanium hastingsitic and ferro-pargasitic hornblendes occur within the vein and are surrounded by epidote (Analysis 2, Table 6B). These aluminum-rich hornblendes are partially overgrown by pale green low-titanium ferro-actinolites (Analysis 3, Table 6B).

Mineral assemblages similar to those described above have been reported from other gabbros in East Greenland (Elsdon 1982; Rose & Bird 1986) and in regionally metamorphosed iron-rich gabbros in Quebec (Klein 1984). These areas of intense alteration and fracturing appear to represent localized zones of high permeability during the latest stages of cooling of the Skaergaard intrusion.

**Cummingtonite-olivine:** In the oxide-rich layers of Trough Band H (Fig. 5C) amphibole mineralized veins contain mineral assemblages that are not found elsewhere within the intrusion (sample 517-EG82, Fig. 13D). These veins are up to 2 mm wide. As shown in

Fig. 30 the vein margins are lined with fine-grained olivine and the vein centers are mostly fine grained aggregates of cummingtonite ( $X_{\text{Fe}_{7}\text{Si}_{8}\text{O}_{22}(\text{OH})_{2}} = 0.55-0.57$ , Analyses 1 & 2, Table 7), magnetite and minor amounts of actinolite ( $X_{\text{Fe}^{2+}} = 0.49-0.55$ , Analysis 3, Table 7). Hydrothermal vein olivines are considerably more iron-rich ( $X_{\text{Fe}_{2}\text{SiO}_{4}} = 0.84$ , Analysis 4, Table 7) than cumulate olivines in the oxide-rich layers where  $X_{\text{Fe}_{2}\text{SiO}_{4}} = 0.65$ . Oxides are recrystallized up to 5 mm from the vein into complex trellis networks of ilmenite ( $X_{\text{Fe}_{2}\text{O}_{3}} = 0.20-0.40$ ) that enclose magnetite ( $X_{\text{FeTiO}_{3}} = 0.15-0.25$ ) and trace amounts of olivine (see Analyses 5 & 6, Table 7). Angular microbreccia fragments of plagioclase and altered Fe-Ti oxides are found in the vein. Because plagioclase is virtually absent from the oxide-rich layers of the Trough Bands, these fragments must have been transported from the adjacent plagioclase-rich layers, a distance of >2 cm. Microfractures filled with olivine and/or actinolite formed subparallel to the main mineralized vein.

Table 6B. Selected electron microprobe analyses of hornblende-actinolite-albite-epidote vein minerals.

	1 H14-1 Ferro- edenite	2 H14-8 Hastingsitic hornblende	3 H14-6 Ferro- actinolite	4 H14-9 Albite	5 H14-23 Epidote	6 H14-7 Stülbite
SiO <sub>2</sub>	42.29	39.31	49.02	68.15	37.71	59.71
Al <sub>2</sub> O <sub>3</sub>	7.45	11.75	3.45	19.68	23.87	15.60
FeO	27.75	26.69	29.42			
Fe <sub>2</sub> O <sub>3</sub>	3.47 <sup>a</sup>	4.91 <sup>a</sup>	0.97 <sup>a</sup>	b.d. <sup>b</sup>	12.04 <sup>b</sup>	0.29 <sup>b</sup>
MgO	2.94	1.59	3.58	n.a.	0.01	n.a.
MnO	n.a.	n.a.	n.a.	n.a.	0.06	n.a.
TiO <sub>2</sub>	0.60	0.14	0.02	n.a.	b.d.	n.a.
CaO	10.58	11.08	11.38	0.38	22.98	4.33
Na <sub>2</sub> O	1.85	1.15	0.31	11.65	n.a.	0.86
K <sub>2</sub> O	0.54	1.73	b.d.	0.07	n.a.	2.40
Total	97.47	98.35	98.15	99.93	96.67	83.19
Basis (Oxygens):	23	23	23	8	13	18
Si	6.772	6.282	7.633	2.982	3.021	6.964
Al <sup>IV</sup>	1.228	1.719	0.367	1.015	0.000	2.036
Al <sup>VI</sup>	0.178	0.495	0.266	0.000	2.256	0.110
ΣAl	1.406	2.214	0.633	1.015	2.256	2.146
Fe <sup>2+</sup>	3.716	3.567	3.832			
Fe <sup>3+</sup>	0.418	0.590	0.114	0.000	0.726	0.025
Mg	0.702	0.379	0.831	—	0.001	—
Mn	—	—	—	—	0.004	—
Ti	0.072	0.017	0.002	—	0.000	—
Ca	1.815	1.897	1.899	0.018	1.973	0.541
Na	0.574	0.356	0.094	0.989	—	0.194
K	0.110	0.353	0.000	0.004	—	0.357
Total	15.585	15.655	15.038	5.008	7.981	10.227

<sup>a</sup> Fe<sub>2</sub>O<sub>3</sub> is midpoint between minimum and maximum. <sup>b</sup> All Fe as Fe<sub>2</sub>O<sub>3</sub>. All abbreviations and analytical techniques as in Tables 1 and 2.

Vein 517-EG82 continues above and below the oxide-rich layer into the plagioclase-rich layers of Trough Band H. Within the plagioclase-rich layer the mineralogy changes abruptly to the albite, hornblende and epidote assemblages described above for sample H14-EG81. This vein system extends to the north of the bleached albite mineralized area within the trough band and merges with an older amphibole-clinopyroxene-biotite vein. It could not be determined from these field relations whether the cummingtonite-olivine veins in the oxide-rich layers are formed by events responsible for the amphibole-clinopyroxene-biotite veins or the hornblende-actinolite-albite-epidote veins. Nevertheless, it is apparent that the local composition of the wall rock

Fig. 28. Compositions of calcic amphiboles from hornblende-actinolite-albite-epidote veins in the Lower Zone c and Upper Zone a gabbros. Solid circles represent early ferro-edenitic hornblende and the stippled circles represent later vein amphiboles. See Fig. caption 16 for explanation and Figs 13A and C for sample locations.

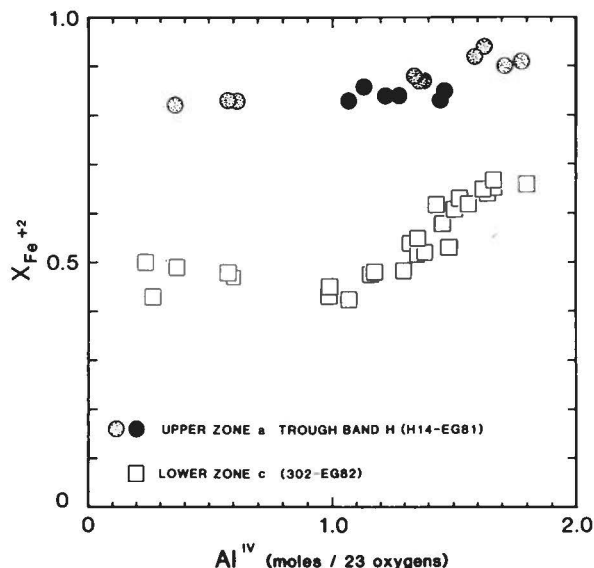
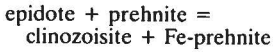
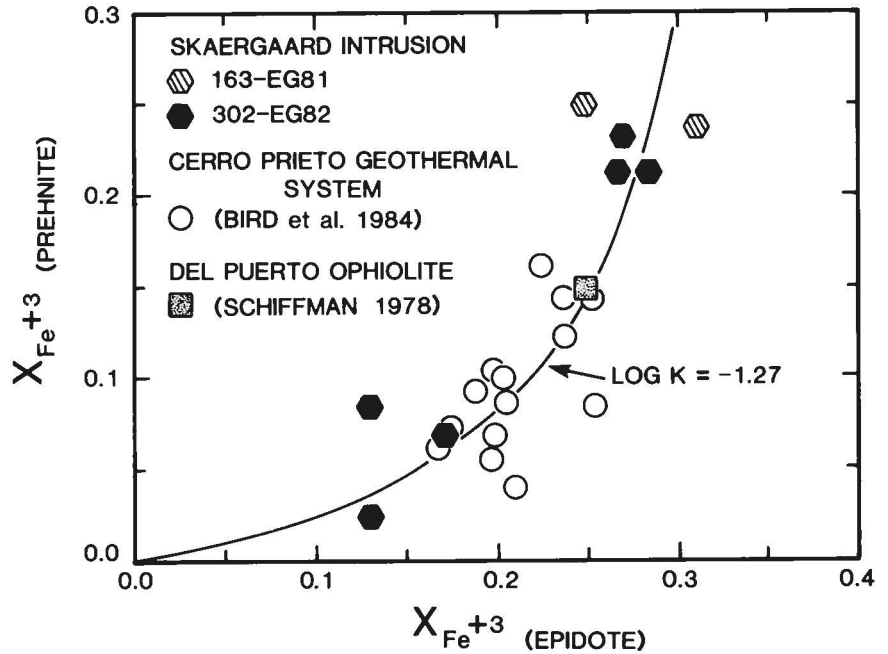




Fig. 29. Compositions of coexisting epidote and prehnite solid solutions in wall rock alteration zones around a hornblende-albite-epidote vein (302-EG82) in Lower Zone c and in an epidote-prehnite-quartz vein (163-EG81) in the basalt host rock. See Figs 3 and 13A for sample locations. The solid line represents  $Al^{+3}-Fe^{+3}$  partitioning consistent with an equilibrium constant of  $10^{-1.27}$  for the exchange reaction



estimated by Bird et al. (1984) based on phase relations among calc-silicates and aqueous solutions in active geothermal systems.



has a dramatic influence on the types of vein mineral assemblages found within hydrothermal fractures within the Trough Bands.

## Fracture systems of the Upper Border Group and the Basistoppen Sheet

Hydrothermal alteration is more pervasive in the Upper Border Group and the Basistoppen Sheet than in the Layered Series gabbros (Wager & Deer 1939; Hughes 1956; Douglas 1964; Naslund 1976, 1980, 1984a,b; Naslund et al. 1983). As with the Layered Series gabbros, the earliest fracturing is associated with the local transport of hybrid materials, such as gabbro pegmatites and granophyres that may be associated with the fusion of upper crustal xenoliths found near the upper portions of the intrusion. High temperature hydrothermal alteration has locally produced talc and iron oxides from olivine (Hughes 1956), and iron-rich green pyroxene and hornblende after brown pyroxene (Wager & Deer 1939). Lower temperature alteration is more pervasive and includes replacement of plagioclase by sericite, chlorite, epidote and/or albite, and pyroxenes by chlorite or actinolite (Hughes 1956; Douglas 1964; Wager & Deer 1939). Ilvaite has locally formed from olivine (Naslund et al. 1983). These hydrothermal assemblages may make up as much as 2 to 20 volume percent of the Upper Border Group rocks (Naslund 1984a).

A major distinction between the hydrothermal alteration of the Upper Border Group and Basistoppen

Sheet and that of the Layered Series gabbros is the greater abundance of low temperature mineral assemblages in the former. These low temperature assemblages are typical of hydrothermal alteration found in active geothermal systems in rocks of basaltic composition, such as in Iceland. Vein minerals such as epidote, calcite, chlorite and albite are common in the upper portions of the intrusion, but have a very limited distribution, or are absent within the underlying Layered Series gabbros. Black weathering amphibole veins similar to those found within the Layered Series gabbros have not been observed above the Sandwich Horizon.

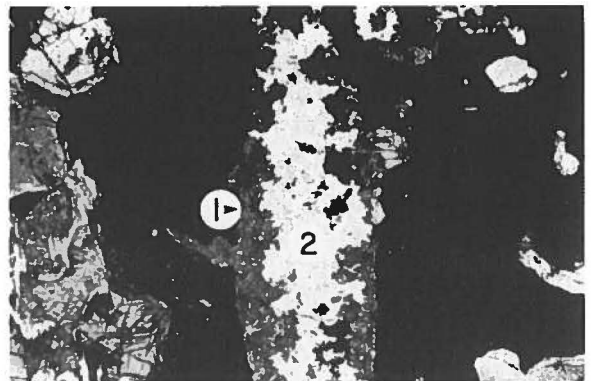


Fig. 30. Photomicrograph of an olivine-cummingtonite vein (517-EG82) in an oxide-rich layer of Trough Band H. The vein wall is lined with fine-grained fayalitic olivine (1) and the vein center is filled with cummingtonite, magnetite and minor amounts of actinolite (2). See Fig. 13C for sample location. Field of view is 3 mm wide.

Table 7. Selected electron microprobe analyses of cummingtonite-olivine vein minerals.

	1 517-14 Cummingtonite	2 517-12 Cummingtonite	3 517-17 Actinolite	4 517-3 Olivine (Ferrohortalite)	5 517-10 Ilmenite	6 517-11 Magnetite
SiO <sub>2</sub>	52.65	50.49	53.22	30.50	b.d.	b.d.
Al <sub>2</sub> O <sub>3</sub>	1.41	1.10	1.48	0.03	0.02	1.96
FeO	26.94	27.44	20.39	61.91 <sup>a</sup>	44.61	48.89
Fe <sub>2</sub> O <sub>3</sub>	0.39 <sup>c</sup>	0.96 <sup>c</sup>	0.45 <sup>c</sup>		3.60 <sup>b</sup>	37.59 <sup>b</sup>
MgO	11.53	12.45	12.03	6.48	0.16	0.11
MnO	0.31	0.36	0.16	0.85	0.57	0.12
TiO <sub>2</sub>	0.14	0.11	0.13	0.04	50.59	7.84
CaO	5.04	3.78	9.86	0.07	0.02	0.03
Na <sub>2</sub> O	0.25	0.21	0.31	0.09	b.d.	b.d.
K <sub>2</sub> O	b.d.	b.d.	b.d.	b.d.	b.d.	b.d.
Total	98.65	96.90	98.03	99.98	99.57	96.54
Basis (Oxygens):	23	23	23	4	3	8
Si	7.860	7.729	7.860	0.988	0.000	0.000
Al <sup>IV</sup>	0.140	0.199	0.140			
Al <sup>VI</sup>	0.108	0.000	0.117			
ΣAl	0.248	0.199	0.257	0.001	0.001	0.199
Fe <sup>2+</sup>	3.364	3.514	2.518	1.678	0.947	2.434
Fe <sup>3+</sup>	0.043	0.111	0.050		0.069	2.907
Mg	2.565	2.840	2.648	0.313	0.006	0.013
Mn	0.039	0.047	0.020	0.023	0.012	0.008
Ti	0.016	0.013	0.014	0.001	0.965	0.457
Ca	0.806	0.620	1.560	0.003	0.001	0.003
Na	0.072	0.062	0.089	0.005	0.000	0.000
K	0.000	0.000	0.000	0.000	0.000	0.000
Total	15.013	15.135	15.016	3.012	2.001	6.001

<sup>a</sup> All Fe as FeO. <sup>b</sup> Fe<sub>2</sub>O<sub>3</sub> calculated by charge balance. <sup>c</sup> Fe<sub>2</sub>O<sub>3</sub> is midpoint between minimum and maximum. All abbreviations and analytical techniques as in Tables 1 and 2.

There is a notable lateral variation in the fracture abundance and hydrothermal alteration mineralogy across the upper portions of the intrusion. The most extensive fracture-related hydrothermal alteration is

found within and above the Basistoppen Sheet (Figs 3 & 31A). East of the Basistoppen Sheet, near Kilen, hydrothermal mineralization and fracture systems are difficult to identify within the coarse-grained weathered expo-

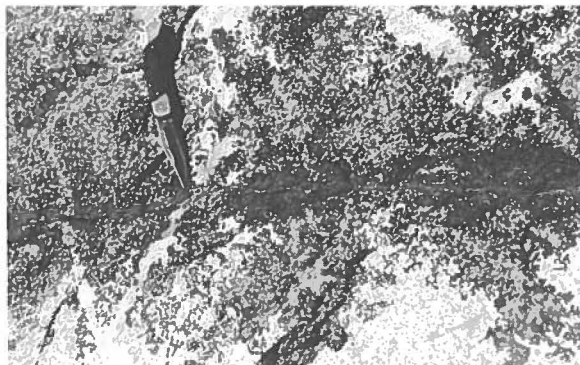


Fig. 31. Epidote vein crosscutting a granophyre near the Basistoppen Sheet near location 61 in Fig. 3. The epidote vein crosscuts the granophyre at the knife tip. The alteration halo about the vein consists of epidote, chlorite and actinolite replacement of the wall rock. Knife is 21 cm long.

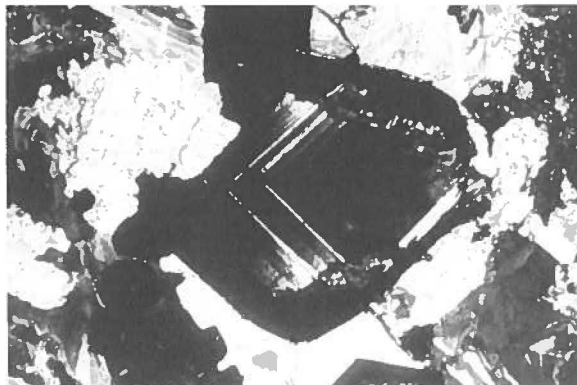


Fig. 32. Photograph of epidote, garnet and pyrite vein (61-EG81, Fig. 3) in the Basistoppen Sheet. Zoning in the garnet in the center of the photo probably represents variations in the extent of hydrogarnet substitution. Field of view is 5 mm wide.

Table 8. Selected electron microprobe analyses of epidote garnet pairs from the Basistoppen Sheet.

	Vein Wall		Vein Center	
	61-7.4 Epidote	61-7.3 Fe-grossular	61-2.3 Epidote	61-2.5 Andradite
SiO <sub>2</sub>	38.51	38.30	38.34	35.41
Al <sub>2</sub> O <sub>3</sub>	27.42	14.79	25.68	0.10
Fe <sub>2</sub> O <sub>3</sub>	9.88 <sup>a</sup>	13.01 <sup>a</sup>	9.91 <sup>a</sup>	31.36 <sup>a</sup>
MgO	0.03	0.10	0.01	0.02
MnO	0.05	0.29	0.01	0.07
TiO <sub>2</sub>	b.d.	b.d.	b.d.	b.d.
CaO	23.27	34.50	23.41	32.75
Na <sub>2</sub> O	0.01	b.d.	0.05	b.d.
K <sub>2</sub> O	0.01	b.d.	b.d.	b.d.
Total	99.18	100.99	97.41	99.71
Basis (Oxygens):	12.5	12	12.5	12
Si	2.977	2.969	3.025	3.001
Al <sup>IV</sup>	0.023	0.031	0.000	0.000
Al <sup>VI</sup>	2.475	1.320	2.387	0.010
ΣAl	2.498	1.351	2.387	0.010
Fe <sup>3+</sup>	0.574	0.759	0.588	2.000
Mg	0.003	0.012	0.001	0.003
Mn	0.003	0.019	0.000	0.005
Ti	0.000	0.000	0.000	0.000
Ca	1.927	2.866	1.979	2.974
Na	0.002	0.000	0.007	0.000
K	0.001	0.000	0.000	0.000
Total	7.985	7.976	7.987	7.993

<sup>a</sup> All Fe as Fe<sub>2</sub>O<sub>3</sub>. All abbreviations and analytical techniques as in Tables 1 and 2.

tures of the Upper Border Group gabbros. Nevertheless, fracture systems and pervasive alteration of the gabbros are clearly more abundant to the west of Kilen (see Fig. 3).

Vein systems within and above the Basistoppen Sheet are characterized by epidote-bearing mineral assemblages, that may contain grandite garnet, calcite, alkali feldspars, serpentine, quartz and/or chlorite. Veins appear to be more abundant than in the Layered Series gabbros, but detailed measurements have not been made. Most veins are <2 mm wide and are continuous for tens of meters (Fig. 31B). Alteration zones about the veins are formed by replacement of the igneous minerals by sericite, chlorite, actinolite and serpentine. Epidote veins up to 2 cm wide have been found, but they are not common.

Within the Basistoppen Sheet the most abundant set

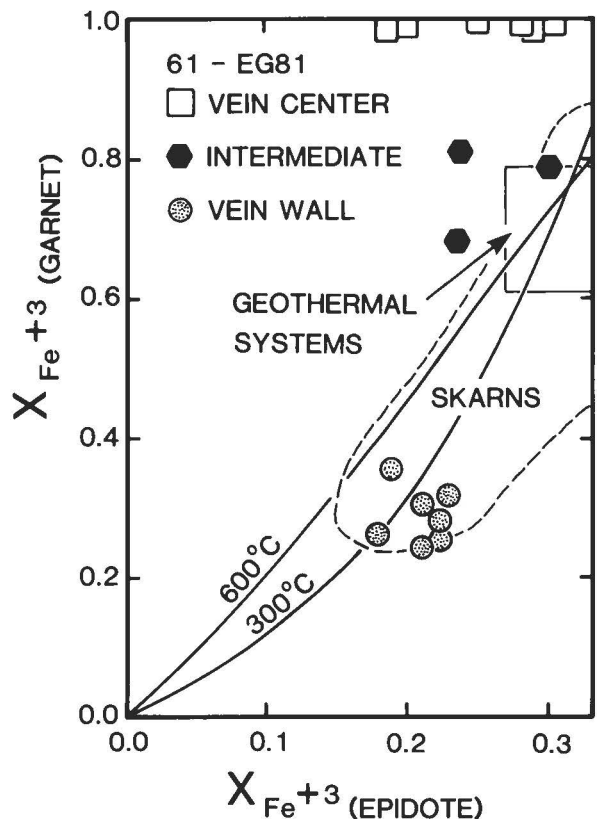


Fig. 33. Compositions of coexisting epidote and garnet solid solutions within vein 61-EG81 from the Basistoppen Sheet (symbols). See Fig. 3 for sample location. The ranges of measured compositions of epidote and garnet solid solutions from contact skarns (dashed lines) and active geothermal systems (box) are also given in the figure (see summary of references given in Bird & Helgeson 1980 and Bird et al. 1984). Solid lines denote equilibrium compositions computed from equations and data reported by Bird & Helgeson 1980.

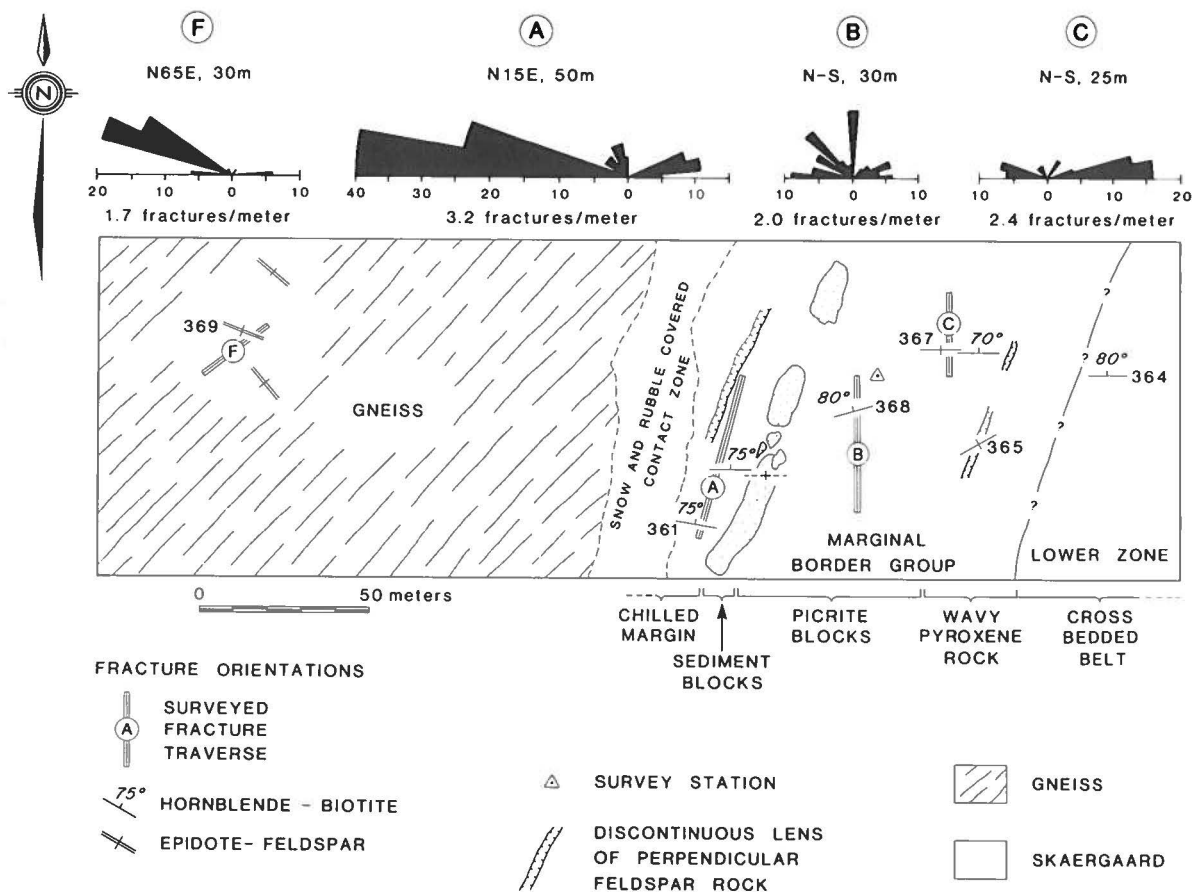


Fig. 34. Map of the contact region between the Skaergaard intrusion and gneisses near Uttental Pass (map location is given in Fig. 13A). Rose diagrams denote the orientation and abundance of veins measured along traverses within the map area. The direction and distance given above the rose diagrams are the orientation and length of the traverses used in the measurements. Fracture abundances reported here and elsewhere in this paper are mineralized fractures per meter computed by dividing the total number of veins within the traverse by the total distance of the traverse.

of epidote veins strike N40–50W (Fig. 31). A N80E fracture set which contains epidote, garnet and pyrite is less abundant and crosscuts the northwest vein set. The average frequency of the northwest fracture set is  $>1$  fracture per meter in the lower half of the Basistoppen Sheet. Near the top of the Basistoppen Sheet miarolitic cavities occur as irregular to subspherical mineralized pores ranging from 5–20 mm in diameter. These pores are partially filled with varying amounts of epidote, calcite, quartz and chlorite. Extensive hydrolysis of plagioclase and olivine occurs near the cavities. Miarolites comprise up to 5% of some of the rocks. Large miarolites, up to 5 cm wide and partially filled with euhedral epidote crystals ( $C_{Ca_2Fe_3Si_3O_{12}(OH)} = 0.28$ ), are found just above the Basistoppen Sheet on Brødretoppen.

The main occurrence of grandite garnet within the Skaergaard and related intrusions is near the lower portions of the Basistoppen Sheet (61-EG81, see Fig. 3 for location). The N80E vein set crosscuts an earlier north-

west quartz and epidote vein at this locality. This vein has a very irregular width ranging from 1–20 mm wide. Mineralized pockets within the vein are elongate lenses up to 10 cm long and 2 cm wide. These pockets exhibit a distinct compositional and textural zoning pattern. The center consists of coarse grained euhedral garnet (up to 2 mm in diameter) together with epidote and pyrite (Fig. 32). The margins of the pocket are very fine-grained mixtures of garnet, epidote, K-feldspar and quartz. Plagioclase is altered to sericite up to 3 cm from the vein margins.

Measured compositions of coexisting epidote and garnet solid solutions within the vein are given in Fig. 33 and Table 8. Several distinct compositional groupings are apparent from the figure. The center of the vein pocket contains isotropic euhedral andradite, whereas the fine-grained vein wall contains anisotropic grossular-rich garnet. Throughout the vein epidote compositions are locally variable, and range from

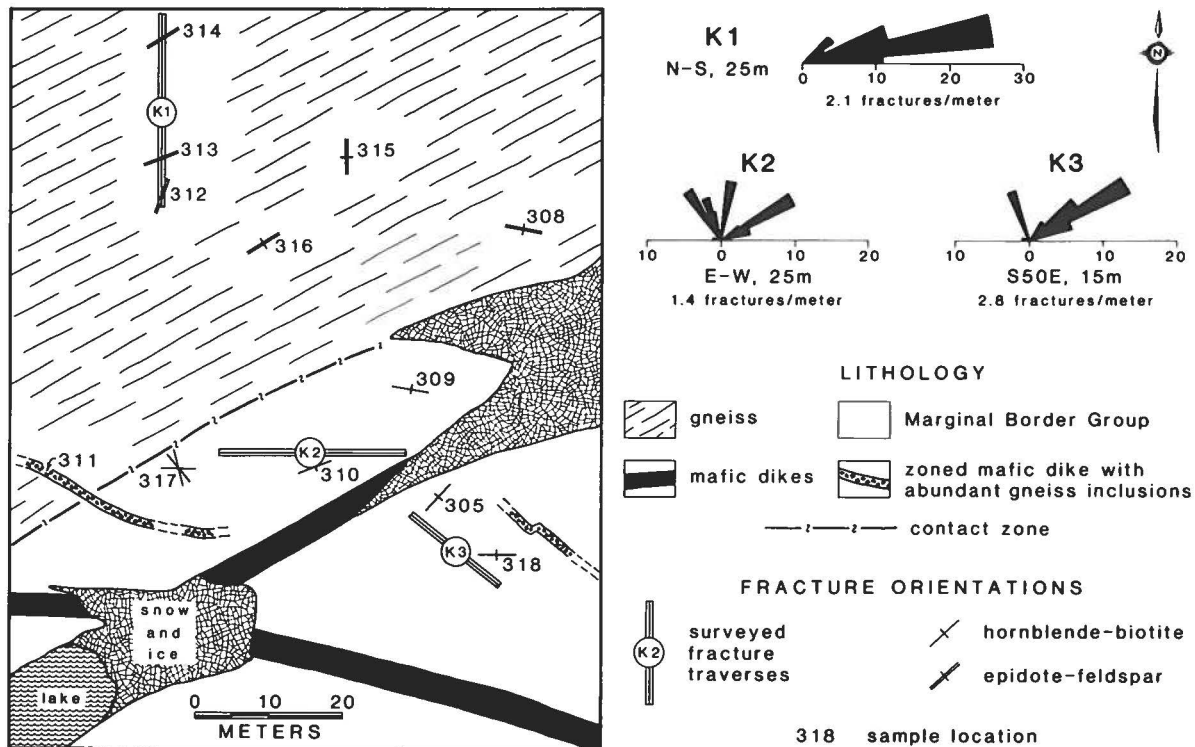


Fig. 35. Map of the contact region between the Skaergaard intrusion and the gneisses on Kraemer Ø showing the location of fracture traverses, and vein abundance and orientations. See Fig. 5A for map location and Fig. 34 caption for explanation.

$X_{\text{Ca}_2\text{Fe}_3\text{Si}_3\text{O}_{12}(\text{OH})} = 0.18$  to 0.31. K-feldspar at the vein margins contains 0.04 mole percent albite. Also shown in Fig. 33 are the ranges of compositions of coexisting epidote and garnet solid solutions from active geothermal systems and hydrothermal skarns. Note that the mineral pairs from the vein wall of 61-EG81 are in close agreement with analyses from other types of hydrothermal systems. It will be shown below that the mineral assemblage within the center of the pocket represents metastable coexistence of epidote and andradite garnet.

From our observations of the subsolidus mineralogy and deformation of the upper portions of the Skaergaard intrusion it is apparent that the intrusion of the Basistoppen Sheet just after solidification of the Sandwich Horizon (Douglas 1964; Naslund 1984a) had a profound effect on the nature of fracturing and hydrothermal fluid flow and reactions on the central and western portions of the Upper Border Group.

### Fracture systems near the contact of the Skaergaard intrusion

The most abundant hydrothermal fracture systems of the Skaergaard intrusion are found within the Marginal Border Group. This lithologic unit contains several distinct rock units, each with its own characteristic miner-

alogic and textural features (Wager & Deer 1939; Wager & Brown 1967; Hoover 1982). The innermost and most voluminous part of the Marginal Border Group is the Banded Division, which exhibits an inward fractionation sequence similar to that of the Layered Series gabbros. The outermost units of the Marginal Border Group may contain abundant xenoliths of sediments, picrites, gneisses and basalts. Although these xenoliths have reacted and partially equilibrated with the liquids of the Marginal Border Group (Kays et al. 1981; Kays & McBirney 1982) they represent extreme gradients in the changes of wall rock composition for hydrothermal fracture systems. These changes in the local bulk rock compositions, represented by large concentrations of the xenoliths, have a dramatic effect on the mineralogy formed within the fracture systems near the intrusive contact. Similar extremes in wall rock compositional gradients are present in fracture systems that pass through the Marginal Border Group into the host rock gneisses.

Within the Marginal Border Group and the host rocks of the Skaergaard intrusion small scale survey maps were made at Uttental Pass (Fig. 34), Kraemer Ø (Fig. 35), Mellemø (Figs 36 & 37), Ivnarmitut (Fig. 38), the south contact (Fig. 39) southeast of Skærgårdshalvø and the east contact (Fig. 40) north of Forbindelsesgletscher (see Figs 3, 5A & 13B for map locations).



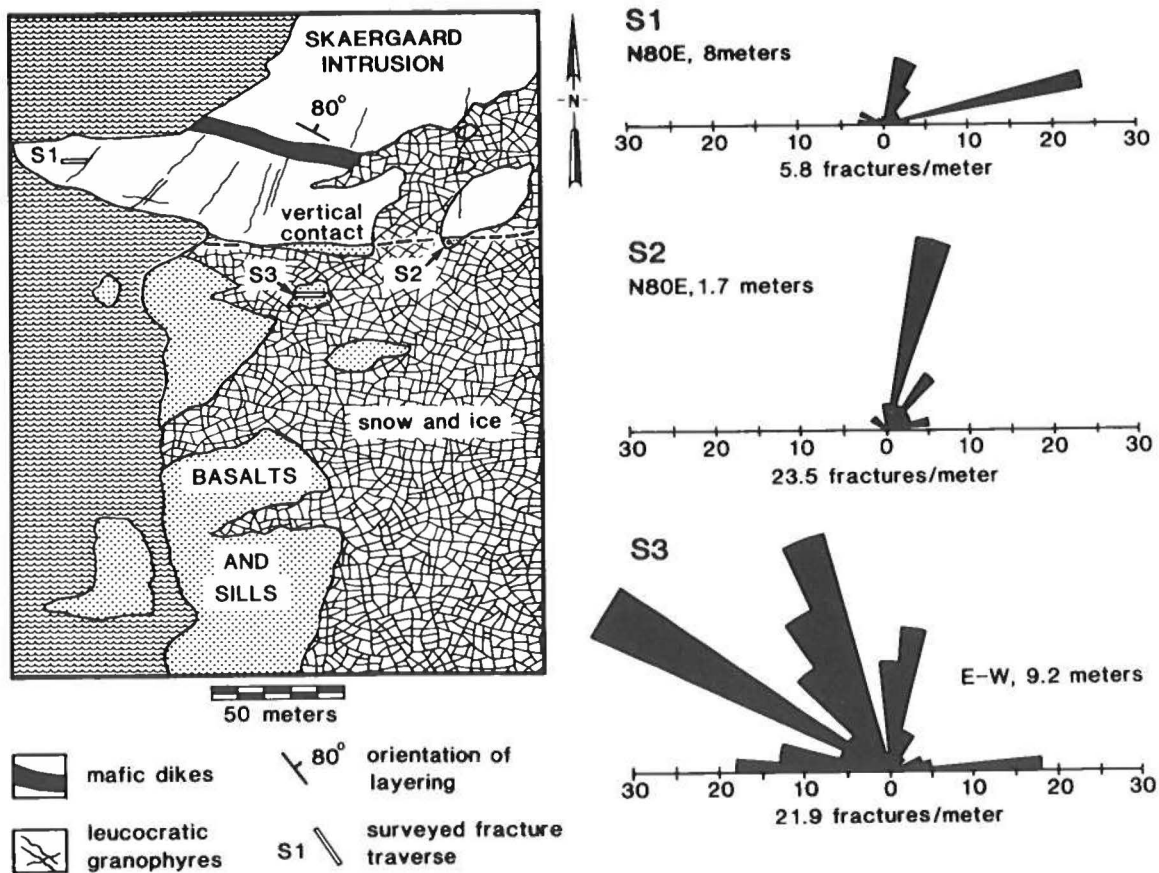


Fig. 39. Map of the southern contact between the Skaergaard intrusion and basalts and sills southeast of Skaergaardshalvø (see Fig. 3 for map location). Rose diagrams denote the abundance of orientation of black and rust-brown weathering amphibole and chlorite veins near the contact. See Fig. 34 caption for explanation.

blende-rich veins are found only in a few locations within the exposures of the coarse grained Banded Division (see traverse T13, Fig. 38). However, this vein type is abundant on either side of the Banded Division (i. e. in the Tranquil Division and in the Layered Series gabbros). We have not been able to explain the apparent absence of hornblende veins in the Banded Division.

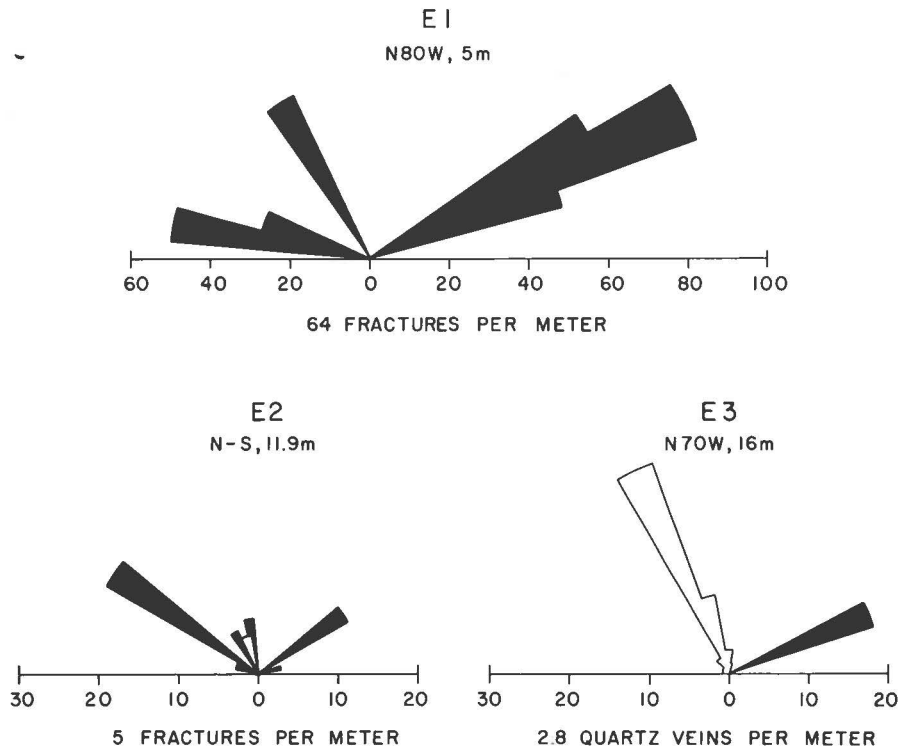
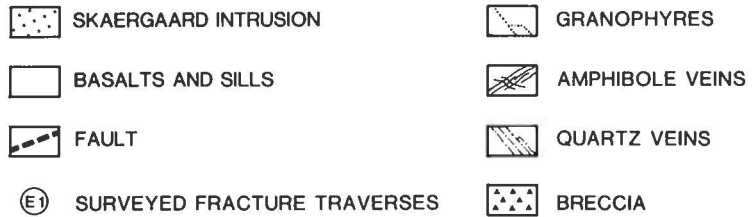
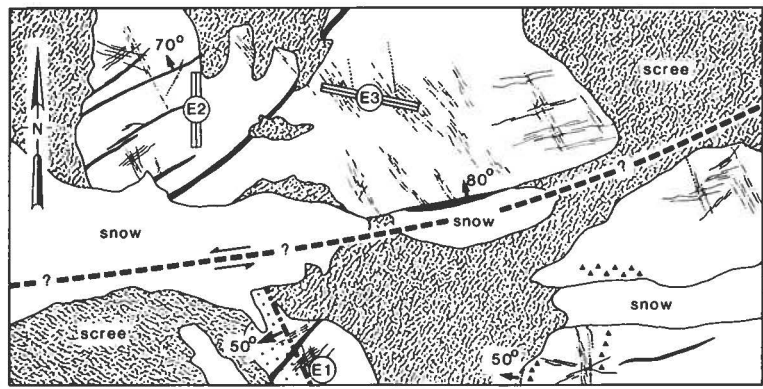
Amphibole-rich veins of the Tranquil Division change to epidote and alkali feldspar veins in the Precambrian gneisses within several meters of the contact. In the basalts near the contact of the intrusion amphibole veins give way after several tens of meters or more to epidote-bearing veins that may contain quartz, prehnite, calcite, salite or grandite garnet.

The abundance of veins near the contact of the Skaergaard intrusion generally decreases as a function of distance from the contact and increases as a function of stratigraphic height within the intrusion. Fig. 41 presents a series of histograms of the abundance of veins measured along traverses within the study areas of Figs 34-40. The histograms of Fig. 41 are arranged in order

of increasing stratigraphic height within the intrusion. Note that veins near the contact between the gneiss and the Skaergaard intrusion are <3 fractures per meter in the deep portions of the system near Kraemer Ø and Uttental Pass. The abundance of veins increases up to 4 fractures per meter near the gneiss-sediment-basalt unconformity at Mellemø and then increases to locally >20 fractures per meter in the metabasalts stratigraphically above the gneisses (see south and east contacts in Fig. 41). The mineralogic phase relations within veins of these study areas are given below.

*Uttental pass:* Rose diagrams given in Fig. 34 depict the orientation and abundance of veins near the deepest exposures of the contact of the Skaergaard intrusion and the Precambrian basement gneisses. In the gneiss host rock less than 100 meters from the intrusion, mineralized fractures are nearly perpendicular to the contact and occur with a frequency of about 1.7 fractures per meter. The frequency of fractures increases in the Marginal Border Group rocks to >2.0 fractures per meter.

Fig. 40. Map of the eastern contact between the Skaergaard intrusion and basalts and sills north of Forbindelsesgletscher (see Fig. 3 for map location). Rose diagrams represent the orientation and abundance of black and rust-brown weathering amphibole and chlorite veins (solid areas) and milky-white quartz veins (open areas). See Fig. 34 caption for explanation.



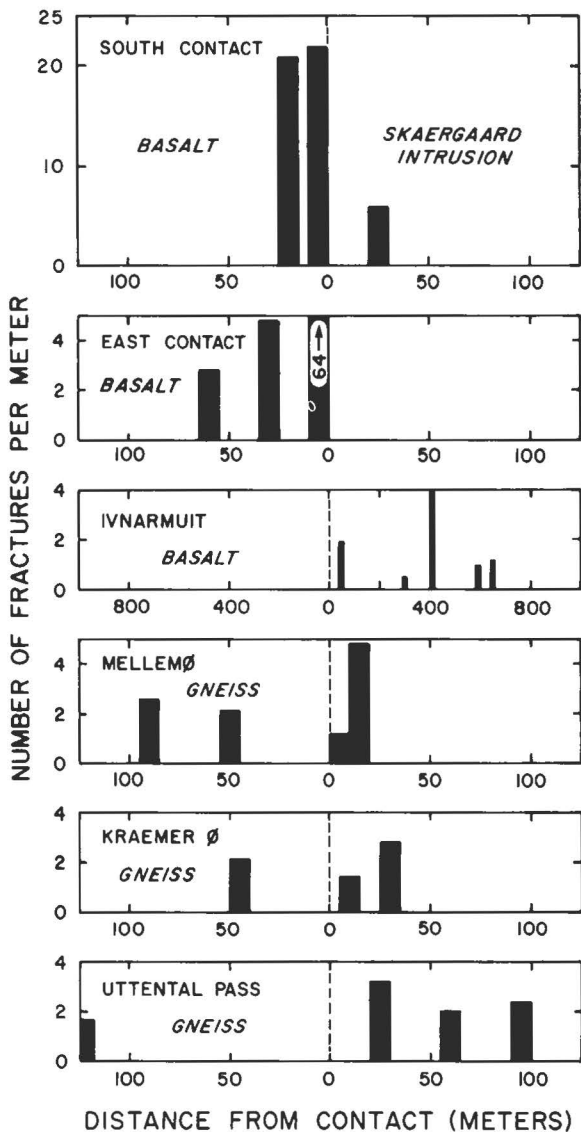


Fig. 41. Histograms of the abundance of amphibole mineralized fractures near the margins of the Skaergaard intrusion. Diagrams are arranged as a function of relative stratigraphic height within the intrusion. For example, Uttental Pass (Fig. 34) is near the lower exposures of the intrusion and the south contact (Fig. 39) is near the uppermost exposures of the intrusion. Data are summarized from rose diagrams given in Figs 34-34 and 38-40.

Fracture sets parallel to the contact zone are more abundant in the Marginal Border Group rocks.

Fracture mineralization changes near the contact from epidote and alkali feldspar assemblages in the gneisses to metasomatically zoned veins in the Marginal Border Group that contain varying amounts of actinolite, hornblende, biotite, talc, chlorite and magnetite (Fig. 42A, Table 9). The fractures in the Marginal Border Group have tan colored centers (0.5 to 5 mm wide)

with dark brown reaction zones in the wall rock (3 mm to 4 cm wide). The centers consist of thin needles of actinolite with lesser amounts of euhedral actinolite crystals. Mg cummingtonite and biotite occur in trace amounts in the vein centers.

Metasomatic reaction zones are best developed in the Marginal Border Group veins within ~50 meters of the contact. Vein margins are defined by the development of brown hornblende, biotite and magnetite. Biotite may form hexagonal crystals parallel to the vein margin that are up to 5 mm wide. Metasomatic reactions marginal to the veins have produced talc pseudomorphs of olivine, chlorite replacing plagioclase (Fig. 42B) and mixtures of Mg cummingtonite and actinolite after pyroxenes. The mole fractions of octahedral iron in hydrous minerals within and near these veins increases with distance from the intrusive contact as shown in Figs 43 & 44. Fig. 44 also demonstrates that the hornblendes formed in the wall rock at distances greater than 1 cm from the veins contain high concentrations of Ti. The width of the metasomatic reaction zones about the veins decreases dramatically outside the zone of picrite xenoliths shown in Fig. 34.

The vein mineralogy described above is restricted to the Marginal Border Group; for example, vein 364-EG82 (Fig. 34) contains chlorite and actinolite with minor replacement of cumulate olivine by talc near the vein wall in the cross-bedded belt of the Lower Zone. No amphibole veins were observed within the xenoliths of sediments at Uttental Plateau. Veins within the sediment blocks are white in outcrop and are filled with albite.

*Kraemer Ø:* At this map locality (Figs 3 and 35) vein abundance near the contact of the Skaergaard intrusion and the gneiss are similar to that at Uttental Pass. Unlike the veins at Uttental Pass, the most abundant vein orientation is parallel to the gneiss-gabbro contact in the map area of Fig. 35. A minor set of veins that is approximately perpendicular to the contact was found in traverses K2 and K3 of Fig. 35. No xenoliths were found in the Marginal Border Group within this study area. The modal abundance of plagioclase is larger and that of olivine is smaller relative to the vein wall samples studied from Uttental Pass.

Veins in the Marginal Border Group within the area of Fig. 35 are thin (<0.5 mm wide) and do not have metasomatic reaction zones like the veins at Uttental Pass. Two types of vein assemblages are found. The earliest consists of hornblende, clinopyroxene, orthopyroxene, biotite, chlorite and talc, whereas the later veins are filled with actinolite, chlorite and minor amounts of quartz and apatite. These two vein types could not be distinguished in the field.

Vein 318-EG82 (Fig. 35) is an example of the early veins. A photomicrograph of the vein mineralogy is given in Fig. 45B and representative mineral compositions are presented in Table 10A. The vein is subparallel

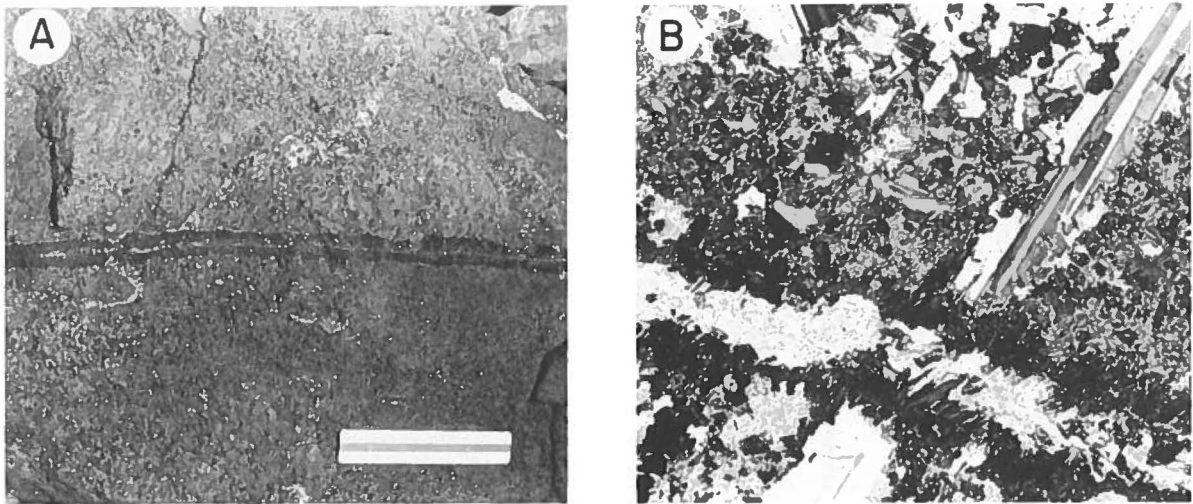


Fig. 42. Veins within the Marginal Border Group near Uttental Pass. A) exposure of a zoned vein (367-EG82, Fig. 34) with a dark marginal zone of talc and chlorite replacing the wall rock gabbros, and a lighter, rust-colored vein center composed of actinolite, cummingtonite, hornblende and biotite (scale is 16 cm long). B) photomicrograph of vein 365-EG82 (Fig. 34) showing actinolite vein center and chlorite replacing plagioclase in a zone of perpendicular feldspar rock (field of view is 1 cm wide).

Table 9. Selected electron microprobe analyses of Marginal Border Group amphibole vein minerals from Uttental Plateau.

	1 368A-1 Actinolite	2 368B-3 Magnesio- hornblende	3 368A-27 Chlorite	4 368A-24 Biotite	5 367A-31 Talc (vein center)	6 367A-24 Talc (replacing olivine)
SiO <sub>2</sub>	55.64	50.64	27.51	37.82	60.76	63.03
Al <sub>2</sub> O <sub>3</sub>	1.64	6.92	20.33	14.68	0.93	0.12
FeO	10.25	8.02	14.58 <sup>a</sup>	7.04 <sup>a</sup>	7.28 <sup>a</sup>	3.18 <sup>a</sup>
Fe <sub>2</sub> O <sub>3</sub>	0.76 <sup>b</sup>	2.59 <sup>b</sup>				
MgO	17.76	16.17	22.98	19.21	26.03	29.83
MnO	0.26	0.24	0.22	2.02	0.08	0.04
TiO <sub>2</sub>	0.13	0.24	0.04	5.33	0.10	0.05
CaO	10.79	11.94	b.d.	0.02	0.08	0.04
Na <sub>2</sub> O	0.62	1.12	0.03	0.74	0.26	0.05
K <sub>2</sub> O	b.d.	b.d.	b.d.	9.05	b.d.	0.01
Cr <sub>2</sub> O <sub>3</sub>	0.02	0.03	b.d.	0.66	0.12	b.d.
Total	97.87	97.91	85.69	94.55	95.63	96.34
Basis (Oxygens):	23	23	14	11	11	11
Si	7.866	7.202	2.797	2.747	3.961	3.994
Al <sup>IV</sup>	0.134	0.798	1.203	1.253	0.039	0.006
Al <sup>VI</sup>	0.139	0.362	1.233	0.004	0.032	0.003
ΣAl	0.273	1.160	2.436	1.257	0.071	0.009
Fe <sup>2+</sup>	1.212	0.954	1.240	0.427	0.397	0.169
Fe <sup>3+</sup>	0.081	0.277				
Mg	3.742	3.427	3.483	2.080	2.529	2.817
Mn	0.031	0.029	0.019	0.001	0.004	0.002
Ti	0.014	0.026	0.003	0.291	0.005	0.002
Ca	1.635	1.819	0.000	0.001	0.006	0.003
Na	0.170	0.309	0.006	0.105	0.033	0.006
K	0.000	0.000	0.000	0.838	0.000	0.001
Cr	0.002	0.003	0.000	0.038	0.006	0.000
Total	15.027	15.206	9.984	7.785	7.012	7.003

<sup>a</sup> All Fe as FeO. <sup>b</sup>Fe<sub>2</sub>O<sub>3</sub> is midpoint between minimum and maximum. All abbreviations and analytical techniques as in Tables 1 and 2.

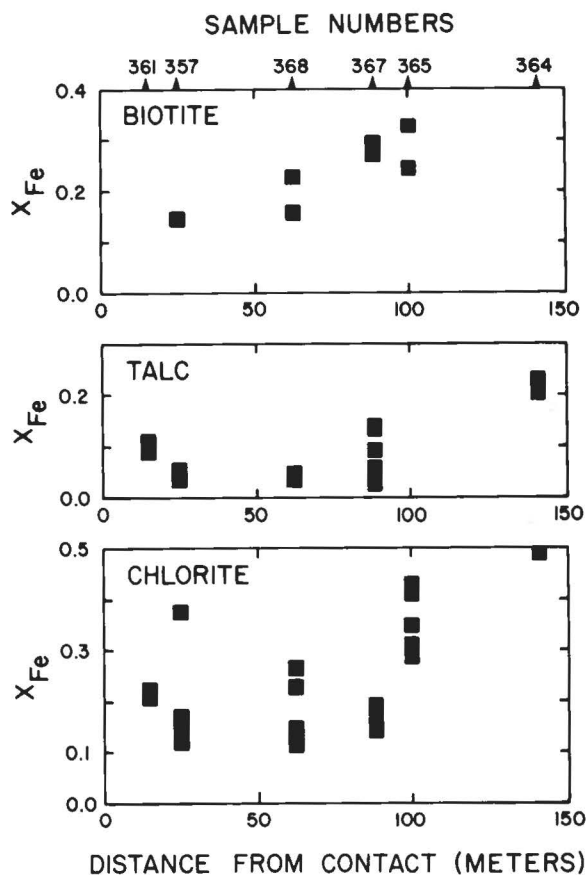


Fig. 43. Mole fractions of total octahedral iron in biotite, talc and chlorite within metasomatic reaction zones about amphibole veins in the Marginal Border Group and the cross-bedded belt of the Lower Zone gabbros as a function of distance from the contact at Uttental Pass (see Figs 13B and 34 for sample locations).

to the intrusive contact and is filled by green actinolitic hornblende ( $X_{Fe^{2+}} = 0.25$ ) where the vein cuts plagioclase, brown hornblende ( $X_{Fe^{2+}} = 0.25$  to  $0.29$  and  $n_{Al^{IV}} = 1.5$  to  $1.6$  per 23 oxygens) where the vein cuts clinopyroxene, and orthopyroxene ( $X_{Fe^{2+}} = 0.30$  to  $0.33$ , see Fig. 20) where the vein cuts relict olivines (Table 10A). Trace amounts of chlorite ( $X_{Fe} = 0.31$  to  $0.44$ ) are also found in the vein.

Plagioclase appears to be only slightly altered near the vein. Equant crystals of plagioclase within the vein are surrounded by actinolitic hornblende and have higher concentrations of the anorthite component than the igneous plagioclase (Analysis 6, Table 10A). This is shown in Fig. 46 where it can be seen that the vein plagioclase contains about 80 mole percent  $CaAl_2Si_2O_8$ , which is about 15–20 mole percent larger than the igneous plagioclase near the vein.

Near the vein margin igneous clinopyroxenes are altered to secondary clinopyroxenes ( $X_{Fe^{2+}} = 0.22$  to  $0.27$ ) that display elemental enrichments and depletions rela-

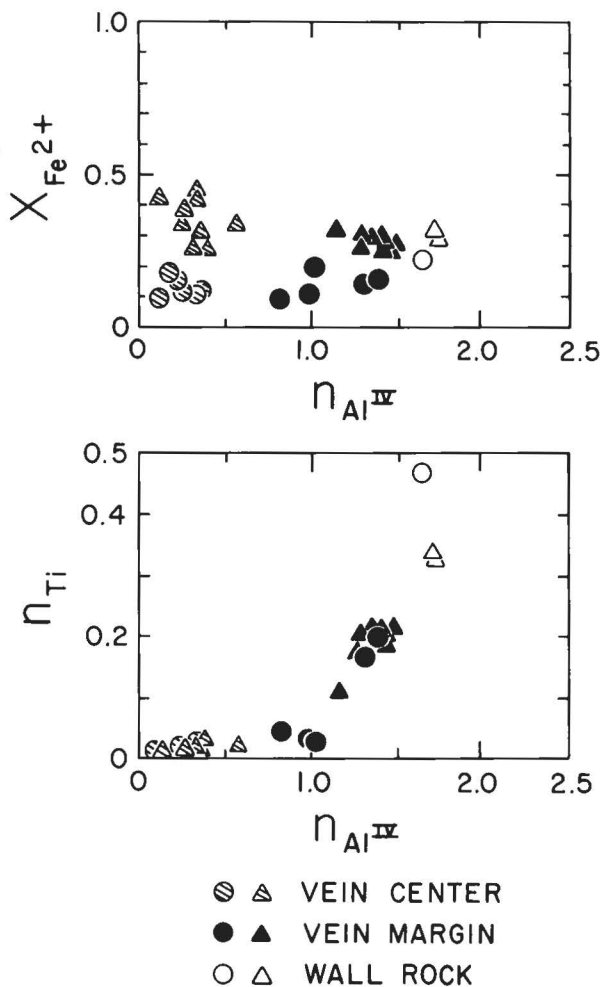


Fig. 44. Compositions of calcic amphiboles within and near veins of the Marginal Border Group near Uttental Pass. Circles represent vein 357-EG82, which is 25 meters from the contact and triangles represent 365-EG82, which is 100 meters from the contact (see Figs 13B and 34 for sample locations). Hatched symbols denote vein center amphiboles, solid symbols are hornblendes at the vein margin and open symbols are paragonitic hornblendes in the Marginal Border Group that are greater than one centimeter from mineralized fractures. See Fig. 16 caption for explanation.

tive to associated igneous augites that are similar to those in pyroxenes of the calcic amphibole-clinopyroxene-biotite veins in the Layered Series (see Fig. 20). Trace amounts of biotite ( $X_{Fe} = 0.29$  to  $0.31$ ) occur with the secondary pyroxenes as well as with oxides. Olivine, although not abundant in these rocks, is commonly pseudomorphed by fine-grained mixtures of talc and magnetite up to 2 mm from the vein margin.

*Mellemø:* Near the contacts of the gneiss, sediment and gabbro at Mellemø (Fig. 36) mineralized fractures occur with a slightly higher frequency than at the Kraemer Ø or Uttental Pass localities (Fig. 41). The prominent vein



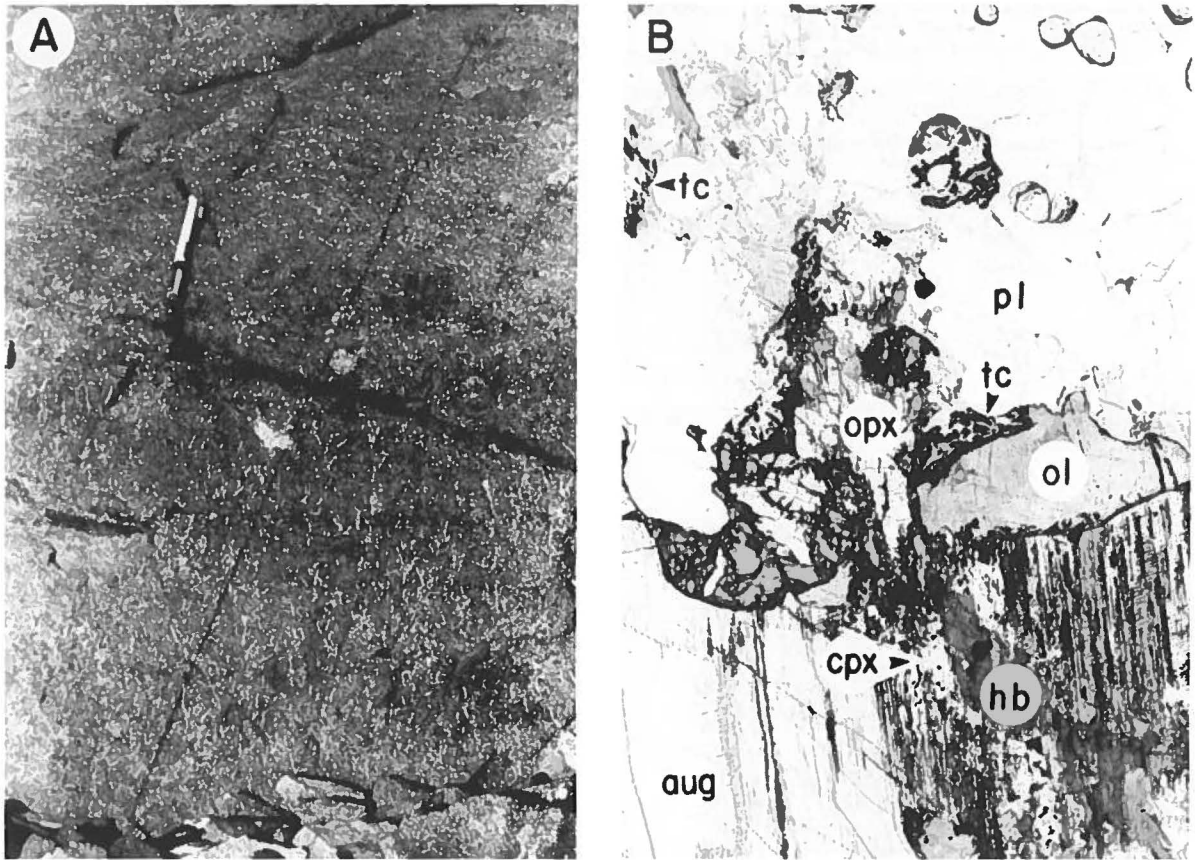


Fig. 45. Photographs of calcic amphibole-pyroxene-biotite veins of the Marginal Border Group. A) exposure of veins in perpendicular feldspar rock of Mellemø (pen is 14 cm long). B) photomicrograph of vein 318-EG82 (see Fig. 35). Magmatic augite (aug) and olivine (ol) are replaced by hydrothermal clinopyroxene (cpx), and talc (tc) and oxides, respectively, at vein margins. Where the fracture cuts augite or plagioclase (pl), the vein-filling mineral is hornblende (hb), but where olivine is cut, it is orthopyroxene (opx) (field of view is 4 mm wide).

sets in the gneisses are approximately parallel to the intrusive contact, which is similar to the Kraemer Ø locality. These veins are filled with quartz and alkali feldspars. In many places open pockets up to 5 cm long are lined by euhedral crystals along these veins. Within the chilled marginal gabbros and the Tranquil Division of the Marginal Border Group thin black weathering amphibole veins occur with a frequency of up to ~4 veins per meter (Fig. 36). The amphibole-rich veins form a prominent set that trends at an angle of ~60° E of the intrusive contact, which strikes roughly north-south and dips 20° E. No black weathering amphibole-rich veins are found within the coarse-grained Banded Division, but a spectacular quartz-rich vein system occurs here that is closely related to pegmatitic clot-like granophyres (see below).

Black weathering veins in the Tranquil Division are typically >0.5 mm wide with thin metasomatic reaction zones that may be up to 3 mm wide (Fig. 45A). These veins are filled primarily with calcic amphiboles, talc and chlorite. Complex textures, fabrics and mineral

zoning indicate that several episodes of fracture mineralization have occurred within many of these veins.

Vein sample 93-EG81 (Fig. 36) contains anorthite-rich plagioclase, ortho- and clinopyroxenes in addition to calcic amphiboles, biotite, talc and chlorite. In this vein and many others that contain hydrothermal pyroxenes, the main hydrothermal phase is brown magnesium-rich hornblende ( $X_{Fe^{2+}} = 0.15$  to  $0.28$ ,  $n_{Al^{IV}} = 1.0$  to 1.6 moles per 23 oxygens) that fills about 80% of the fracture. Actinolite ( $X_{Fe^{2+}} = 0.20$  to  $0.25$ ) and orthopyroxene ( $X_{Fe^{2+}} = 0.27$ , Fig. 20) also occur as vein-filling material. The orthopyroxene (see Fig. 20) is restricted to portions of the vein that cut olivine or plagioclase.

Igneous plagioclase ( $X_{An} = 0.65$  to  $0.75$ ) near the fracture-filling orthopyroxene is replaced by anorthite-rich plagioclase ( $X_{An} \sim 0.85$ ) similar to vein 318-EG82 in Fig. 46. Igneous clinopyroxenes cut by the vein are partially replaced by hydrothermal clinopyroxenes ( $X_{Fe^{2+}} = 0.17$  to  $0.23$ ) that are similar texturally to hydrothermal clinopyroxenes found in 318-EG82 and within the Layered Series gabbros (see Fig. 20). Biotite

Table 10A. Selected electron microprobe analyses of Marginal Border Group early amphibole vein minerals from Kraemer Ø and Mellemø.

	1 318B-58 Actinolite	2 318B-42 Pargasitic- hornblende	3 318B-57 Ortho- pyroxene	4 318A-13 Clino- pyroxene	5 318B-72 Biotite	6 318B-29 Bytownite	7 93A-43 Talc	8 318B-45 Chlorite
SiO <sub>2</sub>	54.77	43.99	54.03	53.21	37.46	47.52	61.44	27.62
Al <sub>2</sub> O <sub>3</sub>	1.52	9.92	0.38	0.89	13.95	33.34	0.65	17.78
FeO	10.28	10.10	19.29	8.84	12.77 <sup>a</sup>		4.12 <sup>a</sup>	24.05 <sup>a</sup>
Fe <sub>2</sub> O <sub>3</sub>	0.48 <sup>b</sup>	1.67 <sup>b</sup>	0.28 <sup>c</sup>	0.00 <sup>c</sup>		0.66 <sup>d</sup>		
MgO	17.27	14.12	24.77	14.39	17.01	b.d.	27.30	16.99
MnO	0.13	0.09	0.34	0.18	0.03	b.d.	b.d.	0.31
TiO <sub>2</sub>	0.13	2.77	0.10	0.18	4.35	b.d.	b.d.	0.03
CaO	11.90	11.46	0.72	21.84	0.11	16.66	0.06	0.11
Na <sub>2</sub> O	0.29	2.08	b.d.	0.23	0.18	2.03	0.31	b.d.
K <sub>2</sub> O	0.06	1.09	b.d.	b.d.	8.96	0.02	b.d.	b.d.
Cr <sub>2</sub> O <sub>3</sub>	0.02	0.11	b.d.	0.03	0.17	b.d.	b.d.	b.d.
Total	97.85	97.40	99.91	99.79	94.99	100.23	93.90	86.89
Basis (Oxygens):	23	23	6	6	11	8	11	14
Si	7.848	6.475	1.985	1.984	2.776	2.178	4.009	2.917
Al <sup>IV</sup>	0.152	1.525	0.015	0.016	1.219	1.802	0.000	1.083
Al <sup>VI</sup>	0.105	0.196	0.002	0.023	0.000		0.050	1.131
ΣAl	0.257	1.721	0.017	0.039	1.219	1.802	0.050	2.214
Fe <sup>2+</sup>	1.232	1.243	0.593	0.276	0.792		0.225	2.124
Fe <sup>3+</sup>	0.052	0.185	0.008	0.000		0.023		
Mg	3.688	3.097	1.356	0.800	1.879	0.000	2.656	2.674
Mn	0.016	0.011	0.011	0.006	0.002	0.000	0.000	0.028
Ti	0.014	0.307	0.003	0.005	0.243	0.000	0.000	0.003
Ca	1.827	1.807	0.028	0.873	0.009	0.818	0.004	0.012
Na	0.081	0.594	0.000	0.017	0.026	0.180	0.040	0.000
K	0.011	0.205	0.000	0.000	0.847	0.001	0.000	0.000
Cr	0.002	0.013	0.000	0.001	0.010	0.000	0.000	0.000
Total	15.028	15.658	4.001	4.001	7.803	5.002	6.984	9.972

<sup>a</sup> All Fe as FeO. <sup>b</sup> Fe<sub>2</sub>O<sub>3</sub> is midpoint between minimum and maximum. <sup>c</sup> Fe<sub>2</sub>O<sub>3</sub> by charge balance. <sup>d</sup> All Fe<sub>2</sub>O<sub>3</sub>. All abbreviations and analytical techniques as in Tables 1 and 2.

is a minor component and is usually associated with iron oxides or altered pyroxenes near the vein margin. Olivine is replaced by fine-grained aggregates of talc ( $X_{Fe} = 0.01$  to 0.03) and magnetite. Chlorite ( $X_{Fe} = 0.17$ ) replaces plagioclase near altered olivines locally within the vein.

In vein 91-EG81 and other veins that do not contain hydrothermal pyroxenes the vein-filling brown hornblende crystals are broken by long continuous straight-walled fractures that are now filled with fibrous green actinolite and minor amounts of chlorite. Selected analyses of vein minerals in these late fractures are given in Table 10B. The late-stage actinolite and chlorite are more iron-rich than the earlier phases ( $X_{Fe} = 0.30$  to 0.50). Minor amounts of calcite, prehnite and serpentine are associated with this secondary fracturing and mineralization.

Within the Banded Division of the Marginal Border Group on Mellemø (Fig. 37) there is a complex array of quartz, actinolite and albite veins that have a very lim-

ited distribution within the Skaergaard intrusion. This vein system appears to be restricted to portions of the Banded Division that contain large amounts of conformable pegmatitic clot-like granophyres that have been described by Wager & Brown (1968) and Kays et al. (1981). Within the map area of Fig. 37 these veins form two prominent sets, one NW and the other ~E-W. The veins are most abundant near large concentrations of pegmatitic bodies and appear in the field to form a set of veins approximately perpendicular to the intrusive contact.

The quartz, actinolite and albite veins within the Banded Division occur as irregular, en echelon vein sets. Some individual veins are up to 50 meters long (see Fig. 37). Most veins are >1 cm wide, with the widest vein being about 4 cm wide. In outcrop these veins are white with pale green pockets of fibrous actinolite near the vein center (Fig. 47A). Quartz and/or albite have formed on the walls of the vein. Vein centers are commonly filled with large crystals (<3 mm long) of fibrous

Table 10B. Selected electron microprobe analyses of Marginal Border Group late amphibole vein minerals from Kraemer Ø and Mellemø.

	1 91B-3 Ferro-Actinolite	2 91B-1 Chlorite	3 91C-1 Biotite
SiO <sub>2</sub>	51.25	29.88	37.66
Al <sub>2</sub> O <sub>3</sub>	1.59	15.24	13.55
FeO	22.32	26.36 <sup>a</sup>	13.78 <sup>a</sup>
Fe <sub>2</sub> O <sub>3</sub>	0.79 <sup>b</sup>		
MgO	8.35	14.77	15.26
MnO	0.72	0.20	0.06
TiO <sub>2</sub>	0.04	0.04	5.31
CaO	11.84	0.04	0.04
Na <sub>2</sub> O	0.25	b.d.	0.37
K <sub>2</sub> O	b.d.	0.81	9.25
Cr <sub>2</sub> O <sub>3</sub>	b.d.	b.d.	0.01
Total	97.15	87.36	95.27
Basis (Oxygens):	23	14	11
Si	7.811	3.180	2.801
Al <sup>IV</sup>	0.189	0.820	1.189
Al <sup>VI</sup>	0.097	1.093	0.000
ΣAl	0.286	1.913	1.189
Fe <sup>2+</sup>	2.845	2.346	0.857
Fe <sup>3+</sup>	0.091		
Mg	1.897	2.342	1.691
Mn	0.093	0.018	0.004
Ti	0.005	0.003	0.297
Ca	1.934	0.005	0.003
Na	0.074	0.000	0.053
K	0.000	0.110	0.878
Cr	0.000	0.000	0.001
Total	15.036	9.917	7.774

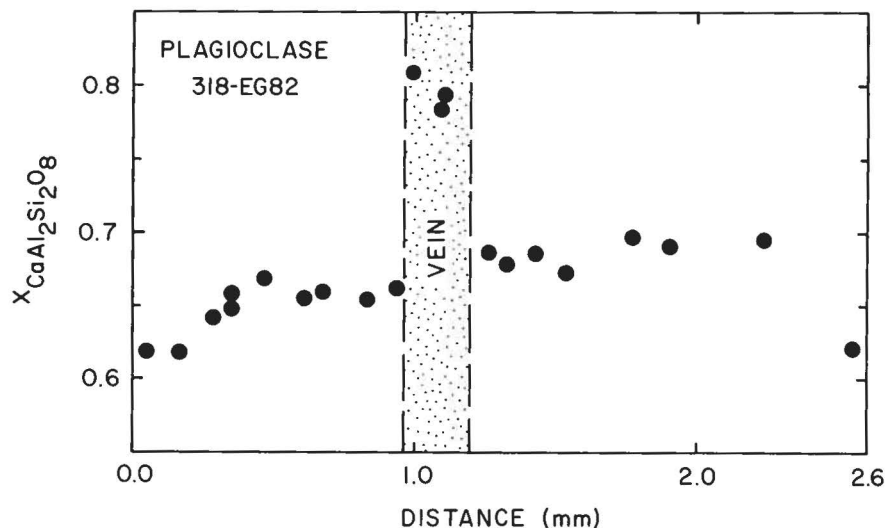
<sup>a</sup> All Fe as FeO. <sup>b</sup> Fe<sub>2</sub>O<sub>3</sub> is midpoint between minimum and maximum. All abbreviations as in Tables 1 and 2.

actinolite ( $X_{Fe^{2+}} = 0.50$  to  $0.63$  with up to 1 wt% F). In some cases euhedral crystals of quartz line or completely fill the fractures, but in others a thin layer of albite ( $X_{An} = 0.01$ ) forms on large plagioclase crystals ( $X_{An} = 0.49$ ) broken by the vein (Fig. 47B & C). In the wider veins micrographic intergrowths of quartz and alkali feldspars formed at the vein margins. Pegmatitic clinopyroxenes near the margins of the clot-like granophyres are replaced by actinolite ( $X_{Fe^{2+}} = 0.48$  to  $0.50$ ) near some of the veins. Minor replacement of plagioclase by sericite and minor amounts of chlorite are formed near the vein, together with thin serpentine veins.

Within the clot-like granophyres many of these individual veins diverge into thinner and more numerous veins that become less distinct towards the centers of the pegmatitic bodies. This geometric relationship suggests that the fluids responsible for the formation of the veins were exsolved from the pegmatitic clot-like granophyres. This is in part supported by the observation that these types of veins only occur near the pegmatitic bodies and do not occur outside the Banded Division of the Marginal Border Group of the Skaergaard intrusion.

*Ivnamut*: On the island of Ivnamut (Figs 38 & 48) the contact between the Skaergaard intrusion and Tertiary basalts is exposed over a distance of ~50 meters at the southwest part of the island (see Wager & Brown 1967: fig 73). Veins within the Marginal Border Group on Ivnamut are similar in mineralogy and abundance to those at Mellemø. Black weathering amphibole veins are abundant in the Tranquil Division and nearly absent in the Banded Division (compare fracture traverses T12 and T13 in Fig. 38). Quartz-rich vein systems similar to those described from the Banded Division on Mellemø

Fig. 46. Compositions of plagioclase within and near an orthopyroxene, hornblende, clinopyroxene, biotite, talc and plagioclase vein in the Marginal Border Group on Kraemer Ø (see Fig. 35 for sample location). Analyses are made on a single crystal of plagioclase 2.5 mm long that is cut by a 0.2 mm wide hydrothermal vein. Anorthite-poor analyses at the extremes of the diagram correspond to the margins of the plagioclase crystal. The anorthite-rich analyses in the vein are of small equant crystals in optical continuity with the wall rock plagioclase and surrounded by greenish-brown hornblende.



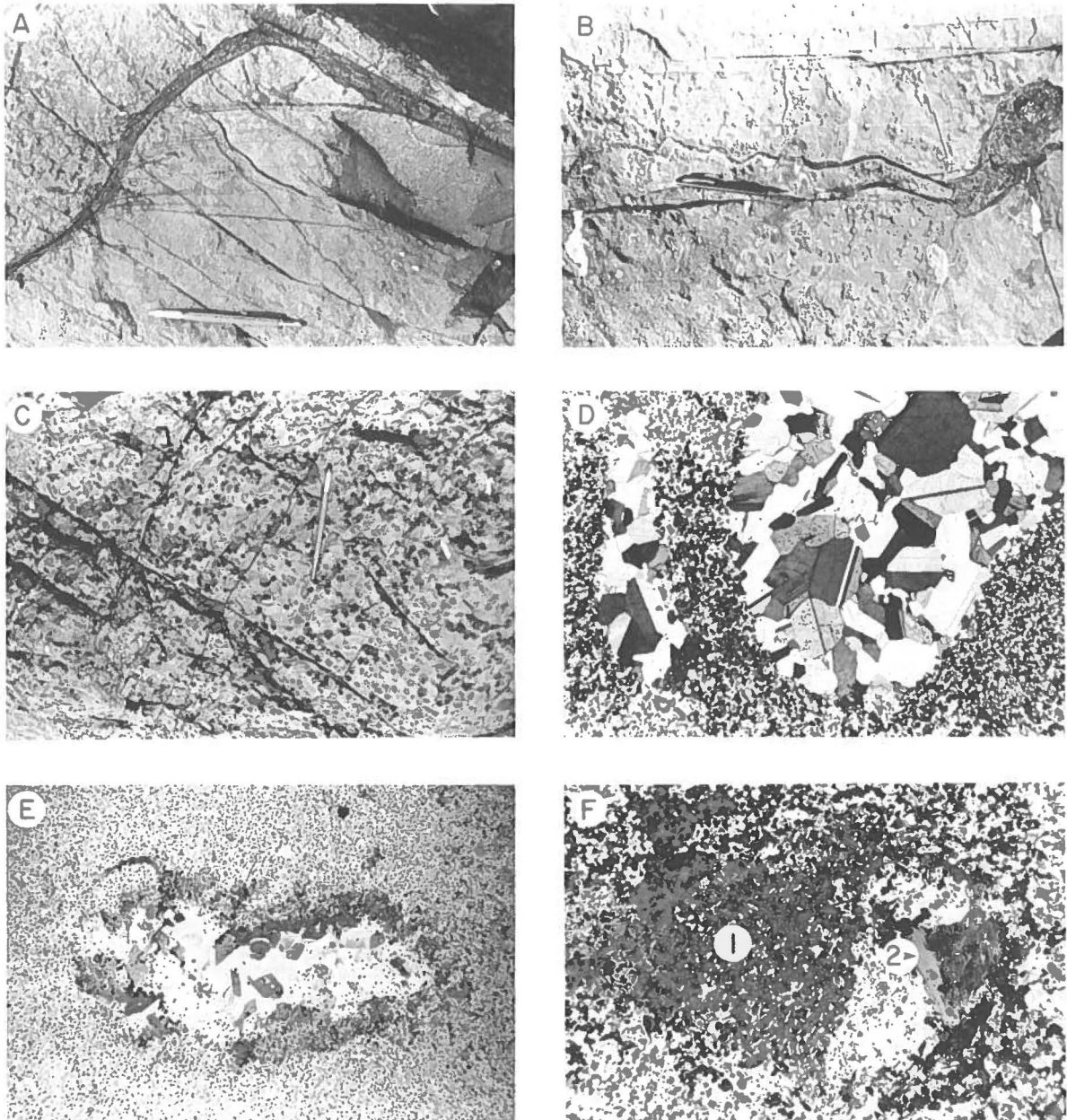


Fig. 49. Vein systems and metamorphism of basalts on Ivnermiut. A) olivine-pyroxene-oxide veins. B) olivine-pyroxene-oxide veins and plagioclase concentrations. C) olivine poikiloblasts in metabasalts. D) plagioclase concentrations in sample 430-EG82. E) amphibole concentrations in sample 441-EG82. F) Olivine poikiloblast (1) with minor amphiboles and biotite mineralization (2). Photomicrographs D, E and F are 1 cm wide, and the pencils in photos A, B and C are 14 cm long.

*South and east contacts:* Vein systems near the Skaergaard intrusion's contact with lavas, hyaloclastites and volcanoclastic breccias of the Vandfaldsdalen and Miki Formations, and the pre-Skaergaard sills occur in the map areas at the southern (Fig. 39) and eastern (Fig. 40) contacts. Black weathering amphibole and chlorite veins form dense and complex fracture systems near the contact zones (Fig. 51B). These veins are typically less

than 1 mm wide with well developed metasomatic reaction zones about the central fracture that may be up to 5 mm wide. Intense recrystallization and ductile deformation of the host rock occurs up to one meter from the contact. This deformation is particularly pronounced where clasts in volcanoclastic breccias are stretched parallel to the intrusive contact.

At the south contact area (Fig. 39) a prominent NNE

Table 11. Selected electron microprobe analyses of metabasalt matrix and deformed amygdules from Ivnamtut.

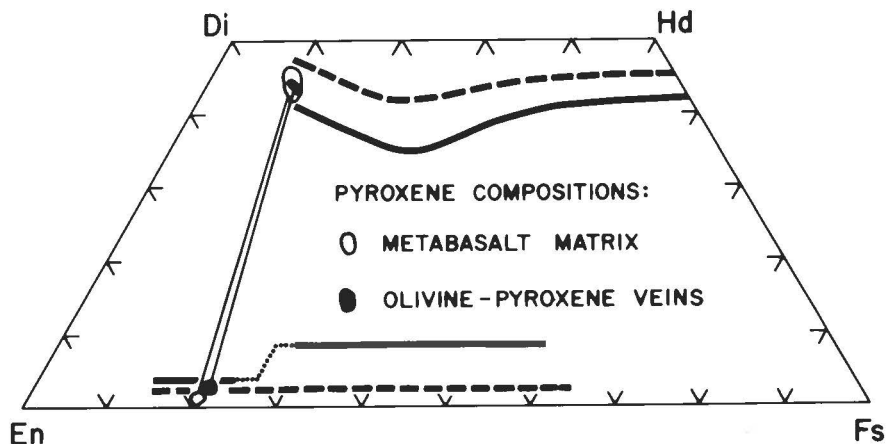
	1 400-29 Ortho- pyroxene	2 Matrix minerals 400-39 Clino- pyroxene	3 429A-18 Olivine (Chrysolite)	4 400-38 Labradorite	5 106C-14 Labradorite	6 Amygdule minerals 106C-4 Pargasitic hornblende	7 106C-5 Biotite
SiO <sub>2</sub>	55.46	51.62	38.83	52.88	52.31	43.96	37.96
Al <sub>2</sub> O <sub>3</sub>	1.14	2.63	b.d.	29.99	29.80	10.20	14.28
FeO	12.86	5.53	20.62 <sup>a</sup>			8.36 <sup>c</sup>	9.56 <sup>a</sup>
Fe <sub>2</sub> O <sub>3</sub>	0.00 <sup>b</sup>	1.44 <sup>b</sup>		0.61 <sup>d</sup>	0.54 <sup>d</sup>	1.19	
MgO	29.18	15.68	40.41	0.03	0.02	15.27	18.03
MnO	0.38	0.22	0.27	b.d.	b.d.	0.04	b.d.
TiO <sub>2</sub>	0.32	0.96	0.01	0.06	0.03	3.65	5.63
CaO	1.03	21.03	0.06	12.54	12.26	11.60	0.03
Na <sub>2</sub> O	b.d.	0.42	b.d.	4.34	4.47	2.33	0.65
K <sub>2</sub> O	b.d.	b.d.	n.a.	0.15	0.06	0.76	9.14
Cr <sub>2</sub> O <sub>3</sub>	b.d.	0.07	b.d.	b.d.	b.d.	0.05	0.07
Total	100.37	99.60	100.20	100.60	99.49	97.41	95.35
Basis (Oxygens):	6	6	4	8	8	23	11
Si	1.968	1.910	0.999	2.385	2.384	6.407	2.764
Al <sup>IV</sup>	0.032	0.090		1.596	1.602	1.593	1.226
Al <sup>VI</sup>	0.016	0.025				0.160	0.000
ΣAl	0.048	0.115	0.000	1.596	1.602	1.753	1.226
Fe <sup>2+</sup>	0.382	0.171	0.444			1.019	0.582
Fe <sup>3+</sup>	0.000	0.040		0.021	0.019	0.130	
Mg	1.543	0.865	1.550	0.002	0.001	3.317	1.957
Mn	0.011	0.007	0.006	0.000	0.000	0.005	0.000
Ti	0.009	0.027	0.000	0.002	0.001	0.400	0.308
Ca	0.039	0.834	0.002	0.606	0.599	1.812	0.002
Na	0.000	0.030	0.000	0.380	0.395	0.659	0.092
K	0.000	0.000	-	0.009	0.003	0.141	0.849
Cr	0.000	0.002	0.000	0.000	0.000	0.006	0.004
Total	4.000	4.001	3.001	5.001	5.004	15.649	7.783

<sup>a</sup> All Fe as FeO. <sup>b</sup> Fe<sub>2</sub>O<sub>3</sub> by charge balance. <sup>c</sup> Fe<sub>2</sub>O<sub>3</sub> is midpoint between minimum and maximum. <sup>d</sup> All Fe as Fe<sub>2</sub>O<sub>3</sub>. All abbreviations and analytical techniques as in Tables 1 and 2.

vein set occurs both within the gabbro and the basalts near the contact zone. These veins are subparallel to the leucocratic granophyres within the Skaergaard intrusion and their abundance is locally >23 veins per meter.

Other prominent fracture sets represented by the rose diagrams in Fig. 39 seem to have a restricted areal distribution relative to the three traverses made within the map area. Similar relationships are apparent from the

Fig. 50. Compositions of Ca-rich and Ca-poor pyroxenes from metabasalts (400-EG82) and from an olivine-pyroxene vein (429A-EG82) at Ivnamtut. See Fig. 48 for sample locations and Fig. 9 for abbreviations.





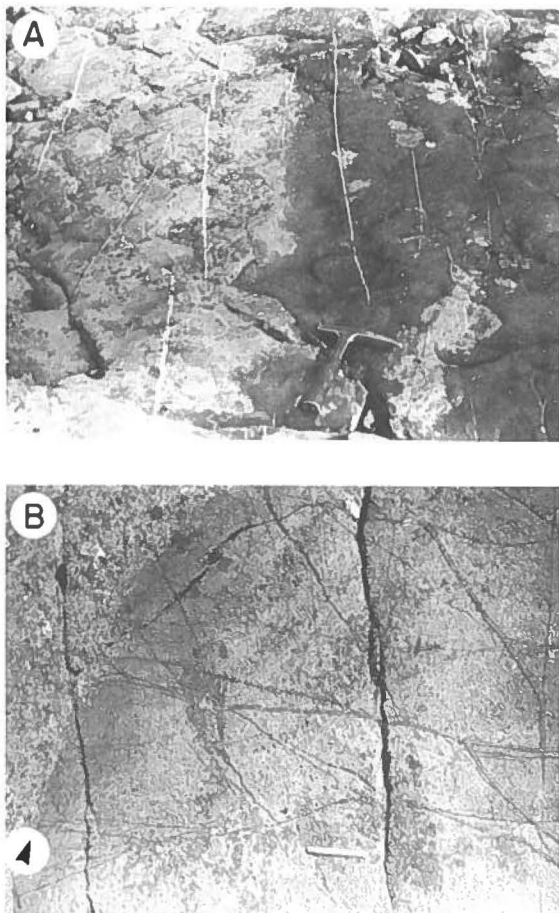


Fig. 51. A) Photograph of the contact parallel milky-white quartz veins in the metabasalts near the east contact of the Skaergaard intrusion (see Fig. 40, hammer is 30 cm long). B) exposure of amphibole veins in a pre-Skaergaard sill at the south contact (Fig. 39). The contact is marked by the arrow, and the Skaergaard intrusion is the coarse-grained rock in the left of the photo (match is 4 cm long).

observations made at the east contact (Fig. 40), but in the latter case the most abundant amphibole mineralized fracture set is subparallel to the intrusive contact.

A remarkably uniform set of quartz veins occurs subparallel to the eastern contact of the Skaergaard intrusion in Fig. 40. These veins occur in the pre-Skaergaard basalts and sills and are not found at distances greater than about 100 meters from the contact. The quartz veins are typically <2 cm wide and are continuous for several meters (Fig. 51A). They form intricate en echelon arrays with curved out-of-plane propagation features near some of their terminations. At several locations within the map area of Fig. 40 it is apparent that thin (<10 cm wide) granitic veins and thin dikes are closely associated with the quartz veins. Veins between 0.5 and 2 cm wide contain subhedral crystals of feldspar

and quartz lining the fracture with central pockets that are filled with pale green amphiboles. These veins appear in the field to be similar to quartz-actinolite-chlorite veins within the Banded Division of the Marginal Border Group (Fig. 37). The spatial and temporal relationships between the quartz veins and the black to rust-brown weathering veins is complex. Crosscutting relations indicate that the quartz veins are both older and younger than all the types of black and rust weathering amphibole and chlorite veins. Some vein sets and breccias appear to be associated with the emplacement and cooling of pre-Skaergaard sills that are found throughout the region (Bird et al. 1985). Late stage drusy quartz and epidote veins crosscut all the vein types described above. These veins may be up to 3 cm wide and contain minor amounts of albite. They were formed approximately parallel to the mafic dikes within the study area and thus may be associated with this later magmatic event.

### Fracture systems in the basalt host rocks

The abundance and orientation of amphibole and chlorite veins in the basalts near the contact with the Skaergaard intrusion have been presented above in Figs 39, 40 & 48. Near the Skaergaard intrusion fractures in the basalts are more abundant by at least an order of magnitude than fractures in the gneisses (compare Figs 34–36 with Figs 39, 40 & 48).

In a traverse east from the Skaergaard intrusion to Miki Fjord from the area of Fig. 40 to point E6 in Fig. 3 the abundance of veins decreases from as many as 64 veins per meter to 1.5 veins per meter as shown by the rose diagrams of vein abundance and orientation given in Figs 40 and 52. This traverse is approximately the same as the east contact traverse used by Taylor & Forrester (1979) to determine the variation in whole rock  $\delta^{18}\text{O}$  in the basalts marginal to the Skaergaard intrusion. In their study they report a change in  $\delta^{18}\text{O}$  from <2 at the contact to >2.5 near point E6 in Fig. 3, then a decrease to 1.8 near the shore of Miki Fjord. The mineralogy of the veins changes as a function of distance from the Skaergaard intrusion and from pre-Skaergaard sills that are <20 meters thick within the basalts. Black to rust-brown calcic amphibole and chlorite veins are the dominant type of veins within distances of ~300 meters from the eastern side of the intrusion. Beyond 300 meters distance from the Skaergaard intrusion the abundance of white quartz, epidote and calcite veins increases relative to black amphibole and chlorite veins; at ~500 meters from the intrusion they are the only vein type found.

Epidote-quartz veins occur at distances greater than ~50 meters east and south of the Skaergaard intrusion. These veins may be up to 3 cm wide and commonly contain prehnite. In sample 163-EG81, which is ~100 me-

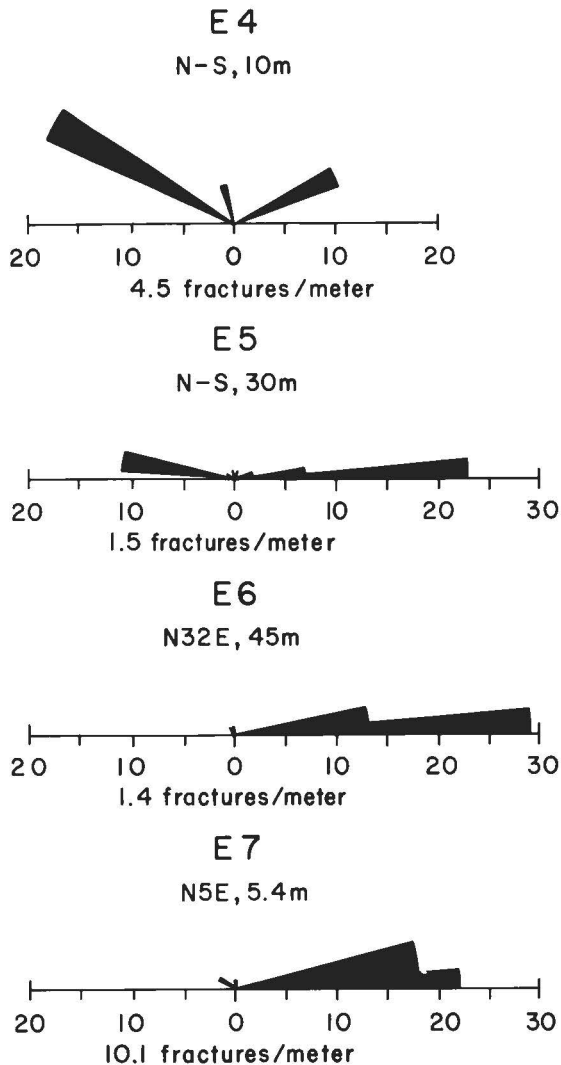


Fig. 52. Rose diagrams of vein abundance and orientation in the basalts east of the Skaergaard intrusion. See Fig. 3 for locations of the fracture traverses and figure caption 34 for explanation. Traverse E7 is located ~80 meters south of point E6 in Fig. 3.

ters south of the Skaergaard intrusion (Fig. 3), a vein 1.5 cm wide contains euhedral crystals of epidote ( $X_{\text{Ca}_2\text{Fe}_3\text{Si}_3\text{O}_{12}(\text{OH})} = 0.25$  and 0.31) and quartz that form layers on the vein walls up to 3 mm thick. Prehnite ( $X_{\text{Ca}_2\text{FeAlSi}_3\text{O}_{10}(\text{OH})_2} = 0.25$ ) fills the central portions of the fracture. Calcite lines or fills small pockets within the center of this vein. Compositions of coexisting prehnite and epidote from this vein are given in Fig. 29. Veins of this type have been found within the basalts to the south and east of the intrusion. They usually strike east-west, similar to the mafic dikes in the area. It could not be determined in the field whether the epidote, prehnite and quartz veins were older or younger than the mafic dikes.

It is important to note, however, that we have never found a vein of this type crosscutting the mafic dikes.

Andradite-rich garnet occurs in calcite filled patches and veins in the Miki Formation basalts east of the intrusion at locality 659-EG84 (see Fig. 3 for location). Near this locality there are veins lined with garnet, epidote and salitic pyroxenes are filled with calcite and quartz. Grandite garnet also occurs near vein 163-EG81 in the basalts south of the Skaergaard intrusion where it fills amygdules together with epidote, actinolite, chlorite and quartz. From our preliminary investigation of the basalts it appears that the formation of grandite garnet is restricted to distances of less than about 800 meters from the contact of the Skaergaard intrusion.

Alteration of the basalts at distances greater than 800 meters east and south of the intrusion are associated with the formation of varied and complex mineral assemblages than may contain epidote, prehnite, chlorite, albite, pumpellyite, calcite, quartz, serpentine and zeolites. A summary of some of these phase relations is given by Bird et al. (1985).

## Physical and chemical conditions of vein mineralization

Evaluation of intensive thermodynamic parameters of the Skaergaard intrusion has been the subject of numerous studies (Lindsley et al. 1969; Williams 1971; McBirney 1975; Naslund 1980; Taylor & Forester 1979; Norton & Taylor 1979; Sato & Valenza 1980; Morse et al. 1980). These studies have primarily addressed conditions associated with the crystallization and cooling of the magmatic phases. In some cases mineral assemblages within and near vein systems of the Skaergaard intrusion allow evaluation of intensive thermodynamic parameters associated with chemical reactions that formed the vein mineralogy. In this respect the vein mineralogy provides a record of the conditions for fluid flow and reaction of aqueous solutions or magmas during the subsolidus cooling history of the intrusion. In this section we present an outline of the experimental and thermodynamic constraints on mineralogic phase relations of some of the characteristic vein systems associated with the Skaergaard magma-hydrothermal system. Emphasis is placed on the temperature,  $O_2$  and  $CO_2$  fugacities, and activities of aqueous species associated with the formation of vein assemblages in the system  $Na_2O$ -CaO-MgO-FeO- $Fe_2O_3$ - $TiO_2$ - $Al_2O_3$ - $SiO_2$ - $H_2O$ - $CO_2$ . A more detailed thermodynamic analysis of mineralogic phase relations in the veins of the Skaergaard intrusion will be presented by Bird & Manning (in prep.).

The pyroxene-oxide veins within Upper Border Group xenoliths in the Middle Zone gabbros are among the earliest veins formed within the Skaergaard intrusion. Fig 9A demonstrates that tie lines between coexisting pyroxenes have orientations similar to those of

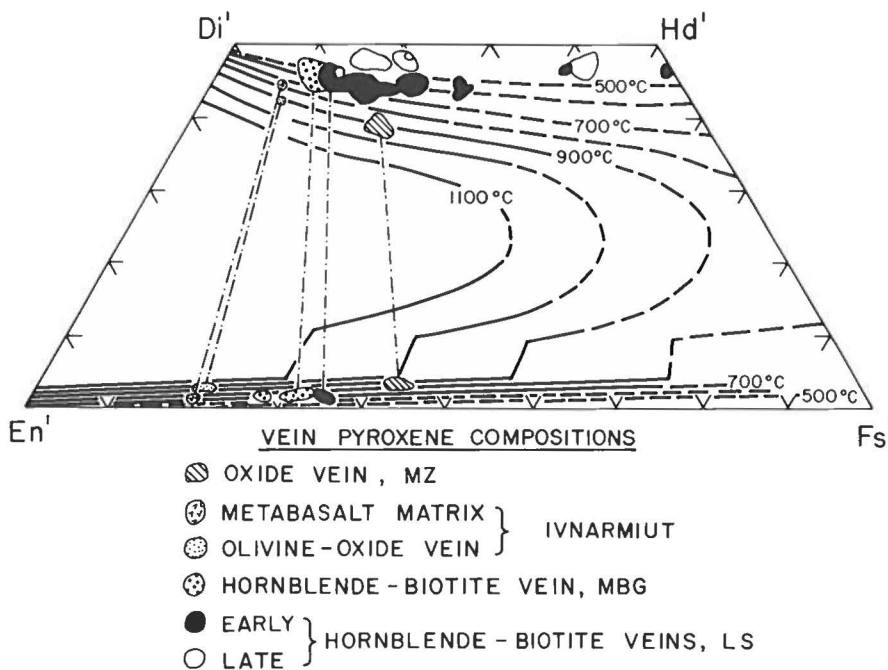


Fig. 53. Compositions of vein pyroxenes from the Skaergaard intrusion represented in a pyroxene quadrilateral with the 1 atmosphere pyroxene solvus of Lindsley & Anderson (1983) and Lindsley (1983). Pyroxene analyses are projected onto the quadrilateral using equations and data presented by Lindsley & Anderson (1983).

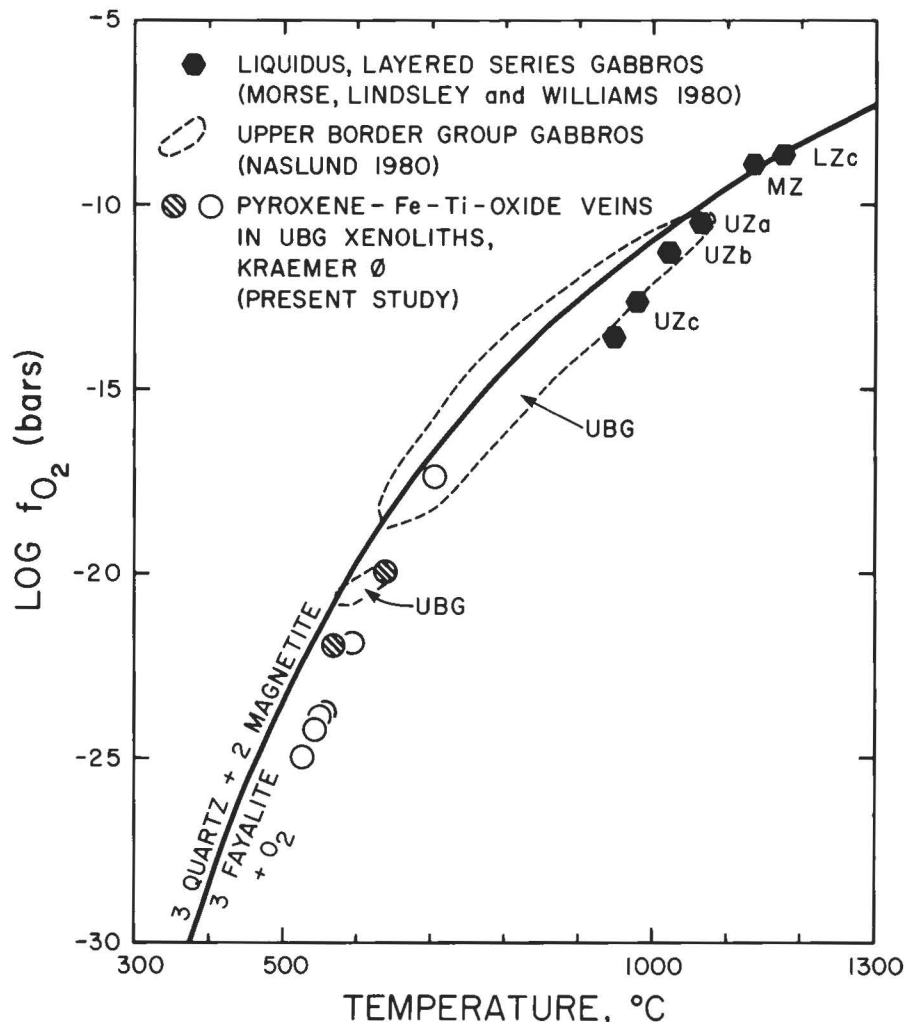
the Middle zone pyroxenes, suggesting that solidus temperatures in the pyroxene-oxide veins were similar to the Middle Zone solidus. Phase relations among ilmenite, and Ca-rich and Ca-poor pyroxenes reported by Bishop (1980), Kretz (1982), Lindsley & Anderson (1983) and Lindsley (1983) can be used to place constraints on the temperatures of subsolidus reactions within the pyroxene-oxide veins. The compositions of pyroxenes from vein 321-EG82 given in Fig. 9A and Table 1, together with the experimentally determined 1 atmosphere isotherms for the pyroxene solvus in the system  $\text{CaFeSi}_2\text{O}_6\text{-CaMgSi}_2\text{O}_6\text{-Mg}_2\text{Si}_2\text{O}_6\text{-Fe}_2\text{Si}_2\text{O}_6$  presented by Lindsley & Anderson (1983) and Lindsley (1983) are given in Fig. 53. This figure suggests that subsolidus equilibration of Ca clinopyroxenes and orthopyroxenes occurred within the range of 800° to 1000°C. Calculations using the equations of Kretz (1982) yield a similar temperature range. These values are consistent with predicted temperatures of 950°C for coexisting pyroxene and ilmenite compositions based on equations reported by Bishop (1980). In contrast to the pyroxenes, titanomagnetite and ilmenite compositions evaluated by both microprobe (Table 1) and XRD analyses, combined with temperature-oxygen fugacity-composition relations reported by Spencer & Lindsley (1981), suggest that reactions among Fe-Ti oxides occurred to temperatures as low as 550° to 750°C. The results of the latter calculations are presented in Fig. 54 together with predicted oxygen fugacities and temperature relations reported for the Upper Border Group rocks by Naslund (1980) and for the Layered Series gabbros by Morse et al. (1980). Temperature and oxygen fugacities of the py-

roxene-oxide veins given in Fig. 54 overlap, in part, with Fe-Ti oxide temperatures and oxygen fugacities in the Upper Border Group rocks, which have reacted extensively with aqueous solutions during the subsolidus cooling of the Skaergaard intrusion (Taylor & Forester 1979; Naslund et al. 1983; Naslund 1984a). The low temperatures predicted from vein Fe-Ti oxide compositions may be the result of irreversible reactions between the oxides and hydrothermal solutions during the subsolidus cooling history of the Skaergaard intrusion. It should be pointed out that these temperatures (550° to 750°C) correspond to predicted minimum temperatures of the early hydrothermal amphibole-clinopyroxene-biotite veins of the Layered Series (see below). The higher temperature predicted from partitioning of  $\text{Fe}^{2+}$  and  $\text{Mg}^{2+}$  between pyroxenes and ilmenite appears to be consistent with slow reaction rate for the reduction of ilmenite-hematite solid solutions relative to the oxidation of magnetite (Hammond & Taylor 1982).

Crosscutting relations have not been observed between all the hydrothermal vein types. However, the relative age of the different veins can be predicted from phase relations and compositions of vein minerals, together with the cooling history of the Skaergaard intrusion presented by Norton & Taylor (1979). In particular, the temperatures predicted from the phase equilibrium constraints within the veins can be combined with the numerical predictions of Norton & Taylor's cooling history of the intrusion to evaluate the relative timing of the fracture mineralization.

Hydrothermal veins in the Layered Series are filled primarily with calcic amphiboles. These veins can be di-

Fig. 54. Predicted oxygen fugacity and temperature relationships for the Skaergaard intrusion based on the compositional relations of Fe-Ti oxides. The circles represent the oxygen fugacities and temperatures for compositions of titanomagnetite and ilmenite in pyroxene-oxide veins in the Upper Border Group xenoliths within the Middle Zone gabbros. The open circles denote calculations made using microprobe analyses and the hatched circles denote calculations made from XRD analyses. The solid curve represents equilibrium between quartz, fayalite and magnetite at 2 kilobars calculated from equations and data reported by Helgeson et al. (1978). See text.



vided into two types: those in which calcic amphiboles display complete solubility of  $Al^{IV}$  within the range of 0.4 to 1.0 moles per 23 oxygens (actinolitic hornblende-biotite-chlorite-talc veins in the Lower Zone and calcic amphibole-calcic pyroxene-biotite veins of the Lower Zone c to Upper Zone gabbros), and those in which calcic amphiboles display a gap in the solubility of  $Al^{IV}$  (hornblende-actinolite-biotite veins throughout the Layered Series, hornblende-actinolite-albite-epidote veins that are associated with the fallen Upper Border Group blocks and the Trough Bands, and amphibole veins associated with the terminations of transgressive granophyres). We have designated pyroxene-bearing amphibole veins that do not have a distinct gap in  $Al^{IV}$  concentrations of calcic amphiboles as "early" veins. This is to distinguish them from veins that contain amphiboles with a gap in the  $Al^{IV}$  concentration, which are referred to as "late" veins. The late veins may contain pyroxenes, but these are enriched in  $CaSiO_3$  relative to the early vein pyroxenes of similar  $Fe^{2+}/Mg$  ratios (see

Figs 20 & 53). The late veins are characterized by paragenetic relations that indicate several stages of amphibole mineralization including formation of actinolite and low-Ti green pargasitic hornblende.

The lack of a gap in  $Al^{IV}$  solubility in calcic amphiboles from the actinolitic hornblende-biotite-chlorite-talc veins of the Lower Zone a and b gabbros suggests that this vein type was probably coeval with the formation of the calcic amphibole-clinopyroxene-biotite veins in the overlying Lower Zone c to Upper Zone gabbros. The different mineral assemblages in these two vein types is apparently a function of changes in the bulk rock composition of the Layered Series as determined by the fractionation trend; in particular, the variations in the modal abundance of olivine, magnetite and clinopyroxene in the vicinity of the Lower Zone c gabbros.

Partitioning of  $Fe^{2+}$  and Mg among hornblende, biotite and clinopyroxene in veins containing calcic amphibole with no gap in  $Al^{IV}$  solubility are similar to amphibole facies metamorphic mineral assemblages repor-

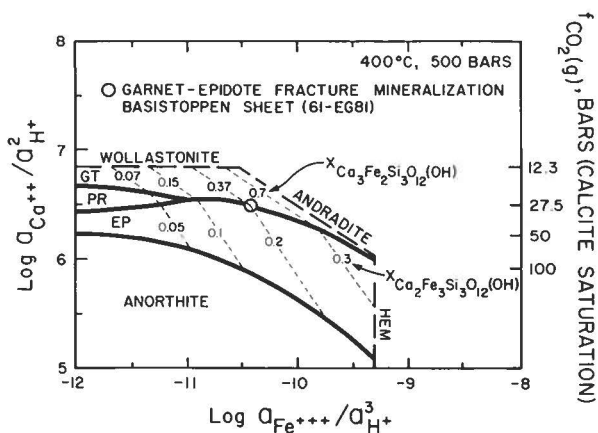


Fig. 56. Activity-activity phase diagram in the system  $\text{CaO-Al}_2\text{O}_3\text{-Fe}_2\text{O}_3\text{-SiO}_2\text{-H}_2\text{O-CO}_2$  at quartz saturation and unit activity of water. The thin dashed lines represent the compositions of epidote and garnet, and the open circle represents the measured compositions within vein 61-EG81. Diagram is computed from equations and data reported by Helgeson & Kirkham (1974a,b, 1976), Helgeson et al. (1978, 1981) and Bird & Helgeson (1980). See text.

transport models presented in Fig. 55 that epidote and garnet within the vein margin are stable between about 320° and 450°C at 500 bars during a period of time from about 350 000 to 450 000 years after the emplacement of the Skaergaard intrusion.

The activity-activity phase diagram given in Fig. 56 illustrates epidote, garnet and prehnite phase relations at 400°C and 500 bars in terms of the activity ratios of  $a_{\text{Ca}^{++}}/a_{\text{H}^+}^2$  and  $a_{\text{Fe}^{+++}}/a_{\text{H}^+}^3$  in the coexisting aqueous solution. The open circle denotes the measured compositions of epidote and garnet near the vein margin for the limiting case of quartz saturation and unit activity of  $\text{H}_2\text{O}$ . It can be seen in this phase diagram that andradite cannot be in equilibrium with epidote of any composition. A maximum value of the fugacity of  $\text{CO}_2$  ( $f_{\text{CO}_2}$ ) can also be determined from the phase diagram. Because calcite is absent from the vein assemblage,  $f_{\text{CO}_2}$  in the vein-forming fluids must have been less than ~27 bars.

Reaction A given in Fig. 55 can also be used to evaluate the maximum temperature of formation of the prehnite, epidote, quartz and calcite vein (163-EG81) in the metabasalts marginal to the intrusion at Hammer Gletscher (Fig. 3). This reaction defines the maximum temperature for the stability of prehnite, epidote and quartz in the absence of garnet. The maximum temperature at 450 bars pressure (see below) computed using the law of mass action for reaction A (Fig. 55), the compositions of epidote and prehnite reported in Fig. 29 and equations and data reported by Helgeson & Kirkham (1974a), Helgeson et al. (1978) and Bird & Helgeson (1980) is about 290°C. Phase relations in the system  $\text{CaO-FeO-Fe}_2\text{O}_3\text{-Al}_2\text{O}_3\text{-SiO}_2\text{-H}_2\text{O-CO}_2$  are given in Fig. 57 at 250° and 300°C at 450 bars for quartz saturation

and unit activity of water. The open circle in diagram B denotes the values of  $a_{\text{Ca}^{++}}/a_{\text{H}^+}^2, a_{\text{Fe}^{+++}}/a_{\text{H}^+}^3$  and fugacity of  $\text{CO}_2$  in the fluid phase in equilibrium with the averaged compositions of the vein assemblage of epidote, prehnite, quartz and calcite. Note that the predicted fugacity of  $\text{CO}_2$  is only ~2 bars. It is also apparent in comparing diagrams A and B in Fig. 57 that prehnite with a composition of  $X_{\text{Ca}_2\text{Fe}(\text{AlSi}_3\text{O}_{10})(\text{OH})_2} > 0.23$  is not stable at 300°C as predicted from the law of mass action for reaction A in Fig. 55 above.

Fluid inclusion freezing and homogenization temperatures were made on four quartz-rich veins within the basalt host rocks near the Skaergaard intrusion. Analyses were made on a nitrogen gas flow heating and cooling stage described by Hollister et al. (1981). Equivalent weight percent of NaCl in the fluids are calculated from equations and data reported by Potter et al. (1978). Results of the homogenization of the low-salinity liquid-rich inclusions in vein quartz are given in Fig. 58 and sample locations are given in Fig. 3.

Quartz vein samples 101 and 104-EG81 are located between 30 and 50 meters from the east contact, just

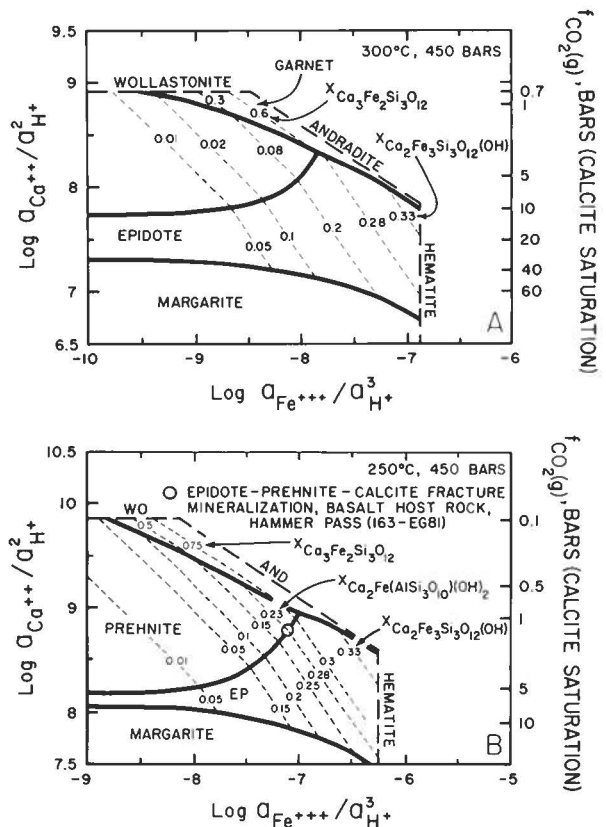


Fig. 57. Activity-activity phase diagram in the system  $\text{CaO-Al}_2\text{O}_3\text{-Fe}_2\text{O}_3\text{-SiO}_2\text{-H}_2\text{O-CO}_2$  at quartz saturation and unit activity of water. The open circle denotes the measured compositions of epidote and prehnite in vein 163-EG81 in the presence of quartz and calcite (sample location is given in Fig. 3). See Fig. 56 caption and text for details.



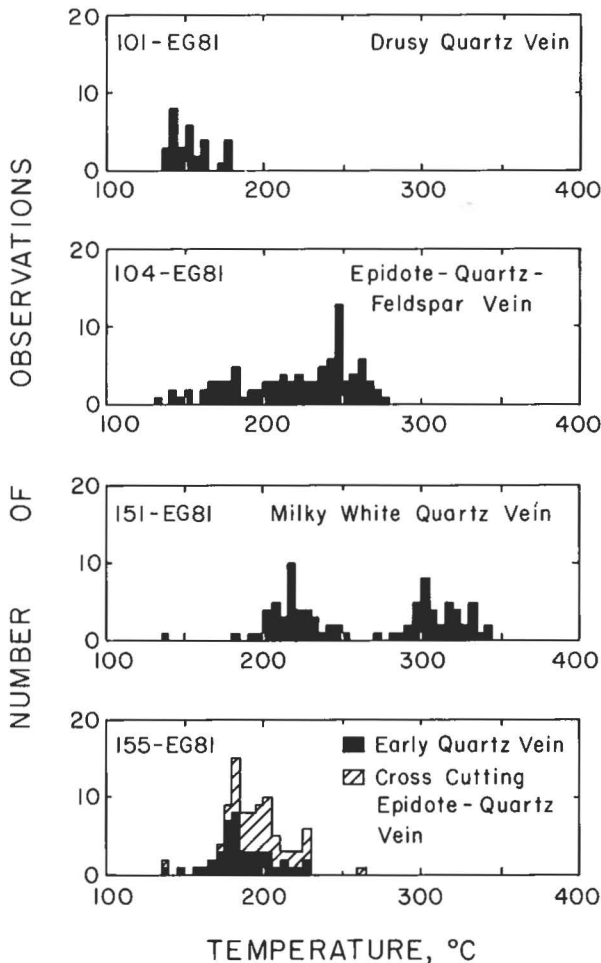


Fig. 58. Histogram of one bar fluid inclusion homogenization temperatures in vein quartz from the metabasalts marginal to the Skaergaard intrusion. See Fig. 3 for sample locations.

south of the location of Fig. 40. The former vein strikes N80E and is a 2 cm wide drusy quartz vein, containing numerous secondary liquid-rich inclusions. Primary inclusions are up to 7  $\mu\text{m}$  long, homogenize between 130° and 180°C and contain low salinity solutions (~2 wt % NaCl equivalent). Vein 104-EG81 strikes N15W and is 5 cm wide. This vein consists of epidote and albite at the vein margin with euhedral quartz crystals terminating in open pockets near the vein center. Two modes in the fluid inclusion homogenization temperatures are apparent in Fig. 58. The low temperature inclusions overlap with analyses from vein 101-EG81, and the higher temperature inclusions homogenize near 250°C and contain fluids with ~6 to 10 weight percent NaCl equivalent.

Samples 151 and 155 are quartz-rich veins near the south contact of the intrusion (Fig. 3). Both samples contain fluid inclusions that homogenize at temperatures between 150° and 250°C. These inclusions appear to be associated with late stage low-salinity fluids (1-

3 wt. % NaCl equivalent) associated with the formation of widespread quartz and epidote veins in the basalts. Vein 151-EG81 is a milky white quartz vein that is cross-cut by epidote and quartz veins. This vein appears to be similar in the field to the contact parallel milky white quartz veins shown in Figs. 40 & 51A from the east contact. Homogenization temperatures of primary fluid inclusions in vein 151-EG81 is between 280° and 340°C and freezing point depression of the fluids indicate an equivalent weight percent of NaCl of >3.4%.

Comparison of these analyses with temperatures computed by Norton & Taylor's (1979) transport model of the Skaergaard intrusion for basalts near the margins of the intrusion indicates that these four quartz-rich veins may have formed during the latest stages of the cooling of the Skaergaard intrusion. For example, their model S2 predicts temperatures of 150° to 350°C occurred marginal to the intrusion between 150 000 to 550 000 years after the inflation of the Skaergaard magma chamber. The milky white quartz veins near the south contact (155-EG81) and the east contact (Figs 40 & 51A) are parallel to the contact of the intrusion and are possibly related to the emplacement and cooling of the intrusion. The other quartz-rich vein that contain epidote may be associated with the emplacement and cooling of the later coast parallel dikes, as indicated by the close geometric association of these vein types with mafic dikes in the basalts.

## Concluding remarks

The Skaergaard intrusion is one of a number of gabbroic plutons in East Greenland (Fig. 1). The style of intrusion for many of these gabbroic plutons appears to be dependent on their relationship to the coast parallel flexure and dike swarms (Wager & Deer 1939; Wager & Brown 1967; Deer 1976; Myers 1980; Brooks & Nielsen 1982a,b). The Skaergaard, located ~5 km from the main flexure and dike swarm, formed by a single flux of tholeiitic magma, and thereafter experienced a simple geologic history (Wager & Deer 1939). In contrast, intrusions located within the flexure zone and the dike swarm are characterized by intensively disturbed layering and reveal petrologic and structural features indicative of multiple magma injection (Brooks & Nielsen 1982b, Myers 1980). The latter intrusive process is similar to those found at mid-ocean ridge spreading centers and described by O'Hara (1977) and Pallister & Hopson (1981). We feel that the style of the formation of the magma chamber will have an important effect on the spatial and temporal characteristics of the subsequent subsolidus fracture permeability and water/rock reactions in these cooling plutons. Because of the Skaergaard intrusion's rather simple magmatic and structural history, it provides a type example of the evolution of

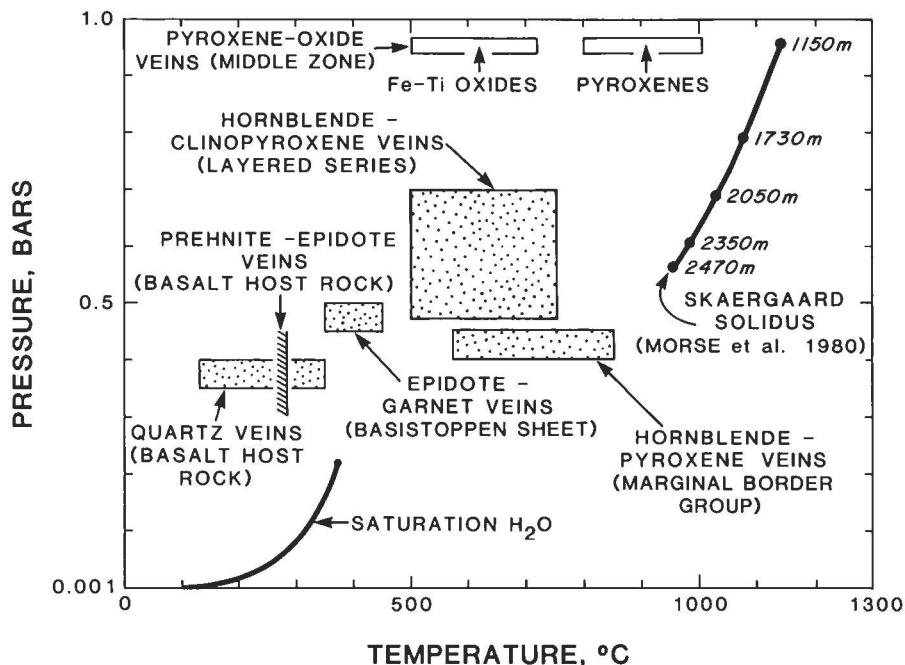


Fig. 59. Pressure and temperature diagram summarizing the estimated conditions of mineralization of fracture systems within and near the Skaergaard intrusion (see text). Pressures shown for the pyroxene-oxide veins are lithostatic pressures. Pressures given for all other vein types are hydrodynamic fluid pressures reported by Norton & Taylor (1979). Elevations reported for the solidus denote the stratigraphic height within the Layered Series.

vein mineralogy during the subsolidus cooling history of gabbroic intrusions.

The pressure-temperature conditions of mineralized fractures within and near the Skaergaard intrusion are summarized in Fig. 59. Pressures for hydrothermal veins shown in the diagram are estimated from the transport model of Norton & Taylor (1979), and for the pyroxene-oxide veins from the lithostatic pressures reported by Morse et al. (1980). Fluid inclusion homogenization temperatures indicate entrapment of fluids within quartz veins of the basalt host rocks occurred between 150° and 350°C. The maximum temperature of epidote and prehnite veins in the basalt host rocks is about 300°C based on the dehydration of prehnite. The temperatures of these assemblages, together with those for the epidote-garnet veins of the Upper Border Group, are similar to measured temperatures of calc-silicate mineralization in active geothermal systems associated with rocks of basaltic composition (Bird et al. 1984). This extensive calc-silicate fracture mineralization, together with the low  $\delta^{18}\text{O}$  values reported by Taylor & Forester (1979) for the Upper Border Group, implies that the portion of the Skaergaard magma-hydrothermal system above the Sandwich Horizon was characterized by large water to rock ratios at temperatures less than about 400°C.

Hydrothermal mineral assemblages within fractures of the Layered Series and the Marginal Border Group provide a record of the evolution of hydrothermal flow conditions and water-rock reactions during the subsolidus cooling history of the deep portions of the Skaergaard intrusion. Hydrothermal mineral assemblages in

these veins indicate reactions spanning conditions from upper amphibolite to zeolite facies metamorphism. However, the early upper amphibolite facies assemblages are more abundant and widespread implying a distinct decrease in hydrothermal fluid flow and reactions during the cooling of the Layered Series gabbros.

The early fracture sets within the Layered Series and Marginal Border Group contain calcic amphibole + clinopyroxene + biotite  $\pm$  orthopyroxene. Hydrothermal mineral compositions in this fracture set are dependent on both the bulk rock composition and on wall rock mineralogy implying minimal advection of chemical components in these veins. As shown above, the temperature dependence of the partitioning of  $\text{Fe}^{3+}$  and Mg between hornblende and clinopyroxene in early veins are in close agreement with experimental observations of Spear (1981) and with high grade metamorphic rocks summarized by Kretz & Jen (1978). Estimated temperatures suggest that the hornblende, clinopyroxene and biotite mineralization in the fractures of the Skaergaard Layered Series occurred at temperatures of >500° to 750°C and <925° to 960°C. These veins are characterized by calcic amphiboles with a continuous range of tetrahedral Al concentration from  $\sim 0.1$  to >1.8 moles per 23 oxygens.

Later fractures in the Layered Series are associated with more extensive wall rock metasomatism and contain only rare hydrothermal pyroxenes that are more calcic than those found in early veins. Amphiboles in these veins have a distinct gap in the solubility of tetrahedral Al, producing both actinolite and hornblende in

the same vein. This discontinuity in the actinolite-hornblende solid solution is indicative of middle amphibolite to greenschist facies metamorphism, and probably suggests vein mineralization at temperatures <500–600°C (e.g. Tagiri 1977; Misch & Rice 1975; Robinson et al. 1982). These later fracture systems are localized within the Layered Series and are less abundant than the high temperature fracture systems. As mentioned above, this is taken to represent a decrease in the volume averaged permeability of the Layered Series gabbros as they cooled below about 500°C. Distinction between the high temperature (> 500°C) pyroxene-bearing veins and the lower temperature actinolite-hornblende-bearing veins usually cannot be made on field evidence alone. Consequently the relative abundance of the two vein types are not given in Fig 13. A decrease in the permeability of the Layered Series with decreasing temperature is also implied by the near absence of low temperature calc-silicate veins that contain predominantly epidote. Epidote veins are common in the Upper Border Group and the basalt host rocks near the intrusion, both of which have extensively reacted with meteoric water as indicated by the oxygen isotope studies of Taylor & Forester (1979).

Extensive metasomatic replacement of the gabbros that occurs in restricted areas of intense fracturing and microbrecciation is associated with secondary ferropargasite, actinolite, chlorite, albite, epidote, prehnite, titanite, apatite, and ilmenite. These areas possibly represent localized regions of high permeability during the later stages of the cooling history of the intrusion. After this event the only evidence of water-rock reactions in fractures of the Layered Series gabbros is the formation of minor amounts of zeolite, albite and prehnite in cavities of the older veins, chlorite veins that are associated with the emplacement of mafic dikes after the cooling of the Skaergaard intrusion (Rogers & Bird 1987), and zeolite, calcite and serpentine mineralization of fault zones.

There are two important aspects of the development of the fracture controlled hydrothermal fluid circulation within the Skaergaard intrusion. First, there was a notable decrease in the permeability of the Layered Series gabbros at temperatures >500°C due to the filling of fractures with amphibole-bearing mineral assemblages. This precluded the formation of widespread epidote-bearing veins in Layered Series. Secondly, the intrusion of the Basistoppen Sheet into the Upper Border Group shortly after crystallization of the Sandwich Horizon (cf. Douglas 1964) resulted in extensive fracturing of the upper portions of the intrusion and the formation of widespread epidote veins.

The relative distribution and abundance of early high temperature veins (>500°C) and later low temperature veins within the Layered Series gabbros is consistent with isotopic and transport properties of the Skaergaard intrusion reported by Taylor & Forester (1979) and Norton & Taylor (1979) which leads to the conclusion that

most of the hydrothermal fluid circulating within the intrusion occurred at >500°C. Our research provides critical mineralogic evidence of high temperature hydrothermal fluid circulation and water/rock reactions within the cooling Skaergaard pluton.

High temperature hydrothermal vein systems are not unique to the gabbros of the Skaergaard intrusion. Recent studies have demonstrated that amphibolite facies mineral assemblages occur in vein systems within the Bushveld igneous complex (Schiffries 1984, 1985), the Artfjället gabbro (Otten 1983, 1984), the Isle of Skye gabbros (Forester & Taylor 1977; Ferry 1985), gabbroic portions of ophiolites (E. G. Liou & Ernst 1979; Stern & Elthon 1979; Evarts & Schiffman 1983) and in dredged samples of oceanic gabbros and ultramafic rocks (Prichard & Cann, 1982; Ito & Anderson 1983; Kimball et al. 1985). Because of its simple geologic history, excellent exposures and well documented geometric and petrologic characteristics, the Skaergaard intrusion is an excellent natural laboratory for investigation of the nature of deep fracture permeability and water/rock reactions that characterize cooling basic intrusions. The subsolidus geochemical and structural history of the Skaergaard intrusion represents an important example of hydrothermal processes associated with a gabbro-hosted magma-hydrothermal system in regions of continental rifting.

#### Acknowledgements

The research presented in this paper has grown from the careful, creative and perceptive observations and interpretations of the many geologists who have studied the Skaergaard intrusion during the past 50 years. The completion of our studies would have been impossible without the support and assistance of D. Norton, H. P. Taylor, Jr., C. K. Brooks, T. F. D. Nielsen, M. T. Rosing, A. R. McBirney, R. Forester, T. Hauge Andersson, S. Adalsteinsson, E. Podovanni, A. Gaines and D. Naslund. We thank Bobbie Bishop, Halldora Hreggvidsdottir, Chuck Karish, Nick Rose and Minik Rosing and the many others among our colleagues at Stanford for their help and encouragement during the course of this research. We gratefully acknowledge the expertise and patience of D. Montgomery in drafting the many versions of the maps and figures. The research was funded by NSF-EAR 82-15120 and NSF-EAR 84-18129 to DKB.

#### References

- Abbott, D. & Deer, W. A. 1972. Geological investigations in East Greenland. IX. The gabbro cumulates of the Kap Edward Holm Lower Layered Series. – *Meddr Grønland* 190, 6: 42 pp.
- Bence, A. E. & Albee, A. L. 1968. Empirical correction factors for the electron microanalysis of silicates and oxides. – *J. Geol.* 76: 382–403.
- Bird, D. K. & Helgeson, H. C. 1980. Chemical interaction of aqueous solutions with epidote-feldspar mineral assemblages in geologic systems. I. Thermodynamic analysis of phase relations in the system CaO-FeO-Fe<sub>2</sub>O<sub>3</sub>-Al<sub>2</sub>O<sub>3</sub>-SiO<sub>2</sub>-H<sub>2</sub>O-CO<sub>2</sub>. – *Am. J. Sci.* 280: 907–941.

- Bird, D. K. & Helgeson, H. C. 1981. Chemical interaction of aqueous solutions with epidote-feldspar mineral assemblages in geologic systems. II. Equilibrium constraints in metamorphic/geothermal processes. – *Am. J. Sci.* 281: 576–614.
- Bird, D. K., Schiffman, P., Elders, W. A., Williams, A. E. & McDowell, S. D. 1984. Calc-silicate mineralization in active geothermal systems. – *Econ. Geol.* 79: 671–695.
- Bird, D. K., Rosing, M. T., Manning, C. E. & Rose, N. M. 1985. Geologic field studies of the Miki Fjord area, East Greenland. – *Bull. Geol. Soc. Denmark* 34: 219–236.
- Bishop, F. C. 1980. The distribution of Fe<sup>2+</sup> and Mg between coexisting ilmenite and pyroxene with applications to geothermometry. – *Am. J. Sci.* 280: 46–77.
- Blank, H. R. & Gettings, M. E. 1973. Subsurface form and extent of the Skaergaard intrusion, East Greenland. – *EOS (Trans. Am. Geophys. Union)* 54: 507.
- Bridgewater, D., Davies, F. B., Gill, R. C. O., Gorman, B. E., Myers, J. S., Pederson, S., & Taylor, P., 1978. Precambrian and Tertiary geology between Kangerdlugssuaq and Angmagssalik, East Greenland. – *Rapp. Grønlands Geol. Unders.* 83: 17 pp.
- Brooks, C. K. 1979. Geomorphological observations of Kangerdlugssuaq, East Greenland. – *Meddr Grønland, Geoscience* 1: 24 pp.
- Brooks, C. K. & Gleadow, A. J. W. 1977. A fission-track age for the Skaergaard intrusion and the age of the East Greenland basalts. – *Geology* 5: 539–540.
- Brooks, C. K. & Nielsen, T. F. D. 1982a. The East Greenland continental margin: a transition between oceanic and continental magmatism. – *J. Geol. Soc. London* 139: 265–275.
- Brooks, C. K. & Nielsen, T. F. D. 1982b. The Phanerozoic development of the Kangerdlugssuaq area, East Greenland. – *Meddr Grønland, Geoscience* 9: 30 pp.
- Brown, G. M. 1957. Pyroxenes from the early and middle stages of fractionation of the Skaergaard intrusion, East Greenland. – *Mineral. Mag.* 31: 511–543.
- Brown, G. M. & Vincent, E. A. 1963. Pyroxenes from the late stages of fractionation of the Skaergaard intrusion, East Greenland. – *J. Petrol.* 4: 175–197.
- Coleman, L. C. 1978. Solidus and subsolidus compositional relationships of some coexisting Skaergaard pyroxenes. – *Contrib. Mineral. Petrol.* 66: 221–227.
- Deer, W. A. 1976. Tertiary igneous rocks between Scoresby Sund and Kap Gustav Holm, East Greenland. – In: Escher, A. & Watt, W. S. (eds), *Geology of Greenland*. – The Geological Survey of Greenland, Denmark: 405–429.
- Douglas, J. A. V. 1964. Geological investigations in East Greenland. VII. The Basistoppen sheet, a differentiated basic intrusion into the upper part of the Skaergaard complex, East Greenland. – *Meddr Grønland* 164, 5: 66 pp.
- Eldson, R. 1982. Autometamorphic alteration of gabbro, Kap Edvard Holm intrusive complex, East Greenland. – *Mineral. Mag.* 45: 219–225.
- Evarts, R. C. & Schiffman, P. 1983. Submarine hydrothermal metamorphism of the Del Puerto ophiolite, California. – *Am. J. Sci.* 283: 289–340.
- Ferry, J. M. 1985. Hydrothermal alteration of Tertiary igneous rocks from the Isle of Skye, northwest Scotland. I. Gabbros. – *Contrib. Mineral. Petrol.* 91: 264–282.
- Forester, R. W. & Taylor, H. P. 1977. <sup>18</sup>O/<sup>16</sup>O, D/H, and <sup>13</sup>C/<sup>12</sup>C studies of the Tertiary igneous complex of Skye, Scotland. – *Am. J. Sci.* 277: 136–177.
- Gilbert, M. C. 1966. Synthesis and stability relations of the hornblende ferropargasite. – *Am. J. Sci.* 264: 698–742.
- Hamilton, E. I. 1963. The isotopic composition of strontium in the Skaergaard intrusion, East Greenland. – *J. Petrol.* 4: 383–391.
- Hammond, P. A. & Taylor, L. A. 1982. The ilmenite/titanomagnetite assemblage: kinetics of re-equilibration. – *Earth Planet. Sci. Lett.* 61: 143–150.
- Helgeson, H. C. & Kirkham, D. H. 1974a. Theoretical prediction of the thermodynamic behavior of aqueous electrolytes at high pressures and temperatures: I. Summary of the thermodynamic properties of the solvent. – *Am. J. Sci.* 273: 1089–1198.
- Helgeson, H. C. & Kirkham, D. H. 1974b. Theoretical prediction of the thermodynamic behavior of aqueous electrolytes at high pressures and temperatures: II. Debye-Huckel parameters for activity coefficients and relative partial molal properties. – *Am. J. Sci.* 274: 1199–1261.
- Helgeson, H. C. & Kirkham, D. H. 1976. Theoretical prediction of the thermodynamic behavior of aqueous electrolytes at high pressures and temperatures. III. Equation of state for aqueous species at infinite dilution. – *Am. J. Sci.* 276: 97–240.
- Helgeson, H. C., Delany, J. M., Nesbitt, H. W. & Bird, D. K. 1978. Summary and critique of the thermodynamic properties of rock-forming minerals. – *Am. J. Sci.* 278-A: 229 pp.
- Helgeson, H. C., Kirkham, D. H. & Flowers, G. C. 1981. Theoretical prediction of the thermodynamic properties of aqueous electrolytes at high pressures and temperatures: IV. Calculation of activity coefficients, osmotic coefficients, and apparent molal and standard and relative partial molal properties to 600°C and 5 kb. – *Am. J. Sci.* 281: 1249–1516.
- Hey, M. H. 1954. A new review of the chlorites. – *Mineral. Mag.* 30: 277–292.
- Hollister, L. S., Crawford, M. L., Roedder, E., Burruss, R. C., Spooner, E. T. C. & Touret, J. 1981. Practical aspects of microthermometry. – In: Hollister, L. S. & Crawford, M. L. (eds), *Fluid Inclusions: Applications to Petrology*. – Mineral. Assoc. Canada Short Course Handbook 6: p. 278–204.
- Hoover, J. D. 1982. Petrology of the Marginal Border Group of the Skaergaard intrusion, East Greenland. – Unpub. Ph. D. Thesis, University of Oregon, Eugene, Oregon: 809 pp.
- Hughes, C. J. 1956. Geological investigations in East Greenland. VI. A differentiated basic sill enclosed in the Skaergaard intrusion, East Greenland and related sills injecting the lavas. – *Meddr Grønland* 137, 2: 28 pp.
- Irvine, T. N. 1980. Magmatic density currents and cumulus processes. – *Am. J. Sci.* 280-A: 1–58.
- Ito, E. & Anderson, A. T. 1983. Submarine metamorphism of gabbros from the Mid-Cayman rise: petrographic and mineralogical constraints on hydrothermal processes at slow spreading ridges. – *Contrib. Mineral. Petrol.* 82: 371–388.
- Kays, A., McBirney, A. R. & Goles, G. G. 1981. Xenoliths of gneisses and the conformable, clot-like granophyres in the Marginal Border Group, Skaergaard intrusion, East Greenland. – *Contrib. Mineral. Petrol.* 76: 265–285.
- Kays, A. & McBirney, A. R. 1982. Origin of the picrite blocks in the Marginal Border group of the Skaergaard intrusion, East Greenland. – *Geochim. Cosmochim. Acta* 46: 23–30.
- Kempe, D. R. & Deer, W. A. 1970. Geological investigations in East Greenland. IX. The mineralogy of the Kangerdlugssuaq alkaline intrusion. – *Meddr Grønland* 190, 3: 95 pp.
- Kimball, K. L., Spear, F. S. & Dick, H. J. B. 1985. High temperature alteration of abyssal ultramafics from the Islas Orcadas Fracture Zone, South Atlantic. – *Contrib. Mineral. Petrol.* 91: 307–320.
- Klein, S. W. 1984. Iron-rich hornblende plus albite in low pressure metabasites, Chibougamau, Quebec. – *Can. Mineral.* 22: 391–399.
- Knapp, R. B. & Knight, J. E. 1977. Differential thermal expansion of pore fluids: fracture propagation and microearthquake production in hot pluton environments. – *J. Geophys. Res.* 82: 2515–2522.
- Kretz, R. 1982. Transfer and exchange equilibria in a portion of the pyroxene quadrilateral as deduced from natural and experimental data. – *Geochim. Cosmochim. Acta* 46: 411–421.
- Kretz, R. & Jen, L. S. 1978. Effect of temperature on the distribution of Mg and Fe<sup>2+</sup> between calcic pyroxene and hornblende. – *Can. Mineral.* 16: 533–537.



- Leake, B. E. 1978. Nomenclature of amphiboles. – *Can. Mineral.* 16: 501–520.
- Leeman, W. P. & Dasch, J. 1978. Strontium, lead and oxygen isotopic investigation of the Skaergaard intrusion, East Greenland. – *Earth Planet. Sci. Lett.* 41: 47–59.
- Lindsley, D. H. 1965. Iron-titanium oxides. – *Carnegie Inst. of Washington Year Book* 64: 144–148.
- Lindsley, D. H. 1983. Pyroxene thermometry. – *Am. Mineral.* 68: 477–493.
- Lindsley, D. H. & Anderson, D. J. 1983. A two pyroxene thermometer. – *J. Geophys. Res.* 88, Supplement, Proceedings of the 13th Lunar and Planetary Science Conference, Part 2: A887–A906.
- Lindsley, D. H., Brown, G. M. & Muir, I. D. 1969. Conditions of the ferrowollastonite – ferrohedenbergite inversion in the Skaergaard intrusion, East Greenland. – *Mineral. Soc. Am. Spec. Paper* 2: 193–201.
- Liou, J. G. & Ernst, W. G. 1979. Oceanic ridge metamorphism of the East Taiwan ophiolite. – *Contrib. Mineral. Petrol.* 68: 335–348.
- Manning, C. E. & Bird, D. K. 1986. Hydrothermal clinopyroxenes of the Skaergaard intrusion. – *Contrib. Mineral. Petrol.* 92: 437–447.
- McBirney, A. R. 1975. Differentiation of the Skaergaard intrusion. – *Nature* 253: 691–694.
- McBirney, A. R. 1979. Effects of assimilation. In: Yoder, H. S. (ed.), *The Evolution of the Igneous Rocks: Fiftieth Anniversary Perspectives*. – Princeton University Press, Princeton, New Jersey: 307–338.
- McBirney, A. R. & Noyes, R. M. 1979. Crystallization and layering of the Skaergaard intrusion. – *J. Petrol.* 20: 487–554.
- Misch, P. & Rice, J. M. 1975. Miscibility of tremolite and hornblende in progressive Skagit metamorphic suite, North Cascades, Washington. – *J. Petrol.* 16: 1–21.
- Morse, S. A., Lindsley, D. H. & Williams, R. J. 1980. Concerning intensive parameters in the Skaergaard intrusion. – *Am. J. Sci.* 280–A: 159–170.
- Myers, J. S. 1980. Structure of the coastal dyke swarm and associated plutonic intrusions of East Greenland. – *Earth Planet. Sci. Lett.* 46: 401–418.
- Nash, W. P. 1976. Fluorine, chlorine and OH-bearing minerals in the Skaergaard intrusion, East Greenland. – *Am. J. Sci.* 276: 546–575.
- Naslund, H. R. 1976. Mineralogical variations in the upper part of the Skaergaard intrusion, East Greenland. – *Carnegie Inst. Washington Yearbook* 75: 640–644.
- Naslund, H. R. 1980. Part I. Petrology of the Upper Border Group of the Skaergaard intrusion, East Greenland; and Part II. An experimental study of liquid immiscibility in iron-bearing silicate melts. – Unpub. Ph. D. Thesis, University of Oregon, Eugene, Oregon.
- Naslund, H. R. 1984a. Petrology of the Upper Border Series of the Skaergaard intrusion. – *J. Petrol.* 25: 185–212.
- Naslund, H. R. 1984b. Supersaturation and crystal growth in the roof-zone of the Skaergaard magma chamber. – *Contrib. Mineral. Petrol.* 86: 89–93.
- Naslund, H. R., Hughes, J. M. & Birnie, R. W. 1983. Ilvaite, an alteration product replacing olivine in the Skaergaard intrusion. – *Am. Mineral.* 68: 1004–1008.
- Nielsen, T. F. D. 1978. The Tertiary dike swarms of the Kangerdlugssuaq area, East Greenland: An example of magmatic development during continental break-up. – *Contrib. Mineral. Petrol.* 67: 63–78.
- Nielsen, T. F. D., Soper, N. J., Brooks, C. K., Faller, A. M., Higgins, A. C. & Matthews, D. W. 1981. The pre-basaltic sediments and the Lower Basalts at Kangerdlugssuaq, East Greenland. – *Meddr Grønland, Geoscience* 6: 25 pp.
- Nobugai, K., Tokonami, M. & Morimoto, N. 1978. A study of subsolidus relations of the Skaergaard pyroxenes by analytical electron microscopy. – *Contrib. Mineral. Petrol.* 67: 111–117.
- Norton, D. & Taylor, H. P. 1979. Quantitative simulation of the hydrothermal systems of crystallizing magmas on the basis of transport theory and oxygen isotope data: an analysis of the Skaergaard intrusion. – *J. Petrol.* 20: 421–486.
- Norton, D., Taylor, H. P. & Bird, D. K. 1984. The geometry and high temperature brittle deformation of the Skaergaard intrusion. – *J. Geophys. Res.* 89: 10,178–10,192.
- Nwe, Y. Y. 1976. Electron-probe studies of the earlier pyroxenes and olivines from the Skaergaard intrusion, East Greenland. – *Contrib. Mineral. Petrol.* 55: 105–126.
- O'Hara, M. J. 1977. Geochemical evolution during fractional crystallization of a periodically refilled magma chamber. – *Nature* 286, 503–507.
- Otten, M. T. 1983. The magmatic and subsolidus evolution of the Artfjället gabbro, central Swedish Caledonides. – Unpub. Ph.D. thesis, University of Utrecht (Netherlands): 185 pp.
- Otten, M. T. 1984. The origin of brown hornblende in the Artfjället gabbro and dolerites. – *Contrib. Mineral. Petrol.* 86: 189–199.
- Pallister, J. S. & Hopson, C. A. 1981. Samail ophiolite plutonic suite: field relations, phase variation, cryptic variation and layering, and a model of a spreading ridge magma chamber. – *J. Geophys. Res.* 86: 2593–2644.
- Papike, J. J., Cameron, K. L. & Baldwin, K. 1974. Amphiboles and clinopyroxenes: Characterization of 'other' than quadrilateral components and estimates of ferric iron from microprobe data. – *Geol. Soc. Am. Abstr. with Programs* 6: 1053–1054.
- Poldervaart, A. & Hess, H. H. 1951. Pyroxenes in the crystallization of basaltic magma. – *J. Geol.* 59: 472–489.
- Popp, R. K., Gilbert, M. C. & Craig, J. R. 1977. Stability of Fe-Mg amphiboles with respect to oxygen fugacity. – *Am. Mineral.* 62: 1–12.
- Potter, R. W., Clynne, M. A. & Brown, D. L. 1978. Freezing point depression in aqueous sodium chloride solutions. – *Econ. Geol.* 73: 284–285.
- Pritchard, H. M. & Cann, J. R. 1982. Petrology and mineralogy of dredged gabbro from Gettysburg Bank, eastern Atlantic. – *Contrib. Mineral. Petrol.* 79: 46–55.
- Robinson, P., Spear, F. S., Schumacher, J. C., Laird, J., Klein, C., Evans, B. W. & Doolan, B. L. 1982. Phase relations of metamorphic amphiboles: natural occurrence & theory. – In: Veblen, D. H. & Ribbe, P. H. (eds), *Amphiboles: Petrology and Experimental Phase Relations*. – Mineral. Soc. Am. Reviews in Mineralogy 9B: 1–227.
- Rogers, R. D. & Bird, D. K. 1987. Fracture propagation associated with dike emplacement at the Skaergaard intrusion, East Greenland. *J. struct. Geol.* in press.
- Rose, N. M. & Bird, D. K. 1986. Hydrothermal mineralogy of the Nordre Aputiteq and Kruise Fjord intrusions; Evidence for multistage hydrothermal alteration in two East Greenland gabbros. – International Association of Geochemistry and Cosmochemistry, Fifth International Symposium on Water-Rock Interaction, Reykjavik, Iceland. Extended Abstracts: 475.
- Sato, M. & Valenza, M. 1980. Oxygen fugacities of the Layered Series of the Skaergaard intrusion, East Greenland. – *Am. J. Sci.* 280–A: 134–158.
- Schiffman, P., Bird, D. K. & Elders, W. A. 1985. Hydrothermal mineralization of Colorado river delta sediments in the Cerro Prieto geothermal system, Baja California, Mexico. – *Mineral. Mag.* 49: 435–449.
- Schiffries, C. M. 1984. The Bushveld intrusion hydrothermal system. – 27th International Geol. Cong. Abstracts 2: 385–386.
- Schiffries, C. M. 1985. Hydrothermal veins in the Bushveld complex: occurrence and field relations. – *EOS (Trans. Am. Geophys. Union)* 66: 1153.
- Semet, M. P. & Ernst, W. G. 1981. Experimental stability relations of the hornblende magnesiohastingsite. – *Bull. Geol. Soc. Am.* 92. (II): 274–358.



- Spear, F. S. 1981. An experimental study of hornblende stability and compositional variability in amphibolite. – *Am. J. Sci.* 281: 697–734.
- Spencer, K. J. & Lindsley, D. H. 1981. A solution model for coexisting iron-titanium oxides. – *Am. Mineral.* 66: 1189–1201.
- Stern C. & Elthon, D. 1979. Vertical variations in the effects of hydrothermal metamorphism in Chilean ophiolites: their implications for ocean floor metamorphism. – *Tectonophysics* 55: 179–213.
- Tagiri, M. 1977. Fe-Mg partition and miscibility gap between coexisting calcic amphiboles from the southern Abakuma plateau, Japan. – *Contrib. Mineral. Petrol.* 62: 271–281.
- Taylor, H. P. & Forester, R. W. 1979. An oxygen isotope study of the Skaergaard intrusion and its country rocks: a description of a 55 m. y. old fossil hydrothermal system. – *J. Petrol.* 20: 335–419.
- Thomas, W. M. 1982. Stability relations of the amphibole hastingsite. – *Am. J. Sci.* 282: 136–164.
- Wager, L. R. 1934. Geological investigations in East Greenland. I. General geology from Angmagssalik to Kap Dalton. – *Meddr Grønland* 105. 2: 46 pp.
- Wager, L. R. 1947. Geological investigations in East Greenland. IV. The stratigraphy and tectonics of Knud Rasmussens Land and the Kangerdlugssuaq region. – *Meddr Grønland* 134, 5: 64 pp.
- Wager, L. R. & Deer, W. A. 1938. A dyke swarm and coastal flexure in East Greenland. *Geol. Mag.* 75: 39–46.
- Wager, L. R. & Deer, W. A. 1939. Geological investigations in East Greenland. III. The petrology of the Skaergaard intrusion, Kangerdlugssuaq, East Greenland. – *Meddr Grønland* 105, 4: 352 pp.
- Wager, L. R. & Brown, G. M. 1967. *Layered Igneous Rocks.* – W. H. Freeman, San Fransisco: 588 pp.
- Westrich, H., Navrotsky, A. & Holloway, J. 1976. Thermodynamic data for pargasite, fluorpargasite, fluorapatite, and fluorphlogopite. – *EOS (Trans. Am. Geophys. Union)* 57: 1020–1021.
- Williams, R. J. 1971. Reaction constants in the system Fe-MgO-SiO<sub>2</sub>-O<sub>2</sub>: intensive parameters in the Skaergaard intrusion, East Greenland. – *Am. J. Sci.* 271: 132–146.

## Instructions to authors

Two copies of the manuscript, each complete with illustrations, tables, captions, etc. should be sent to the Secretary, Kommissionen for videnskabelige Undersøgelser i Grønland. Manuscripts will be forwarded to referees for evaluation. Authors will be notified as quickly as possible about acceptance, rejection or desired alterations. The final decision on these matters rests with the editor.

Manuscripts corresponding to less than 16 printed pages (of 6100 type units) including illustrations are not accepted, unless they are part of a special theme issue. Manuscripts that are long in relation to their content will not be accepted without abridgement.

## Manuscript

**Language.** – Manuscripts should be in English (preferred language), French or German. Authors who are not writing in their native language must have the language of their manuscript corrected before submission.

**Place names.** – All Greenland place names used in the text and in illustrations must be names authorised by The Greenlandic Language Committee. Authors are advised to submit sketch-maps with all required names to the Secretary for checking before the manuscript is submitted. Names of Greenland localities outside the area with which the paper is concerned should be accompanied by coordinates (longitude and latitude).

**Title.** – Titles should be as short as possible, with emphasis on words useful for indexing and information retrieval.

**Abstract.** – An abstract in English must accompany all papers. It should be short (no longer than 250 words), factual, and stress new information and conclusions.

**Typescript.** – Typescripts must be clean and free of handwritten corrections. Use double spacing throughout, and leave a 4 cm wide margin on the left hand side. Avoid as far as possible dividing words at the right-hand end of a line. Consult a recent issue for general lay-out.

Page 1 should contain 1) title, 2) name(s) of author(s), 3) abstract, 4) key words (max. 10), 5) author's full postal address(es). Manuscripts should be accompanied by a table of contents, typed on separate sheet(s).

Underlining should *only* be used in generic and species names. The use of italics in other connections can be indicated by a wavy line in pencil under the appropriate words.

Use at most three grades of headings, but do not underline. The grade of heading can be indicated in soft pencil in the left hand margin of one copy of the typescript. Avoid long headings.

**References.** – References to figures and tables in the text should have the form: Fig. 1, Figs 2–4, Table 3. Bibliographic references in the text are given thus: Shergold (1975: 16) ... (Jago & Daily 1974b).

In the list of references the following style is used:

- Boucot, A. J. 1975. Evolution and extinction rate controls. – Elsevier, Amsterdam: 427 pp.  
Sweet, W. C. & Bergström, S. M. 1976. Conodont biostratigraphy of the Middle and Upper Ordovician of the United States midcontinent. – In: Bassett, M. G. (ed.). The Ordovician System: Proceedings of a Palaeontolog-

ical Association symposium, Birmingham, September 1974: 121–151. Univ. Wales Press.

Tarling, D. H. 1967. The palaeomagnetic properties of some Tertiary lavas from East Greenland. – Earth planet. Sci. Lett. 3: 81–88.

Titles of journals should be abbreviated according to the latest (4th) edition of the World List of Scientific Periodicals and supplementary lists issued by BUCOP (British Union-Catalogue of Publications). If in doubt, give the title in full.

*Meddelelser om Grønland, Bioscience (Geoscience, Man & Society)* should be abbreviated thus: *Meddr Grønland, Biosci. (Geosci., Man & Soc.)*

## Illustrations

**General.** – Submit two copies of all diagrams, maps, photographs, etc., all marked with number and author's name. Normally all illustrations will be placed in the text.

All figures (including line drawings) must be submitted as glossy photographic prints suitable for direct reproduction, and preferably have the dimensions of the final figure. Do not submit original artwork. Where appropriate the scale should be indicated on the illustration or in the caption.

The size of the smallest letters in illustrations should not be less than 1.3 mm. Intricate tables are often more easily reproduced as text figures than by type-setting; when lettering such tables use "Letraset" or a typewriter with carbon ribbon.

Colour plates may be included at the author's expense, but the editor must be consulted before such illustrations are submitted.

**Size.** – The width of figures must be that of a column (76.5 mm), 1½ columns (117 mm) or a page (157 mm). The maximum height of a figure (including caption) is 217 mm. Horizontal figures are preferred. If at all possible, fold out figures and tables should be avoided.

**Caption.** – Captions to figures must be typed on a separate sheet and submitted, like everything else, in duplicate.

## Proofs

Authors receive two page proofs. Prompt return to the editor is requested. Only typographic errors should be corrected in proof; the cost of making alterations to the text and figures at this stage will be charged to the author(s).

Twenty-five copies of the publication are supplied free, fifty if there are two or more authors. Additional copies can be supplied at 55% of the retail price. Manuscripts (including illustrations) are not returned to the author after printing unless specifically requested.

## Copyright

Copyright for all papers published by Kommissionen for videnskabelige Undersøgelser i Grønland is vested in the commission. Those who ask for permission to reproduce material from the commission's publications are, however, informed that the author's permission must also be obtained if he is still alive.

**Meddelelser om Grønland**

**Bioscience**

**Geoscience**

**Man & Society**

**Published by  
The Commission  
for Scientific  
Research  
in Greenland**